

# DISSIPATION AND EXTRA LIGHT IN GALACTIC NUCLEI: III. “CORE” ELLIPTICALS AND “MISSING” LIGHT

PHILIP F. HOPKINS<sup>1</sup>, TOD R. LAUER<sup>2</sup>, THOMAS J. COX<sup>1,3</sup>, LARS HERNQUIST<sup>1</sup>, & JOHN KORMENDY<sup>4</sup>

*Submitted to ApJ, June 5, 2008*

## ABSTRACT

We investigate how “extra” or “excess” central light in the surface brightness profiles of cusp or power-law elliptical galaxies relates to the profiles of ellipticals with cores. The envelopes of cusp ellipticals are established by violent relaxation in mergers acting on stars present in gas-rich progenitor disks, while their centers are structured by the relics of dissipational, compact starbursts. Ellipticals with cores are formed by the subsequent merging of the now gas-poor cusp ellipticals, with the fossil starburst-components combining to preserve a dense, compact component in these galaxies as well (although mixing of stars smooths the transition from the outer to inner components in the profiles). By comparing extensive hydrodynamical simulations to observed profiles spanning a broad mass range, we show how to observationally isolate and characterize the relic starburst component in core ellipticals. Our method recovers the younger starburst population, demonstrating that these dense concentrations survive spheroid-spheroid mergers and reflect the degree of dissipation in the initial mergers that formed the penultimate galaxy progenitors. The degree of dissipation in the mergers that produced the cusp ellipticals is a strong function of stellar mass, roughly tracing the observed gas fractions of disks of the same mass over redshifts  $z \sim 0-2$ . The strength of this component strongly correlates with effective radius at fixed mass: systems with more dissipation are more compact, sufficient to explain the discrepancy in the maximum phase-space densities of ellipticals and their progenitor spirals. The survival of this component together with scattering of stars into the envelope in re-mergers naturally explain the high-Sersic index profile shapes characteristic of very massive core ellipticals. This is also closely related to the kinematics and isophotal shapes: only systems with matched starburst components from their profile fits also reproduce the observed kinematics of boxy/core ellipticals. The final “core-scouring” phase of core formation occurs when a black-hole binary formed in the merger scatters stars out of the innermost regions of the extra-light component. It is therefore critical to adopt a physically-motivated profile-decomposition that accounts for the fossil starburst component when attempting to quantify scouring. We show that estimates of the scoured mass that employ single-component forms fitted to the entire galaxy profile can be strongly biased.

*Subject headings:* galaxies: elliptical and lenticular, cD — galaxies: evolution — galaxies: formation — galaxies: nuclei — galaxies: structure — cosmology: theory

## 1. INTRODUCTION

Early work to incorporate gas physics and star formation in models of the formation of bulges and elliptical galaxies through mergers demonstrated (Mihos & Hernquist 1994a,b,c) that dissipation in disk-disk mergers leads to central starbursts like those observed in ULIRGs (Joseph & Wright 1985). Mihos & Hernquist (1994a) predicted that this process should leave an observable signature by imprinting a two-component structure into the surface brightness profiles of merger remnants. That is, the compact stellar remnant of the starburst should have a steeper density profile than the inward extrapolation of the outer de Vaucouleurs (1948)  $r^{1/4}$ -law shape of the main body of the galaxy. The “extra light” in the starburst remnant is required (Hernquist et al. 1993) to explain the high mass and phase space densities of bulges and elliptical galaxies (Ostriker 1980; Carlberg 1986; Gunn 1987; Kormendy 1989) and their fundamental plane correlations (Dressler et al. 1987; Djorgovski & Davis 1987; Kormendy & Sanders 1992; Rothberg & Joseph 2006; Hopkins et al. 2008b).

When predicted by Mihos & Hernquist (1994a), extra light was not known to exist in normal ellipticals. Sersic (1968) functions were replacing  $r^{1/4}$  laws as standard machinery to interpret brightness profiles (Caon et al. 1993). The steepest central profiles were called “power laws” (Ferrarese et al. 1994; Kormendy et al. 1994; Lauer et al. 1995; Byun et al. 1996). Both descriptions could be taken to imply, absent cores or nuclear star clusters,<sup>5</sup> that the brightness profiles of elliptical galaxies are almost power laws with no breaks indicative of two-component structure. However, Kormendy (1999) discovered in a small sample of normal ellipticals – and later Kormendy et al. (2008), in all the known low-luminosity ellipticals in the Virgo cluster – that the inner “power-law” or “cusp” indeed represented a central “extra light” component – the inner profile of a dense, centrally concentrated rise above the inward extrapolation of an outer Sersic profile. Ferrarese et al. (2006) and Côté et al. (2007) identified

<sup>5</sup> It is important to distinguish nuclear clusters (stellar “nuclei”) from extra light components – we demonstrate the clear distinction in Hopkins et al. (2008a). Nuclei are extremely small (typical radii  $\sim 1-10$  pc, and mass fractions  $\sim 10^{-3} M_{\text{gal}}$ ) relative to starburst/extra light components (radii  $\sim 0.2-2$  kpc and mass fractions  $\sim 0.1 M_{\text{gal}}$ ). The structural scalings and fundamental plane relations of stellar nuclei are similar to those of globular clusters, nearly perpendicular to and with an opposite physical sense from extra light components. Likewise their stellar population ages, metallicities, and kinematics are very different from extra light and elliptical galaxies (Carollo 1999; Böker et al. 2004; Walcher et al. 2006; Côté et al. 2006; Hopkins et al. 2008a).

<sup>1</sup> Harvard-Smithsonian Center for Astrophysics, 60 Garden Street, Cambridge, MA 02138

<sup>2</sup> National Optical Astronomy Observatory, Tucson, AZ 85726

<sup>3</sup> W. M. Keck Postdoctoral Fellow at the Harvard-Smithsonian Center for Astrophysics

<sup>4</sup> Department of Astronomy, University of Texas, 1 University Station C1400, Austin, Texas 78712-0259

qualitatively similar features – “luminosity excess” in the central regions of ellipticals (for a detailed comparison of these features, see the discussion in Hopkins et al. 2008a). Extension of this to the profiles of recent gas-rich merger remnants observed by Rothberg & Joseph (2004) showed similar signatures. The “power law” profiles identified by previous authors form a part of this extra light; the conclusion that there are two components, however, did not become clear until observations from a variety of telescopes made it possible to create profiles with sufficiently large dynamic range. These authors suggested that the observed extra light is the signature of merger-induced starbursts, as predicted by Mihos & Hernquist (1994a), and it is now becoming empirically established that essentially all “power-law” or “cusp” ellipticals show this behavior.

In Hopkins et al. (2008d) (hereafter Paper I) we showed that observed extra light can indeed be identified with the central density excess produced in simulations of gas-rich mergers. We developed a formalism to fit surface brightness profiles with two-component models in a manner that accurately recovers the *physical* decomposition between a central dissipational component (the remnant of the merger-induced starburst) and an outer dissipationless component (the product of violent relaxation acting on stars formed in the pre-merger disks before the coalescence of the merging galaxies). We used this machinery in Hopkins et al. (2008a) (hereafter Paper II) to analyze observed “cusp ellipticals”<sup>6</sup>. We showed that this method could be used to recover the dissipational components in cusp ellipticals, and that such components were ubiquitous in the local cusp elliptical population (in samples of  $\sim 100$ s of such galaxies from Lauer et al. (2007a) and Kormendy et al. (2008)). In essentially every case, simulated dissipative merger remnants provided good matches to the observed profiles of cusp ellipticals. Mutually consistent decompositions of the observed galaxy profiles and the simulated merger remnants demonstrated that the structure of cusp ellipticals as a function of mass corresponds to that predicted for the remnants of gas-rich, spiral-spiral mergers with realistic properties. That is, the degree of dissipation needed for mergers to explain the densities and scaling laws of ellipticals corresponds well with our empirically recovered starburst components and agrees with the gas fractions available in observed progenitor disk galaxies of appropriate masses.

However, it has been argued that the situation may be different for more massive ellipticals, which appear to exhibit central “cores,” and are known to display boxy isophotal shapes and slow rotation in contrast to the disk isophotal shapes and rapid rotation seen in less massive cusp ellipticals (Kormendy & Illingworth 1982; Davies et al. 1983; Davis et al. 1985; Jedrzejewski et al. 1987; Bender 1988; Bender et al. 1989, 1992; Peletier et al. 1990). Cores were first seen in ground-based observations of nearby, high-luminosity ellipticals as central regions of nearly constant surface brightness (King 1978; Young et al. 1978; Lauer 1985b; Kormendy 1985a, 1987a). They were cuspier than isothermal cores, but the functional form of the density profile as  $r \rightarrow 0$  was unknown. Later, *HST* images showed that nearly all ellipticals have singular starlight distributions in the sense that the surface brightness diverges as  $\Sigma(r) \sim r^{-\gamma}$  (Lauer et al.

1991, 1992a,b; Crane et al. 1993; Kormendy et al. 1994; Ferrarese et al. 1994; Lauer et al. 1995). In low-luminosity, early-type galaxies,  $\gamma$  typically decreases only slowly as the center is approached, and a steep  $\gamma > 0.5$  cusp continues in to the *HST* resolution limit. Lauer et al. (1995) classified these as “power-law” galaxies. In more luminous ellipticals, the steep outer density profile shows a robust break to a shallow, inner power-law cusp with  $\gamma < 0.3$  (Lauer et al. 1995). The “break radius”  $r_b$  corresponds to the “core radius”  $r_c$  measured in ground-based observations (Kormendy et al. 1994). Lauer et al. (1995) continued to call these “core galaxies,” even though the shallow cusps in projected brightness imply steep and singular cusps in luminosity density (Lauer et al. 1995; Gebhardt et al. 1996).

The division of central structure into two families was motivated by the observed bimodal distribution of cusp slopes  $\gamma$  (Gebhardt et al. 1996; Lauer et al. 2007a), but this aspect of central slopes participates in a larger, longer-recognized division of the elliptical population: the typical giant, core elliptical has different physical properties from the typical normal-luminosity, cusp elliptical (e.g. Davies et al. 1983; Davis et al. 1985; Jedrzejewski et al. 1987; Bender 1988; Bender et al. 1989, 1992; Peletier et al. 1990; Kormendy & Bender 1996; Faber et al. 1997; Simien & Prugniel 1997a,b,c; Emsellem et al. 2004, 2007; McDermid et al. 2006; Cappellari et al. 2007). Massive giant ellipticals rotate slowly and have “boxy” (rectangularly-distorted) isophotal shapes, characteristic of systems supported by anisotropic velocity dispersions (Schwarzschild 1979; de Zeeuw 1985; Binney & Tremaine 1987); Faber et al. (1997) showed that these relate to the observed “core” population. In contrast, less massive ellipticals (and S0 galaxies), where the power-law population predominates, rotate more rapidly; they have more isotropic velocity dispersions and look like they have embedded disks (“disky” isophotal shapes).

These differences thus led naturally to the idea, developed, in e.g. Faber et al. (1997); Kormendy (1999); Quillen et al. (2000); Rest et al. (2001); Ravindranath et al. (2001); Laine et al. (2003); Lauer et al. (2005, 2007a); Ferrarese et al. (2006); Côté et al. (2007); Kormendy et al. (2008, and references therein), that disk, rapidly rotating cusp ellipticals are direct products of gas-rich (“wet”) mergers, whereas boxy, slowly rotating core ellipticals have been shaped by subsequent dissipationless (“dry”) re-mergers of two or more (initially cuspy gas-rich merger remnant) ellipticals. Several questions therefore arise. How did core ellipticals form? What were their progenitors? It has been shown that mergers of bulgeless disks fail to reproduce the shapes and kinematic properties of these galaxies (see e.g. Barnes 1988; Hernquist 1992, 1993; Naab et al. 2006a; Cox et al. 2006b). Furthermore, if disks are their progenitors, then these systems would not be able to avoid dissipation, because spiral galaxies contain gas. If lower-mass cusp ellipticals are the progenitors of core ellipticals, what happened to the extra light in those cusp ellipticals?

Nearly all numerical experiments find that light profile shapes are, to lowest order, preserved in dissipationless mergers (e.g., Boylan-Kolchin et al. 2005). So, core ellipticals should be “extra light” ellipticals in the same sense as cusp ellipticals – i.e. their profile reflects a combination of an outer, low phase-space density violently relaxed remnant of stellar disks, and an inner, compact component originally formed via dissipational processes (in whatever process formed the progenitors, that would allow gas to lose angular momentum and

<sup>6</sup> The term “cusp elliptical” is used in various ways in the literature. Unless otherwise stated, we use this name to refer to ellipticals that do not have a central resolved core. In published papers, these are called “power-law ellipticals”, “coreless ellipticals”, or “extra light ellipticals.”

reach these densities in the first place). If their last merger was dissipationless, is the amount of dissipation in the “original” spheroid forming merger (i.e. that which formed their progenitors, if these are re-merger remnants) important or relevant to the properties of the  $z = 0$  galaxy? Is any memory of the merger history preserved, and is there any way to observationally recover this information?

There have been suggestions of interesting behavior in the observations, but they have largely lacked an interpretive context. Models of core galaxies generally presume that the projected stellar brightness decreases monotonically outside the core with a monotonically increasing logarithmic slope – the fact that many core ellipticals can be reasonably well-fitted by such descriptions has made the multi-component structure of such objects more ambiguous. A closer look at the existing data, however, shows evidence in some galaxies of characteristic features such as inflection points in the slope outside the core, similar to a “smoothed” version of the features often seen in cusp ellipticals where the profile transitions from being dominated by a dissipational (“extra light”) component superimposed on a background dissipationless outer envelope (see e.g. Ratcliff & Burstein 1982; Barbon et al. 1984; Lauer 1985b; Lauer et al. 2007a; Kormendy et al. 2008). Moreover, even where profiles are smooth and monotonic, the inner portions of core galaxies typically rise well above an  $r^{1/4}$  law fitted to the envelope. Instead, single profiles fitted to the galaxies are forced to higher Sérsic indices that rise more steeply at small radii, reflecting and including the dense, high surface brightness central extra light component, and yielding the high Sérsic indices ( $n_s \sim 6 - 8$ ) characteristic of core ellipticals fitted in this manner (e.g. Prugniel & Simien 1997; Trujillo et al. 2002; Ferrarese et al. 2006; Kormendy et al. 2008). Côté et al. (2007) point out that there appears to be a smooth transition from low- $n_s$  outer profiles with a steep central rise above the corresponding inward extrapolation, to high- $n_s$  outer profiles with a corresponding rise implicit in the Sérsic profile, and hence not explicitly appearing above this threshold. Without a physical motivation for decomposing this inner rise and outer envelope, interpretation of this phenomenon has been restricted to the empirical notation of the best-fit Sérsic indices. In the context of the present work, however, it highlights the potentially composite nature of core galaxies.

It is generally believed that the connection between the merger history of galaxies and their nuclear profile slope (“cusp” or “core,” on scales much less than the effective radius or the scales of the extra light) arises because of “scouring” by a binary black hole (for a review, see Gualandris & Merritt 2007). Begelman et al. (1980) first pointed out that binary black holes coalescing in a dissipationless galaxy merger stall (i.e. are no longer efficiently transported to the center via dynamic friction) at radii  $\sim \text{pc}$ , larger than the radii at which gravitational radiation can efficiently dissipate energy and merge the binary – the so-called “last parsec problem.” They noted that significant gas content can provide a continuous source of drag and friction and solve this problem in gas-rich mergers, but that in “dry” mergers, the binary will remain stalled for some time, and will harden by scattering stars in the nucleus in three-body interactions. This will continue, flattening the nuclear slope, until sufficient mass in stars ( $\sim M_{\text{BH}}$ , by simple scaling arguments) is ejected to merge the binary. It is therefore of particular interest to estimate the stellar mass which must be scattered to explain the slopes of cores, as a

test of scouring models and (in such models) a probe of the galaxy merger history. However, such estimates have been ambiguous (and often controversial; see e.g. Ferrarese et al. 2006; Lauer et al. 2007a,b; Côté et al. 2007; Kormendy et al. 2008), in large part because of the lack of an *a priori* physical model for the profile shape. Understanding the global profile shapes and extra light in core ellipticals is therefore important to reliably estimating how their nuclear profiles have, in detail, been modified by scouring.

It is also important to recognize that there can be both continuity and bimodality in the cusp/core populations. Because the expected number of major mergers in the formation history of a typical elliptical is not large ( $\sim$  a couple), it should be a relatively Poisson process: a significant number of ellipticals (especially at low masses) will have experienced only the original, single major gas-rich merger that transformed them into ellipticals since  $z \sim 2 - 3$  (see e.g. Maller et al. 2006; Hopkins et al. 2008e,c; Somerville et al. 2008; Lin et al. 2008); others (especially at high masses) will have experienced  $\sim$ one or two subsequent major mergers, which will tend to be “dry” spheroid-spheroid mergers. Although there might be some intermediate cases, to the extent that properties (such as kinematics and isophotal shapes) are affected by the last major merger, there should be significant differences between those whose last merger was dissipational (with a disk that contains some mass in gas) or dissipationless (spheroid-spheroid).

However, although the last merger may be dissipational or dissipationless, the total amount of dissipation in the formation history – the mass fraction formed dissipationally, from gas losing angular momentum in mergers and participating in nuclear starbursts – should be continuous across either population (for e.g. a given mass and original formation time). Although some objects may have had subsequent dry mergers, they still formed stars in a dense central concentration in the original, gas-rich merger that formed the progenitor spheroid; this process will be the same regardless of whether or not the system is destined for a future dry merger. As a function of mass, this should broadly reflect the gas fractions of ultimate progenitor disks at the spheroid formation times, and as such is a continuous function of mass, star formation history, and formation time. This continuity in dissipational content, to the extent that it effects the structure, fundamental plane correlations, and stellar populations of spheroids, is reflected in the continuity of e.g. the fundamental plane (recently, see Cappellari et al. 2006; Bolton et al. 2008; Hyde & Bernardi 2008), the stellar age and metallicity versus mass relations (Trager et al. 2000; Nelan et al. 2005; Thomas et al. 2005; Gallazzi et al. 2005, 2006), and the color-magnitude relation (Strateva et al. 2001; Baldry et al. 2004). As there has been considerable observational debate regarding the degree of continuity or bimodality between cusp and core populations (see e.g. Ferrarese et al. 2006; Lauer et al. 2007a; Côté et al. 2007; Kormendy et al. 2008), it is clearly of interest to identify properties that are or are not expected to be continuous across detailed merger and re-merger histories within the spheroid population.

In order to understand the structure and formation history of the core elliptical population, we therefore extend our study of merger remnants and cusp ellipticals in Paper I and Paper II to the core population in this paper. We wish to test the hypotheses that these systems were, in fact, originally formed (i.e. their progenitors were formed) in gas-rich mergers (albeit potentially modified in gas-poor re-mergers), and that the

original degree of dissipation can be empirically recovered, and is the critical parameter that can explain their densities, scaling relations, profile shapes, and sizes.

In § 2 and § 3 we describe our set of merger simulations and the observational data sets we consider, respectively. In § 4 we study how light profiles of gas-rich mergers, which we studied in detail in Paper I and Paper II, evolve in subsequent re-mergers of such ellipticals, and demonstrate that our fitting procedures designed to recover the original dissipational/starburst component in gas-rich merger remnants can be applied to re-merger remnants. In § 5 we investigate how gradients in stellar populations, imprinted by the extra light and original gas-rich merger, are affected by re-mergers. Readers interested primarily in our comparison of the properties and scalings of dissipational components in observed core ellipticals may wish to skip to § 6, where we compare our simulations with and apply our fitted galaxy decomposition to a wide range of observed systems. In § 7 we use these comparisons to study how structural parameters of the outer stellar light and inner extra light component scale with galaxy properties, and compare them with the extra light components in gas-rich merger remnants and cusp ellipticals, and examine how the existence and strength of the extra light component is related to galaxy structure and drives galaxies along the fundamental plane. In § 8 we consider the global isophotal shapes and kinematic properties of re-merger remnants and how they depend on extra light content. In § 9 we examine how re-mergers and issues of profile fitting relate to the outer Sersic profiles of core ellipticals and re-merger remnants, and compare results obtain with different choices of empirical fitting functions. In § 10 we demonstrate that this can affect estimates of “missing light” on small scales, and explain how this effect arises and what it means for a proper physical understanding of nuclear light profiles. Finally, in § 11 we discuss our results and outline future explorations of these correlations.

Throughout, we adopt a  $\Omega_M = 0.3$ ,  $\Omega_\Lambda = 0.7$ ,  $H_0 = 70 \text{ km s}^{-1} \text{ Mpc}^{-1}$  cosmology, and appropriately normalize all observations and models shown, but note that this has little effect on our conclusions. We also adopt a Chabrier (2003) initial mass function (IMF), and convert all stellar masses and mass-to-light ratios to this choice. The exact IMF systematically shifts the normalization of stellar masses herein, but does not substantially change our comparisons. All magnitudes are in the Vega system, unless otherwise specified.

## 2. THE SIMULATIONS

Our merger simulations are described in Paper I and Paper II (for details, see Springel 2005; Springel & Hernquist 2002, 2003; Springel et al. 2005). They are fully hydrodynamic simulations of galaxy-galaxy mergers, including physical and empirically motivated models for black hole accretion, star formation, a multi-phase interstellar medium, and feedback from supernovae, stellar winds, and black hole growth (we show in Paper II that our conclusions are robust to variations in these prescriptions). The typical gravitational softening is  $\sim 20 - 50 \text{ pc}$  ( $\sim 0.01 R_e$ ), and hydrodynamic gas smoothing lengths in the starbursts are smaller, which we show in Paper I and Paper II is sufficient to properly resolve not only the mass fractions but also the spatial extent of the extra light components of interest here.

We consider a series of several hundred simulations of colliding galaxies, described in Robertson et al. (2006a,b) and Cox et al. (2006a,b). We vary the numerical resolution, the or-

bit of the encounter (disk inclinations, pericenter separation), the masses and structural properties of the merging galaxies, initial gas fractions, halo concentrations, the parameters describing star formation and feedback from supernovae and black hole growth, the equation of state of the interstellar medium gas, initial merger redshifts, halo virial velocities, merger mass ratios<sup>7</sup>, and initial black hole masses.

To this, we add a subset of spheroid-spheroid “re-mergers,” representative of gas-poor or “dry” mergers of elliptical galaxies. In these cases, we collide two remnants of previous disk-disk mergers, in order to explore how their properties are modified through re-merging. We typically merge two identical remnants (i.e. two identical copies of the remnant of a given disk-disk merger), but have also explored re-mergers of various mass ratios (from 1:1 to 4:1), and mixed morphology re-mergers (i.e. merging an elliptical remnant with an unmerged gas-rich disk). In the former case, we generally find a similar division in mass ratio at which a “major” merger is significant. In the latter, we find the properties are more akin to those of other gas-rich (disk-disk) mergers, and the remnant should for most purposes still be considered the direct product of a gas-rich merger. In our re-merger series, we vary the orbital parameters, both of the initial gas-rich merger and re-merger, and consider systems with a range of initial gas fractions in the (pre gas-rich merger) progenitor disks. Our re-mergers span a similar range in virial velocities and final stellar masses to our gas-rich mergers.

Each simulation is evolved until the merger is complete and the remnants are fully relaxed, then analyzed following Cox et al. (2006b) in a manner designed to mirror the methods typically used by observers (for details see Paper II). The projected surface brightness profile is fitted with standard elliptical isophotal fitting algorithms (e.g. Bender et al. 1987; Bender 1988) and radial deviations of the iso-density contours from the fitted ellipses determine the boxyness or diskyness of each contour (the  $a_4$  parameter). Throughout, we show profiles and quote our results in terms of the major axis radius. The effective radius  $R_e$  is the projected half-mass stellar effective radius<sup>8</sup>, and the stellar mass  $M_*$  refers to the total stellar mass of the galaxy. When we plot quantities such as  $R_e$ , we typically show just the median value for each simulation across  $\sim 100$  sightlines. The sightline-to-sightline variation in these quantities is typically smaller than the simulation-to-simulation scatter, but we explicitly note where it is large.

## 3. THE DATA

We compare our simulations to and test our predictions on an ensemble of observed surface brightness profiles of ellipticals from Kormendy et al. (2008) and Lauer et al. (2007a). The important aspects of the observations for our purposes are also summarized in Paper II. Briefly, first is the V-band Virgo elliptical survey of Kormendy et al. (2008), based on the complete sample of Virgo galaxies down to extremely faint systems in Binggeli et al. (1985) (the same sample studied in Côté et al. 2006; Ferrarese et al. 2006). The HST images

<sup>7</sup> The results here are primarily from equal-mass mergers; however the behavior does not change dramatically for mass ratios to about 3:1 or 4:1, appropriate mass ratios for comparison with the observations of ellipticals used in this paper. At higher mass ratios, the result is a small bulge in a still disk-dominated galaxy (see e.g. Younger et al. 2008; Hopkins et al. 2009, 2008f), which we do not study here.

<sup>8</sup> This differs from what is sometimes adopted in the literature, where  $R_e$  is determined from the best-fitting Sersic profile, but because we are fitting Sersic profiles to the observed systems we usually quote both.

alone, while providing information on the central regions, typically extend to only  $\sim 1$  kpc outer radii, which is insufficient to fit the outer profile. Kormendy et al. (2008) therefore combine observations from a large number of sources (including Bender et al. 1988, 2007; Caon et al. 1990, 1994; Davis et al. 1985; Kormendy et al. 2005; Lauer 1985a; Lauer et al. 1995, 2005; Liu et al. 2005; Peletier et al. 1990) and new photometry from McDonald Observatory, the HST archive, and the SDSS for each of their objects which enables accurate surface brightness measurements over a wide dynamic range: profiles spanning  $\sim 12$ – $15$  magnitudes in surface brightness, corresponding to a range of nearly four orders of magnitude in physical radii from  $\sim 10$  pc to  $\sim 100$  kpc.

We also add surface brightness profiles from Lauer et al. (2007a), further supplemented by Bender et al. (1988). Lauer et al. (2007a) compile  $V$ -band measurements of a large number of nearby systems for which HST imaging of the galactic nuclei is available. These include the Lauer et al. (2005) WFPC2 data-set, the Laine et al. (2003) WFPC2 BCG sample (in which the objects are specifically selected as brightest cluster galaxies from Postman & Lauer (1995)), and the Lauer et al. (1995) and Faber et al. (1997) WFPC1 compilations (note that issues of completeness and environment are not important for any of our conclusions). This extends our sampling of the high-mass end of the mass function, but at the cost of some dynamic range in the data: Lauer et al. (2007a) combine these data with ground-based measurements to construct profiles that typically span physical radii from  $\sim 10$  pc to  $\sim 10$ – $20$  kpc. We have compared these data with additional profiles used in Bender et al. (1988, 1992, 1993, 1994), and in some cases subsequently updated. These are more limited, extending from  $\sim 30$ – $50$  pc out to  $\sim$  a few kpc, but they allow us to construct multicolor ( $V$ ,  $R$ ,  $I$ ) surface brightness, ellipticity, and  $a_4/a$  profiles, which we use to estimate our sensitivity to the observed waveband and photometric quality/dynamic range.

When comparing to cusp populations and gas-rich mergers from Paper I and Paper II, we occasionally refer to the sample of local remnants of recent gas-rich mergers from Rothberg & Joseph (2004). Details of these observations are summarized in Paper I; they are  $K$ -band profiles of remnants spanning a range in merger stage, from ULIRGs and (a few) unrelaxed systems to shell ellipticals. As demonstrated therein, these systems will almost all become (or already are, depending on the classification scheme used) typical  $\sim L_*$  cusp ellipticals.

Here, we are specifically interested in testing the hypothesis that core ellipticals retain some memory of extra light, even if they have subsequently been modified by dry re-mergers. We therefore divide our sample into those systems which are confirmed via HST observations as being either cusp or core ellipticals. We will specifically focus on the core ellipticals, but will compare their properties to those of cusp ellipticals and gas-rich merger remnants which we study in detail in Paper I and Paper II. We exclude spheroidals, as they are not believed to form in major mergers as are ellipticals (e.g. Kormendy 1985b, 1987b; Kormendy et al. 2008) (they also predominate as satellites at extremely low masses, and not as core galaxies). We also exclude S0 galaxies: these likely form a continuous family with low-luminosity cusp ellipticals (and their properties are consistent with our gas-rich merger remnants in Paper II), but robustly separating the dissipational extra light and violently relaxed components in such objects would require ideal subtraction of the large-scale disk (and fitting

three-component models involves large degeneracies). Furthermore, S0 galaxies are almost uniformly classified as cusp ellipticals in the literature.

This yields a final sample of  $\approx 110$  unique core elliptical galaxies spanning masses  $\lesssim 0.1 M_*$  to  $\gtrsim 10 M_*$ , with fitted parameters presented in Table 1 (with a comparison sample of  $\approx 80$  cusp ellipticals and  $\approx 50$  gas-rich merger remnants from Paper I and Paper II). There is overlap in the samples used; we have  $\sim 300$  surface brightness profiles for our collection of unique ellipticals, including (for many objects) repeated measurements in multiple bands and with various instruments. This provides a useful means to quantify error estimates in fits to these profiles and check for systematic sources of error, as the variations between fit parameters derived from observations in different bands or made using different instruments are usually much larger than the formal statistical errors in the fits to a single profile. For sources with multiple independent observations, we define error bars (Table 1) for each fit parameter representing the  $\sim 1\sigma$  range in parameters derived from various observations, typically from three different surface brightness profiles but in some cases from as many as  $\approx 5$ – $6$  sources (where there are just 2 sources, the “error” is simply the range between the two fits)<sup>9</sup>.

We convert the observations to physical units given our adopted cosmology and compile global parameters and calculate stellar masses as described in Paper II (our conclusions are not sensitive to either of these procedures). The data often cover a dynamic range and have resolution comparable to our simulations, provided we do not heavily weight the very central ( $\lesssim 30$  pc) regions of HST nuclear profiles. Experimenting with different smoothings and imposed dynamic range limits, we find it is unlikely that resolution or seeing differences will substantially bias our comparisons. They can introduce larger scatter, however: the robustness of our results increases considerably as the dynamic range of the observed profiles is increased.

Throughout, we will usually refer interchangeably to the observed surface brightness profiles in the given bands and the surface stellar mass density profile. In Paper I and Paper II we test this assumption in simulations, and show that once the system is relaxed, the optical bands become good proxies for the stellar mass distribution, with  $\lesssim 20\%$  variation in our  $M/L$  over the entire fitted range of radii, in good agreement with what is inferred using the observed color gradients or full resolved stellar population data to determine  $M/L$  versus radius (systems have been corrected or excluded for the effects of dust, the observed color gradients are weak, age and metallicity gradients tend to offset in  $M/L$ , and the ages of the observed systems are uniformly old, all leading to relatively little bias). Furthermore, comparison of systems observed in different bands demonstrates that our conclusions are unchanged regardless of the observed bands in which we analyze these systems.

#### 4. LIGHT PROFILE EVOLUTION IN RE-MERGERS

##### 4.1. *Physical Consequences of the Re-Merger*

We first examine how the surface brightness profiles of typical merger remnants are modified by re-mergers. To lowest order, since the gas is mostly exhausted, the re-merger will be

<sup>9</sup> In many cases the different observations are comparable; in some there are clearly measurements with larger dynamic range and better resolution: the errors derived in this manner should in such cases be thought of as the typical uncertainties introduced by lower dynamic range or less accurate photometry.

dissipationless, and merging two dissipationless, similar systems  $M_1$  and  $M_2$  on a parabolic orbit should roughly preserve their profiles. This leads to the energy conservation equation (Hausman & Ostriker 1978; Hernquist et al. 1993)

$$E_f = k(M_1 + M_2)\sigma_f^2 = E_i = kM_1\sigma_1^2 + kM_2\sigma_2^2 \quad (1)$$

where  $\sigma_f$  is the velocity dispersion of the final remnant, and  $k$  is a constant that depends on the shape of the profile. For a 1:1 merger of initially similar systems, then, the mass doubles and the velocity dispersion is unchanged,  $\sigma_f = \sigma_i$ . This implies that the effective radius must double as well. Modulo a simple overall rescaling of the profile, we therefore have reason to believe that our two component approach, applied successfully to cusp ellipticals in Paper II, should be able to identify the original dissipational and dissipationless components of the pre-re-merger galaxies.

Figure 1 compares this simple expectation to a subset of our re-merger simulations. We plot the “final” specific binding energy (binding energy per unit mass  $\epsilon_{\text{final}}$  of a given stellar particle after the system relaxes following a 1:1 spheroid-spheroid re-merger) as a function of “initial” specific binding energy (specific binding energy  $\epsilon_{\text{initial}}$  before the re-merger, but after the initial spheroid-forming merger). Equation (1) generalized to the individual stars implies that this should be conserved in a re-merger, and indeed, we see a tight correlation of the form  $\epsilon_{\text{final}} \approx \epsilon_{\text{initial}}$ . It has been well-established for some time that particles tend to preserve their rank order in binding energy in dissipationless mergers (Barnes 1988), and we confirm this here (with a scatter in  $\epsilon_{\text{final}}/\epsilon_{\text{initial}}$  of  $\sim 0.15$  dex). In detail, fitting the correlations in our simulations gives  $\epsilon_{\text{final}} \approx 1.1 \epsilon_{\text{initial}}$ . The highly bound particles are slightly more bound after the re-merger, because we are considering the stellar mass here, not the total mass – relatively more of the energy is transferred to the less bound outer halo compared to the tightly bound inner spheroid (something like this must happen, since some material is scattered to positive energies in the re-merger, removing energy from the more bound particles).

If the particle orbital distributions are conserved, then, we expect from our estimate above that their radii (or, for non-circular orbits, their apocentric radii) should approximately double after a re-merger. We therefore compare the “final” and “initial” radii of stellar particles in the same manner. Note that although technically an instantaneous three-dimensional stellar particle radius has no inherent physical meaning for non-circular orbits, even an instantaneous snapshot (e.g. viewing a galaxy at some moment) will capture most particles near their apocenter (in the mean over any ensemble of particles, effectively one will recover the apocentric radii, because this is where any given orbit spends most of its time). We therefore show in Figure 1 the radii at a given instant before and after the re-merger but find that measuring a time-averaged radius or the apocentric radii averaged over some time interval yields nearly identical results. We consider a narrow range of initial radii and examine where the stars at these radii end up after a re-merger, plotting the median and  $\pm 1\sigma$  range of their final radii (each plotted bin contains at least  $> 100$  particles, and most contain  $> 1000$ ). To lowest order, the median final effective radii are roughly twice the initial radii.

In detail, fitting the points shown yields a mean increase in radius of a factor of 1.8 (slightly less than 2, because of the fact noted above that energy is preferentially transferred to less bound material in the outer halo; in fact this factor 1.8

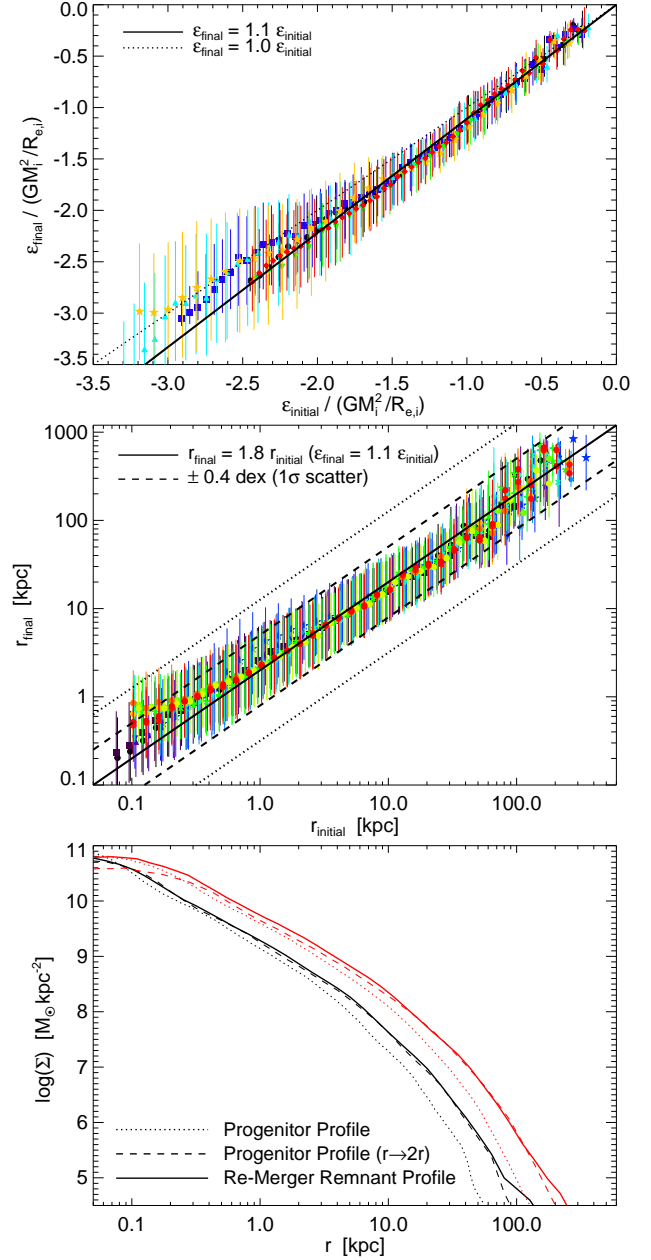


FIG. 1.— The impact of re-mergers on the stellar light profile. *Top:* Final specific binding energy ( $\epsilon_{\text{final}}$ ) of stellar particles after a spheroid-spheroid re-merger is plotted relative to their specific binding energy after the first, spheroid forming gas-rich merger ( $\epsilon_{\text{initial}}$ ; both  $\epsilon$  are in units of the characteristic energy  $GM_i^2/R_{e,i}$ , where  $M_i$  and  $R_{e,i}$  are the galaxy mass and effective radius before any mergers). Each plotted point is the median value for  $> 100$  particles within  $\pm 0.025$  dex in  $\epsilon_{\text{initial}}$ , with error bars showing the  $\pm 1\sigma$  range of  $\epsilon_{\text{final}}$ . Different colors and symbols denote different simulations. Dotted line represents exact conservation of specific binding energy; solid line is the best-fit constant rescaling  $\epsilon_{\text{final}} \approx 1.1 \epsilon_{\text{initial}}$  (representing the fact that energy is preferentially redistributed to the less bound parts of the halo). *Middle:* Same, but for the radii of each stellar particle before ( $r_{\text{initial}}$ ) and after ( $r_{\text{final}}$ ) a re-merger (reflecting their pre and post-merger orbital apocentric radii). Solid line represents the expectation from the  $\epsilon_{\text{final}} - \epsilon_{\text{initial}}$  relation and the virial theorem:  $r_{\text{final}} \approx 1.8 r_{\text{initial}}$ . Dashed and dotted lines indicate the  $\pm 1\sigma$  ( $0.4$  dex) and  $\pm 2\sigma$  range. *Bottom:* Comparison of initial progenitor projected surface mass density profile, and that profile with all radii increased by a uniform factor of 2 (the total mass also doubled) with that of the re-merger remnant (two representative examples shown).

corresponds exactly to the  $\epsilon_{\text{final}} = 1.1 \epsilon_{\text{initial}}$  change in specific energies, given the virial theorem). At small radii, there appears to be a deviation from this, but this can be explained entirely by a combination of resolution effects and the fact that the distribution is one-sided (there are only positive radii). To lowest order, then, the mass profile is preserved, with all radii “inflated” or “puffed up” by a factor  $\sim 2$ . We show this explicitly in the figure; comparing the final profiles with the progenitor profiles expanded by this factor. Correspondingly (given mass conservation), the effective surface brightness  $I_e$  decreases by a factor  $\sim 2$  and  $\sigma$  is conserved; however, typical elliptical profiles are sufficiently steep that this “puffing up” leads to a final surface brightness profile that is everywhere (at each fixed radius) brighter than the progenitors (with the effect larger at large radii).

In short, we have recovered the conventional wisdom that that particles tend to preserve their rank order in binding energy in dissipationless mergers (Barnes 1988), which also leads to their mass profiles and central mass concentrations being preserved, at least in mergers of systems with certain distributions, such as the NFW profile (Navarro et al. 1996), the Hernquist (1990) profile, or the de Vaucouleurs (1948)  $r^{1/4}$  law (e.g. Boylan-Kolchin et al. 2005).

However, for a given initial orbital apocentric radius or specific binding energy, there is in fact a wide range of final orbital apocentric radii, which we will show in § 10 has important consequences for the details of the observed profile. In detail, the distribution of final radii for a given initial radius is close to log-normal (out to  $\sim 3\sigma$  in the wings), with a median a factor of  $\sim 1.8$  larger than the initial radius and a  $1\sigma$  dispersion of 0.38 dex (factor  $\approx 2.5$ ). Most of this scatter owes to mixing in specific binding energy (the scatter in  $\epsilon_{\text{final}}/\epsilon_{\text{initial}}$  of  $\sim 0.15$  dex translates to a scatter in  $r_{\text{final}}/r_{\text{initial}}$  of 0.3 dex), and would be present even if individual orbital structures were perfectly conserved; the rest owes to mixing altering the nature of individual orbits (i.e. changing the isotropy of the system and moving stars between tube and box orbits); only a small component of the scatter is attributable to the inherent uncertainty in defining an orbital “radius” in a non-trivial potential. Figure 1 shows the  $1\sigma$  range for each bin in initial radius and this fit to the entire distribution.

Figures 2 & 3 show how the surface density profile of the final galaxy is modified by a re-merger. We show the surface brightness profiles for two gas-rich merger remnants, one in which the “extra light” signature in the center of the galaxy is plainly obvious (a good match to e.g. NGC 4459 in Virgo), and one in which it is more subtle (i.e. the extra light blends more smoothly into the outer profile; analogous to e.g. NGC 4886a). For each, we also show the profile of those stars specifically formed in the central starburst and those not. We then show the surface density profiles after a re-merger (for each, we show the profile after two different re-mergers with different orbital parameters – the choice of orbital parameters has only a weak impact on the profile). We can follow the stars which originally formed in the gas-rich merger-induced starburst, and plot their profile as well (even though there is no new starburst in the re-merger, since the systems are gas-depleted). In both cases, the profiles are roughly preserved, as expected based on the arguments above. The starburst light profile, while stretched by a similar factor  $\sim 2$  by the re-merger, remains relatively centrally concentrated and continues to dominate the profile at radii  $\lesssim 1$  kpc, while the non-starburst stars that were originally relaxed into an outer

Sersic-like profile continue to follow a similar distribution.

The light profile is, however, smoothed out by this re-merger. In the case where the original remnant shows a sharp departure from the outer profile, the departure remains relatively prominent and detectable even after a re-merger. But, when the original starburst light is more smoothly distributed, the re-merged light profile can be smooth, without any obvious feature. This case demonstrates that because the inner parts of the outer/non-starburst component shape (already being “hot”) are not affected much in the re-merger, while the starburst component is heated, we often find the starburst component is less dominant in the center after the re-merger (they have mixed). It is still important to the central profile and much more concentrated than the outer light, but the distinction is less sharp. It is therefore interesting to test whether our empirical fitting routines reliably recover the mass profile of what was, originally, the starburst light, even after a re-merger.

#### 4.2. Decomposing the Remnant Profile

We therefore adopt a two-component approach, described in Paper I and Paper II, to fit the final (post re-merger) surface brightness profile of each system. The methodology arrived at and tested in these papers amounts to a simple prescription: we fit the total observed light profile (temporarily ignoring the known true physical decomposition of the light profile) to the sum of two Sersic components. Based on the arguments and tests in Paper I and Paper II, we fit to an outer Sersic plus cusp or extra light model, with an outer component for the original pre-starburst/dissipationless stars with a free Sersic index, and an inner component reflecting the remnant of the dissipational/starburst population. Where data are limited at small radii, or in the case of our simulations where we do not resolve the structure on very small nuclear scales, we find the best results (in an average sense) adopting a fixed Sersic index  $n_s = 1$  for the inner component, but we note (as demonstrated in Paper II), that the same mean results are recovered for a free inner Sersic index, and that where the data are of sufficient quality (i.e. for systems with HST nuclear profiles extending to very small radii), it is possible to free this parameter.

Our fitting procedure then takes the following form:

$$I_{\text{tot}} = I' \exp \left\{ -b'_n \left( \frac{r}{R_{\text{extra}}} \right)^{1/n'_s} \right\} + I_o \exp \left\{ -b_n \left( \frac{r}{R_{\text{outer}}} \right)^{1/n_s} \right\}, \quad (2)$$

where  $R_{\text{extra}}$  and  $R_{\text{outer}}$  are the effective radii of the inner ( $n'_s \sim 1$ ) and outer (free  $n_s$ ) components (which we identify with the starburst and old bulge or pre-starburst components, respectively),  $I'$  and  $I_o$  are the corresponding normalizations,  $n'_s$  is the Sersic index of the inner (extra light) component (fixed  $n'_s = 1$  where resolution limits apply) and  $n_s$  is the Sersic index of the outer bulge or pre-starburst component. The constant  $b_n$  is the appropriate function of  $n_s$  such that  $R_{\text{extra}}$  and  $R_{\text{outer}}$  correspond to the projected half-mass radii. We stress that these fits are intended to recover the appropriate profile and fit where these components are physically relevant – i.e. at radii  $\gtrsim 30 - 50$  pc where our simulations are well-resolved (note that the typical effective radii of even the inner component are much larger than this,  $\sim 0.5 - 1$  kpc). For most of the galaxy observations considered here, this corresponds to radii  $\gtrsim 0.5''$ , a factor  $\sim 10$  larger than the HST diffraction limit.



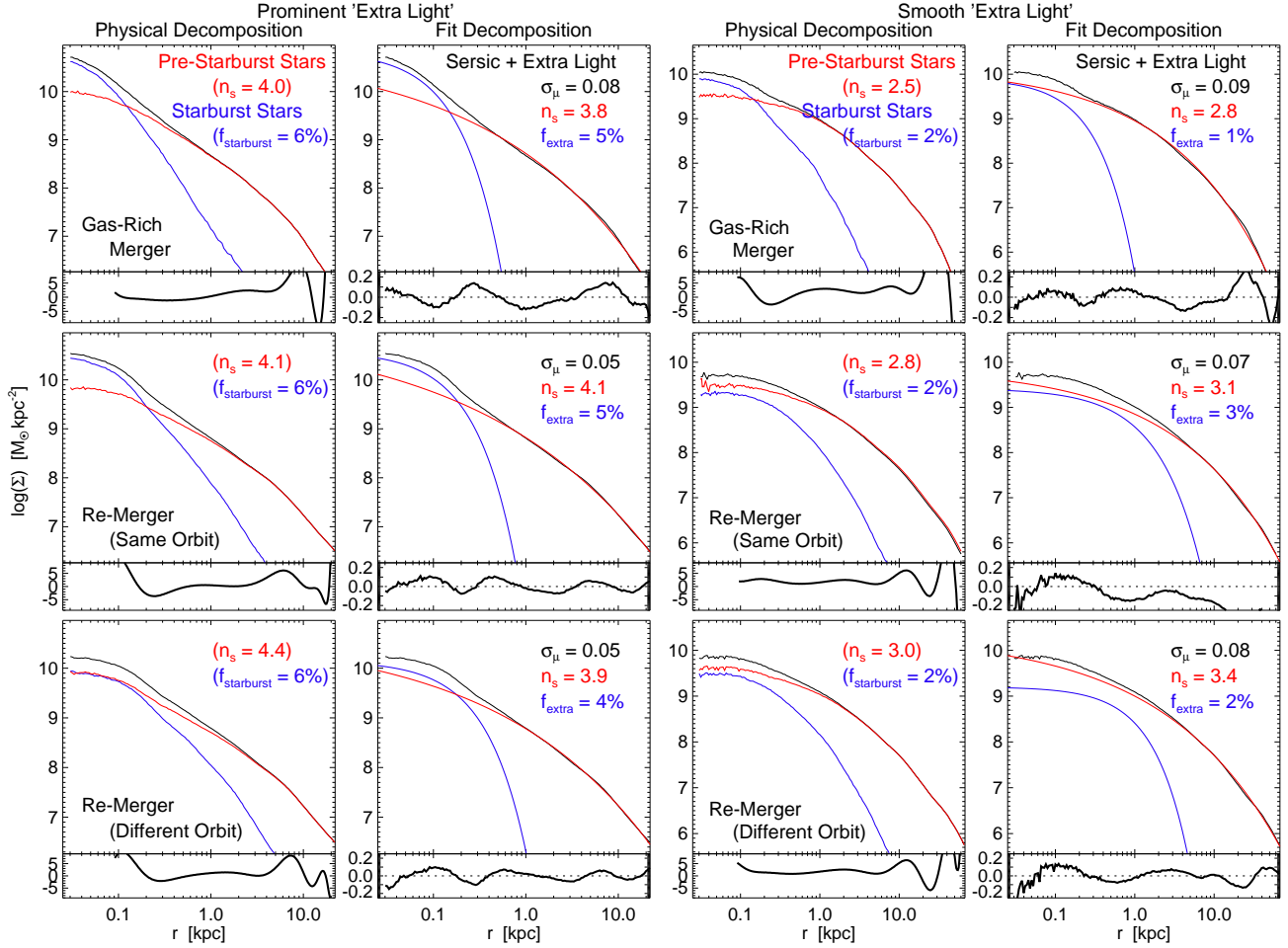


FIG. 2.— *Top*: Surface mass density of a gas-rich merger remnant (black), physically decomposed into stars formed prior to the final merger (which are then violently relaxed; red) and stars formed in the dissipational starburst (blue). The pre-starburst component follows a Sersic law closely, with best-fit index shown, and the starburst mass fraction is labeled. The second derivative of the light profile ( $d^2\mu/(d\log r)^2$ ) is shown below. We compare this with our two-component (Sersic plus cusp or extra light) fit (inner exponential and outer Sersic) to the total light profile, with the Sersic index of the outer component and mass fraction of the inner component, and rms scatter ( $\sigma_\mu$ ) about the fit. Residuals from the fit are shown below. *Middle*: The same, after a spheroid-spheroid re-merger of the remnant above. The (post re-merger) profile of the stars originally formed in the starburst is now shown, and the re-merger remnant is fitted with the same procedure. *Bottom*: Same, but for a re-merger with different orbital parameters. We show a system with a prominent transition to the extra light (*left panels*), and a more typical system with a smoother transition between outer and extra light (*right panels*). Our two-component, cusp plus Sersic function fit accurately recovers the profile of the violently relaxed component and mass fraction of the starburst component, even after a re-merger. The remnant of the original starburst (extra light) is less obvious, however, after re-mergers.

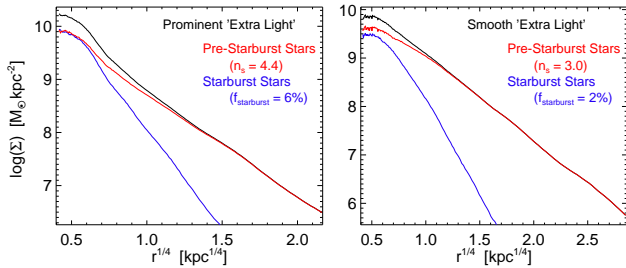


FIG. 3.— As Figure 2 (bottom panels); showing the re-merger remnant profiles and physical breakdown, in  $\mu - r^{1/4}$  instead of  $\mu - \log r$ . The smooth case (*right*) retains its extra light in a physical sense (and it is successfully recovered by our decomposition procedure), but the profile shows no obvious upward “break” relative to an outer Sersic index.

The results of applying these fits are shown in Figure 2. Despite the smearing of the transition to the extra light that owes to the re-merger, this approach still reliably recovers both the true outer Sersic index of the violently relaxed non-starburst stellar material and the mass fraction in the dissipational central starburst. We have tested this for our entire library of

re-merger simulations, and find that while the smoothing of the profile makes the object-to-object errors somewhat larger, it does not alter the ability of this method to recover, on average, the appropriate breakdown between physical components of the galaxy light profile. This is in part because the fitting does not inherently rely on a “break” in the profile – if there is a smooth but significant change in e.g. the effective concentration of the system going from inner to outer regions (or equivalently the rate of change of the logarithmic slope), it will be reflected in the fits by a dense inner component and more extended outer component.

Figure 4 shows the result of these fits to our gas-rich disk-disk merger and gas-poor re-merger simulations. We directly compare the fitted extra light mass fraction to the mass fraction and size of the known physical starburst component, and find that the fitted components recover the appropriate values in the mean with a factor  $\sim 2$  scatter. This result is robust with respect to e.g. the mass, orbital parameters, mass ratios, initial gas content, treatment of feedback and model for the ISM equation of state, and redshift of our simulations. We refer



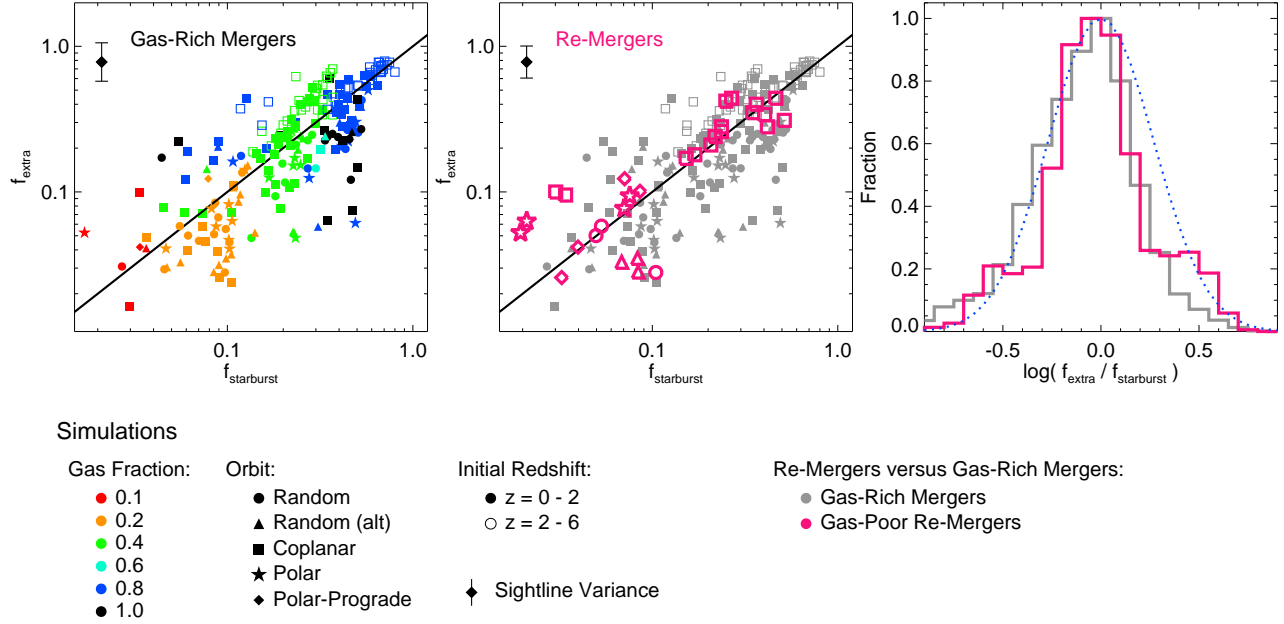


FIG. 4.— Success of our proposed two-component empirical decomposition at recovering the known physical parameters of the galaxy starburst and pre-starburst (violently relaxed) components. *Left:* Mass fraction in the fitted “extra light” component  $f_{\text{extra}}$  versus the known mass fraction of the physical starburst  $f_{\text{sb}}$ , in our gas-rich (disk-disk) merger simulations. Each point is the average across  $\sim 100$  sightlines to a given simulation; median sightline-to-sightline variance is shown ( $\approx 0.15$  dex; plotted error bar). Various colors and symbols denote different initial disk gas fractions, orbital parameters, and merger redshifts (key). *Center:* Same, but comparing our gas-rich simulations (grey, for clarity) with our gas-poor (dry) re-merger simulations (magenta). The starburst fraction  $f_{\text{sb}}$  represents the sum of the starburst masses in the two ellipticals re-merged. Symbol shapes denote original orbits of the progenitors in the gas-rich mergers (although the re-mergers follow a mix of orbits). Each of these points is close to its progenitor gas-rich merger (progenitor initial gas fractions can be inferred from the location relative to points in left panel; this is less significant than  $f_{\text{sb}}$ ). *Right:* Distribution of  $f_{\text{extra}}/f_{\text{sb}}$ , including sightline-to-sightline and simulation-to-simulation variation. Histograms are for our gas-rich (grey) and re-merger (magenta) simulations. Dotted blue line shows a Gaussian with  $\sigma = 0.27$  dex. The fitted  $f_{\text{extra}}$  recovers the physical  $f_{\text{sb}}$  on average, with a factor  $\sim 2$  scatter, and without any significant bias from any varied simulation parameters. Re-mergers yield a similar result – the error bars only significantly increase for systems with either very little starburst components (where the smoothing is significant; see Figure 2) or a large number of re-mergers.

to Paper I for a more detailed comparison where we similarly demonstrate the ability to recover the starburst effective radius and outer component Sersic index. There is no significant bias evident in our re-merger sample: although it is considerably more limited, the representative systems we have re-merged appear to lie in a similar location in this space to their progenitors, with similar scatter. At the very lowest starburst fractions, the scatter does increase in re-mergers, owing to the smoothing of the profile and mixing of the (small) extra light mass with the outer dissipationless mass (shown in Figure 2).

We note that these simulations do not directly model the process of “scouring,” or the gravitational scattering of individual stars by a coalescing black hole binary. Unfortunately, it is prohibitively expensive to model these processes self-consistently in a galaxy-scale simulation, as they require resolving the masses of individual stars and sub-parsec spatial scales. We instead adopt a standard gravitational softening prescription, and for this reason the predicted profiles should not be taken literally within the simulation smoothing lengths ( $\sim 50$  pc). In fact, scouring is expected to alter the galaxy profile significantly only near the radius of influence of the central black hole, i.e.  $\ll 30 - 50$  pc for most of the systems of interest (where the enclosed mass of the galaxy is  $\sim M_{\text{BH}}$ ; as generally expected from theoretical models and simple scaling arguments; Milosavljević et al. 2002; Merritt 2006; Sesana et al. 2007), which is below our simulation resolution limits and well below the relevant size scale at which the extra or starburst light we model is important ( $\sim 0.5 - 1$  kpc). While a very small fraction of stars at these

radii may pass near the black hole on centrophilic orbits, there is no scenario, in any plausible scouring calculation, in which the profile at radii  $\sim 0.5 - 1$  kpc, enclosing a stellar mass  $\gtrsim 100 M_{\text{BH}}$ , could be sufficiently altered by this particular process in order to change our conclusions that the original extra light is recovered after re-mergers. In other words, scouring flattens (“cores out”) the central peak in the dissipational or “extra light” profile – it changes the exact slope/shape of the central light profile as  $r \rightarrow 0$ , but not its total mass or  $\sim$ kpc extent (and we have tested in numerical experiments that our adopted fitting procedures are robust to changes in the nuclear profile shape). In short, the effects of “scouring” on this specific calculation are no different than the effects of our finite spatial and mass resolution.

Figure 5 summarizes the physical properties of the surface brightness profiles of gas-rich merger remnants and gas-poor (“dry”) re-merger remnants. The original gas-rich merger remnant is fundamentally two-component, with a Sersic-like violently relaxed envelope (with characteristic Sersic index  $n_s \sim 2.7 \pm 0.7$ , discussed in Paper II) and an inner dissipational/extra light component that dominates the light profile inside of  $\sim 0.5 - 1$  kpc. The inwards extrapolation of this extra light forms the central cusp, a (roughly) power-law like continuation (with characteristic power-law slopes  $d \ln I / d \ln r \sim -0.7 \pm 0.3$ ). The extra light, and by extension the cusp (insofar as it is simply the inwards continuation of the extra light profile), as well as embedded kinematic subsystems (see Cox et al. 2006b; Naab et al. 2006a) which make the remnant isophotal shapes more disk-like and

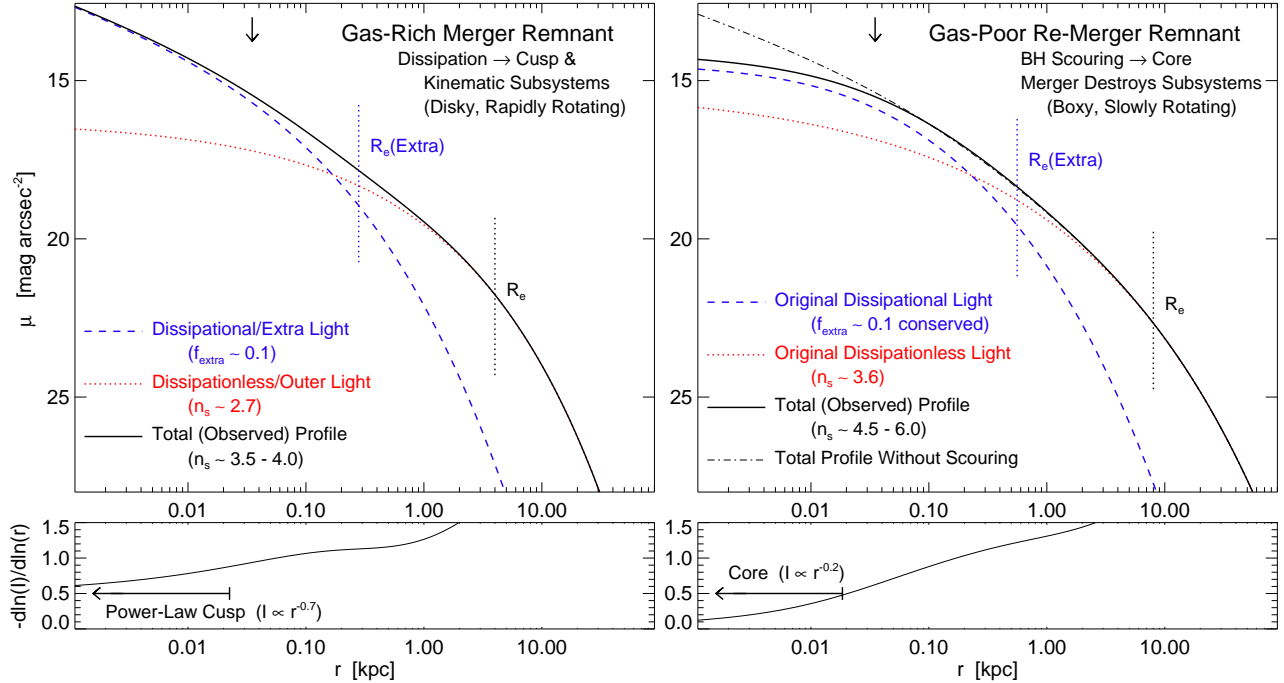


FIG. 5.— Summary of the physical properties of spheroid profile shapes (here for a typical  $\sim L_*$  elliptical), as formed in a major, gas-rich merger (*left*) and then modified by a major gas-poor, spheroid-spheroid re-merger (*right*). Lower panels show the logarithmic derivative of the total (observed) profile. In the original merger, stars from the pre-merger disks are violently relaxed into an extended Sersic-like envelope ( $n_s \sim 2.7$ ). Conservation of phase-space density prevents this component alone from reaching the high densities of observed ellipticals. Gas dissipation, however, yields a nuclear starburst, leaving a dense “extra light” component on top of the outer component, dominating the profile at  $r \lesssim 0.5 - 1$  kpc. The nuclear “cusp” is the inwards continuation of this dissipational component. Together this yields a global profile with typical  $n_s \sim 4$  and densities of observed ellipticals (much higher than their progenitor spirals). In a re-merger, both components are “puffed up” by a factor  $\sim 2$ , and scattering of stars broadens the original dissipationless/envelope component (to  $n_s \sim 3.6$ ). There is no new dissipation, but the remnant of the original dissipational component continues to dominate the profile within  $\sim 1$  kpc and is (in principle) separable. Black hole “scouring” scatters stars from the nuclear cusp/extra light – evacuating  $\sim M_{\text{BH}}$  worth of stars and flattening the central profile to form a nuclear “core.” Although the apparent effects on the extra light profile can be large, the total mass in the “scoured” region here (the “missing mass”) is only  $\sim 2\%$  of the *extra light* mass (most of which is near  $\sim 0.5 - 1$  kpc). Arrows denote the typical resolution limits of our simulations (sufficient to model the structure of the extra light and outer components, but insufficient to simultaneously resolve the transformation of cusps into cores).

yield rapid rotation, are formed by the dissipational star formation event(s). Rapid rotation and disky structure are also frequently observed in what we now recognize as the extra light regions of cuspy ellipticals (e.g., Emsellem et al. 2004, 2007; Kormendy et al. 2008).

In a dissipationless re-merger, both the original dissipational and dissipationless components are “puffed up” by a uniform factor  $\sim 2$ . The scattering of stars (the scatter in Figure 1) makes the envelope of the original dissipationless component broader, raising its Sersic index (discussed in § 9). The mass of the original dissipational component is conserved, as is its dominance within the central  $\sim \text{kpc}$  – this is a consequence of the overall preservation of profile shape. However, heating of the inner component and mixing of stars according to the scatter in Figure 1 makes the relative prominence (the rise above the outer profile) somewhat more smooth. With no scouring mechanism, the central slope would still eventually rise about as steeply as the progenitor cusp (again, reflecting the conservation of profile shape). Scouring, or scattering of stars by a nuclear binary black hole, will however evacuate the central regions and flatten this slope.

Here we have applied a toy scouring model following Gualandris & Merritt (2007), which kicks out a total of  $\sim 2 M_{\text{BH}}$  worth of stars. The scoured region (i.e. the scoured or missing mass) is therefore represented by the area between the scoured and un-scoured profiles. Because the extra light dominates the stellar density in the central regions (and formed the original cusp), scouring acts primarily on the stars in the nuclear region of the extra light. This leaves a central core

with a shallow slope ( $d \ln I / d \ln r \sim -0.2 \pm 0.2$ ). The re-merger also tends to destroy the embedded kinematic subsystems (see Cox et al. 2009) and no new source of dissipation is available to re-form them, leaving a remnant with boxy isophotal shapes and less rotation.

#### 4.3. Caveats and Limitations

We emphasize here the clear hierarchy of scales: the large scale profile and envelope is made primarily from the dissipationless violently relaxed component. The extra light dominates the profile within  $\sim \text{kpc}$  scales, a factor of a few to an order of magnitude smaller than the effective radius. Processes such as scouring and the observational distinctions between cusps and cores occur at scales yet another order of magnitude (or more) smaller,  $< 100 \text{ pc}$ . Because of this hierarchy, although scouring can appear to alter the shape of the “extra light” profile significantly, it has a negligible effect on the estimate of the total extra light mass fraction (here, the entire mass content inside the “scoured” radius is just  $\sim 2\%$  of the extra light mass) or effective radius (this  $R_e \sim 1 \text{ kpc}$ ). In general, we can continue to treat galaxy profiles as multi-component (in a physical sense) after a moderate number of dry mergers, because the mixing of stars over factors  $\sim 2$  in radii in major re-mergers is insufficient to eliminate the differences between such different scales.

This will no longer be true after a sufficiently large number of re-mergers (if there is an initial order-of-magnitude difference in the scales of the extra and outer light, then simple scalings suggest  $\sim 3$  1:1 mass ratio re-mergers, or  $\sim 5 - 10$

more likely 1:2 – 1:3 mass ratio re-mergers, could completely “blend” the dissipational and dissipationless components). However, cosmological simulations, clustering measurements, and halo occupation models (Maller et al. 2006; Zheng et al. 2007; Masjedi et al. 2008; Hopkins et al. 2008c) suggest this will only be important in the most extreme  $M_* \gtrsim 10^{12} M_\odot$  BCG populations (which constitute only  $\sim 10$ – $20\%$  of the mass density *within* the core elliptical population, and only  $\sim 3$ – $5\%$  of the mass density in ellipticals). In this regime, there are other reasons to treat our models with caution: such systems almost all experienced their first mergers at very high redshifts where the progenitors are less well-understood, they live in unusual environments, and at these masses it may be the case that growth by a large series of minor mergers becomes more important than growth by major mergers. We do not intend, therefore, for our models here to be considered as analogs for these systems; our intention is to understand the bulk of the core elliptical population at masses  $\lesssim$  a few  $L_*$  (constituting  $\sim 80$ – $90\%$  of the mass density in core ellipticals), the vast majority of which still live in less extreme environments (e.g. Blanton et al. 2005; Wang et al. 2006; Masjedi et al. 2006) and are expected to have experienced a small number ( $\sim$  a couple) of major re-mergers since redshifts  $z \sim 2$ – $4$ .

Ellipticals with cores, then, if they are the products of the re-mergers of cuspy progenitors, should have just as much “extra light” (dissipational content) as cusp ellipticals, and we will show in § 6 and § 7 that this surviving dissipational component obeys the same correlations and has similar properties to the extra light in observed cusp systems. However, the term “extra light” has not generally been applied to core ellipticals, because observations typically show less (compared to what is seen in cusp ellipticals) of an obvious upward break in the profile at small radii relative to the inwards extrapolation of their outer Sersic profiles. In fact, core ellipticals are sometimes referred to as “missing light” ellipticals, because they show a deficit in their central light profiles, relative to the extrapolation of an outer Sersic profile. These differences arise naturally from the smoothing and mixing processes in re-mergers, and in fact are completely consistent with our advocated formation scenario (see § 9).

As discussed above, “extra light” should be physically identified with stellar populations originally formed in dissipational starbursts (on top of more extended violently relaxed populations from dissipationlessly merged stellar disks), whereas “missing light” is associated with the deficit of stars in the nucleus owing to scattering of some small mass by a merging binary black hole. In a *physical* sense then, *ellipticals can be both “extra” and “missing” light ellipticals* – the terms as we mean them are not mutually exclusive. Indeed, if “extra light” means stars from dissipation (on top of dissipationlessly assembled stars) – as we use the term – then all ellipticals *must* have “extra light” at some level. And if a black hole binary does not merge sufficiently rapidly (if there is little gas in a recent major merger), scouring *will* happen. In this physical scenario, cored or “missing light” ellipticals are re-merged extra light ellipticals where the inwards extrapolation of the original extra light (which constituted the original “cusp”) has been flattened by scouring, forming a core in the center of the dissipational extra light profile.

For these reasons, we will continue to refer to our fitted central components as “extra light” and interpret them as the surviving dissipational components from the gas-rich mergers

that formed the core elliptical progenitors. Given our interpretive context and calibration from our re-merger simulations, we will show that such components appear ubiquitous in core ellipticals and obey well-defined scaling laws closely related to those of the dissipational components in cusp ellipticals.

However, that is not to say that core ellipticals would necessarily be identified as “extra light” galaxies in the sense of certain traditional observational metrics. Specifically, the smoothing of the transition between inner and outer components in re-mergers and raising the outer Sersic profile  $n_s$  by scattering stars to large radii means that the extra light may appear less pronounced. Re-mergers also tend to destroy kinematic subsystems and mix stellar orbits (Cox et al. 2009), potentially wiping out obvious changes in isophotal shapes or kinematics near the radius where the estimated extra light begins to dominate the profile. Absent such features or a physical model (as we have in the form of our simulations) to lend an interpretive physical context and suggest a multi-component nature in the first place, there will always be an infinite space of functional forms that fit the observed profiles with arbitrarily high accuracy and do not include an *explicit* “extra” or secondary component. This does not mean, of course, that the remnant dissipational populations are not manifest in the fits (after all, both our fit and others equally represent the data to a meaningful physical accuracy  $\sigma_\mu \lesssim 0.1 \text{ mag arcsec}^{-2}$ , comparable to the inherent point-to-point variance in simulations and observed systems). The parameters of interest here will simply be reflected in more indirect fashion (in some combination(s)) in whatever fitting function is adopted. We discuss some of these comparisons with alternative fitting functions commonly applied to core ellipticals in the literature in § 9. Given our aims and desire to compare simulations and observations on a uniform footing, however, we proceed with this specific machinery as a means to interpret the observed profiles of core ellipticals.

## 5. IMPACT ON STELLAR POPULATION GRADIENTS

In Paper II, we demonstrated that dissipation can give rise to strong stellar population gradients in ellipticals, and that this relates e.g. the gradient strengths, sizes, and extra light masses. We therefore briefly examine how these gradients might be modified in re-mergers; and show that the gradients tend to survive, preserving our predictions from Paper II.

Figure 6 shows the metallicity as a function of radius from several representative simulations, comparing the evolution with time of gradients in simulated ellipticals that evolve passively after the original gas-rich merger to (originally identical) systems that have had another (dry) re-merger in the intervening time. The details of our methodology are described in Paper II, but, briefly, we model every stellar particle as a single burst population with an age and metallicity given self-consistently by the star formation model in the simulation. Stars formed before the original gas-rich merger (i.e. those in our initial conditions) are placed on the mass-metallicity relation for disks of the appropriate mass at the corresponding redshift for our simulation. We project the remnant (along  $\sim 100$  sightlines, but the results depend only weakly on viewing angle) and calculate the light-weighted metallicity, stellar population age, and other properties in small radial annuli.

Naively comparing the profile in e.g. metallicity or age after a re-merger to that immediately after a gas-rich merger, it appears that there is a significant difference. However, this owes largely to age effects (the stars in the re-merger have aged significantly during the merger). Clearly the correct procedure is

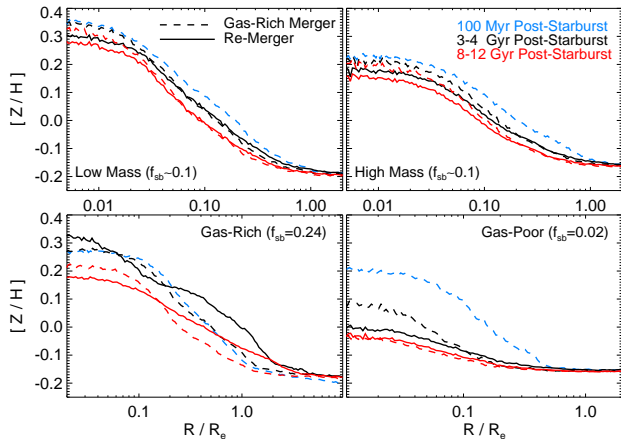


FIG. 6.— Illustration of the typical effects of a re-merger on the stellar population gradients of spheroids. For four distinct original gas-rich mergers ( $a < L_*$  and  $> L_*$  case with typical starburst mass fractions  $f_{sb} \sim 10\%$ , and a highly gas-rich and very gas-poor  $\sim L_*$  case, as labeled), we show the metallicity as a function of radius (plotted line is the median, variation across  $\sim 100$  sightlines is  $\approx 0.05 - 0.1$  in  $[Z/H]$  at each  $r$ ). We show the  $B$ -band light-weighted metallicity, at each of three approximate times after the major starburst corresponding to the original gas-rich merger (the gas-rich merger remnant is evolved passively, the re-merger case experiences a re-merger between  $t = 0 - 3$  Gyr). At the same mean stellar population age, the re-merger has had little effect on the profile, washing it out only slightly. The starburst mass fraction and overall stellar age are much more important to the gradient strength. We find similar results for age,  $[\alpha/Fe]$ , and color gradients.

to compare at fixed age or post-original gas-rich merger time. It is also important to rescale the systems by their effective radii, as we expect a roughly uniform puffing up of the remnant in a re-merger.

Figure 6 shows that when we do this, there is relatively little smearing out of the gradients by re-mergers. There is some effect, but it is generally of the order of the scatter in the gradients across sightlines, and is generally weaker than the effects of age or variation in initial gradient strength across our simulations owing to different degrees of dissipation. This is expected – Figure 1 demonstrates that the rank order in radii is preserved in a mean sense. Although there is some scatter in the particle radii, it is not dramatic as far as gradients are concerned. Note in Figure 6, the change in metallicity with radius is quite smooth, typically decreasing from the central metallicity over  $\sim 2$  orders of magnitude in radius. Compared to this dynamic range, the typical dispersion in final radii for stellar particles at a given initial radius ( $\sim 0.4$  dex) is significant, but not large. Thus even strong gradients are relatively robust to the smoothing effect in re-mergers.

Figure 7 summarizes these results for our re-merger simulations, plotting the gradient strength (quantified as the logarithmic slope in metallicity or age versus radius at  $\sim 0.1 - 1 R_e$ ; for details see Paper II) as a function of central (averaged within an aperture of  $R_e/8$ , comparable to typical observations) metallicity or stellar population age. We show both gas-rich merger remnants and the products of dry re-mergers of those same systems. Quantified in this manner, there is no significant offset between the re-mergers and the passively evolved gas-rich merger remnants.

In Paper II we showed that these distributions and the gradient strength as a function of mass and velocity dispersion, as well as color gradients as a function of elliptical age, all agree well with those observed in elliptical populations. Because these are not entirely washed out in re-mergers, this agreement continues to hold for re-mergers and core ellipticals. It has been specifically noted observationally

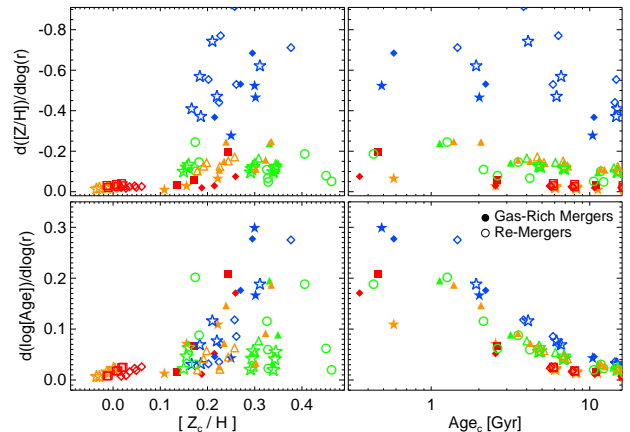


FIG. 7.— Stellar population gradients in metallicity or age as a function of central metallicity or age, in a subset of gas-rich merger remnants (filled symbols) and re-mergers of these same systems (open symbols). Color denotes the initial gas fraction of the original gas-rich mergers, and symbol type denotes orbital parameters, as in Figure 4. The dilution of gradients in re-mergers is weak – they continue to trace the same trends as gas-rich mergers of the same stellar age. The effect of increased dissipation in the original merger is dominant, and the re-merger is less important in general than the simple subsequent aging of the stellar populations by  $\sim$  a few Gyr after the gas-rich merger.

(e.g. Lauer et al. 2005; Ferrarese et al. 2006; Kuntschner et al. 2006; McDermid et al. 2006) that core ellipticals and even BCGs exhibit typical color and stellar population gradients compared to other galaxies of similar mass and age. To the extent that they may represent re-mergers of (originally) cusp ellipticals, our simulations imply that this is the natural expectation.

## 6. DISSIPATIONAL CONTENT IN ELLIPTICAL GALAXIES WITH CORES

### 6.1. Fitting Surface Brightness Profiles

If the preceding discussion is correct, extra or starburst light survives a galaxy merger in some sense. We expect, then, that even if core ellipticals have been shaped by spheroid-spheroid re-mergers, and their profiles smoothed, they should show a central stellar density similar to our simulations corresponding to what was (originally) their starburst light content, which should be recovered (on average) by our applied decompositions. Are observed systems consistent with this scenario?

Figure 8 shows the surface brightness profiles of three core ellipticals from moderate mass (NGC 3379, a  $\sim M_*$  core elliptical) to very massive (NGC 4874, a  $\gtrsim 10 M_*$  elliptical). In these systems, there is a distinct shoulder in the light profile, which is evident in a completely non-parametric sense in the first and second logarithmic derivatives of the profiles – the slope of the profile is clearly non-monotonic with radius over a brief range. Moreover, the shape of this feature is similar in all three cases. There are perhaps alternative explanations for these features (NGC 3379 may in fact be a face-on S0, see De Lorenzi 2008, and NGC 4874 is a very massive galaxy with a large envelope, albeit not technically a BCG) but these are not unique systems – there are a significant number of other such cases, as we describe below.

The features in these observed light profiles are similar, both in their shape and characteristic radii, to the physical transition in our simulations where the extra or starburst light begins to dominate with respect to the dissipationless, non-starburst light. Applying our two-component fit decomposi-

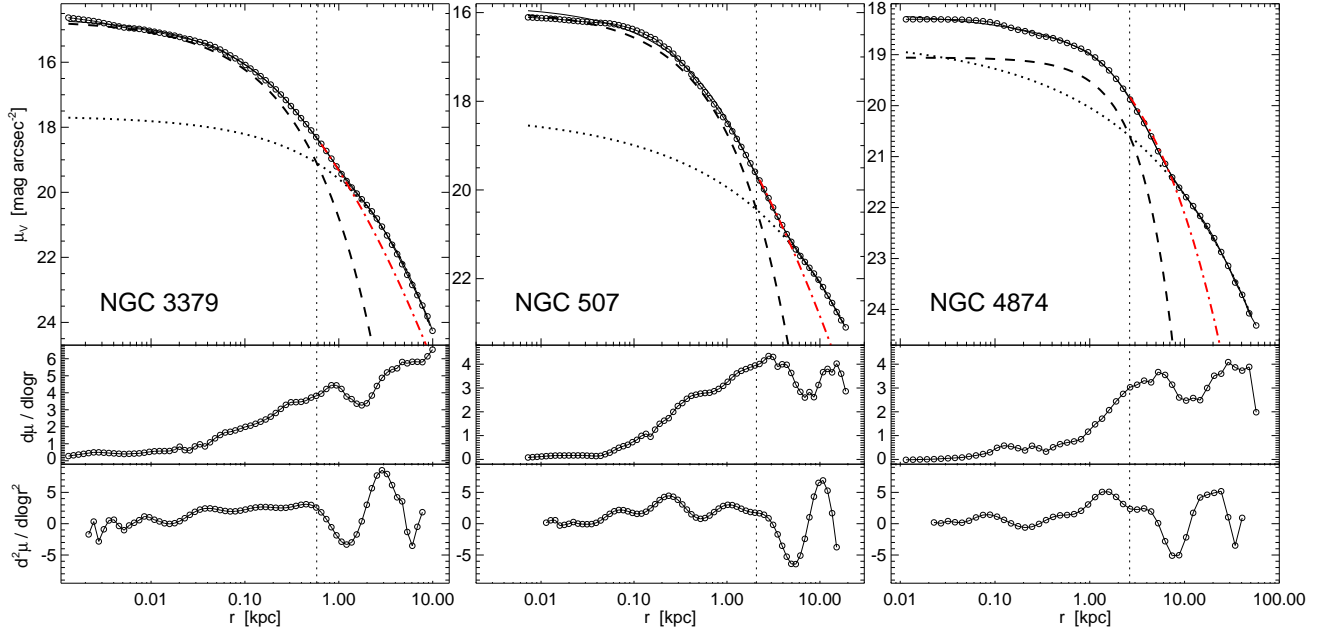


FIG. 8.— Examples of core ellipticals with possible surviving signatures of starburst or “extra” light from cusp progenitors in their nuclei (preserved, albeit smoothed out, from the original, gas-rich spheroid forming merger). *Top*: Observed surface brightness profile (open circles) and best-fit two-component model (solid line). The inner (starburst remnant; black dashed line) and outer (violently relaxed dissipationless remnant; black dotted line) components of the best-fit model are shown, with the radius (vertical dotted line) at which the two are equal. Nuker fits (red dot-dashed) to the profile between the central  $\sim 100$  pc (inside which the core dominates the fit) and radius of the shoulder are shown – these fall short where our fitted outer component dominates the light, reflecting a significant change in the curvature of the profile. *Middle*: First derivative of the surface brightness with respect to  $\log r$ . *Bottom*: Second derivative of the profile. Characteristic features or shoulders in the profiles can survive re-mergers, manifest plainly in a non-parametric fashion in both first and second derivatives, corresponding to the radius at which our method estimates the starburst component begins to dominate. (The specific objects are discussed further in the text.)

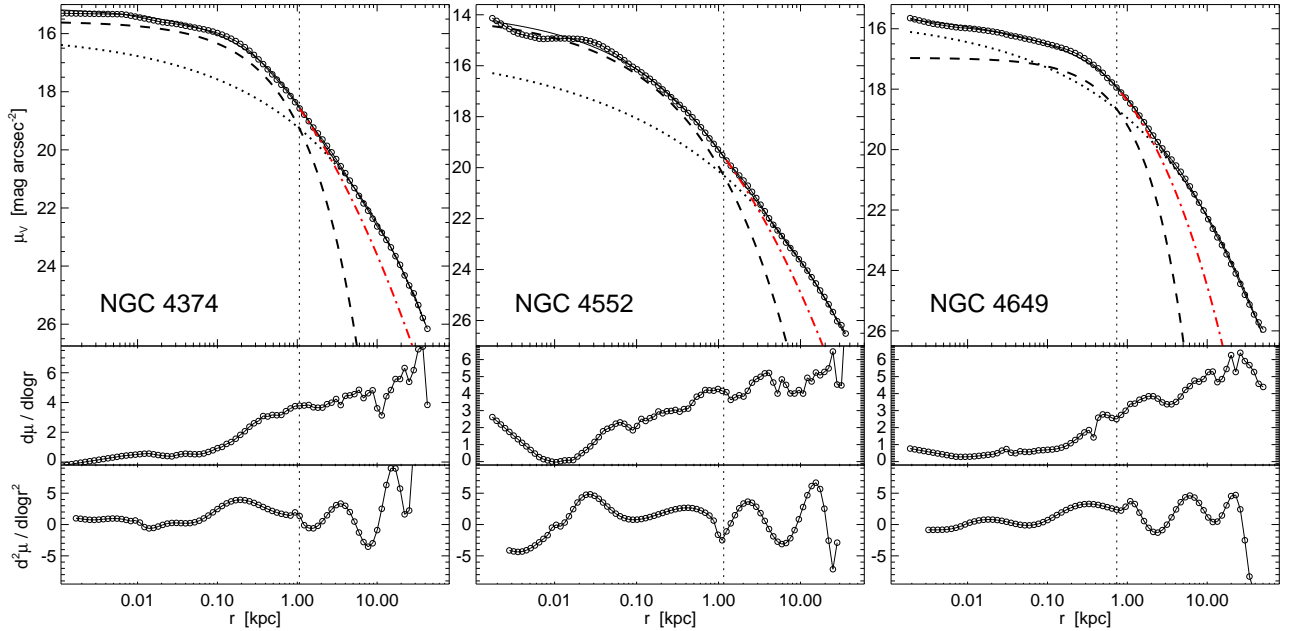


FIG. 9.— As Figure 8, but for systems with less prominent/obvious features. Despite being weaker, a similar transition is seen, and the amplitude in the first and second profile derivatives is comparable. The Nuker fits to the central profile similarly underpredict the outer component, as expected if a second physical component becomes important.



tion to these profiles, we find a good fit that (as expected) is able to explain these shoulder-like features as the transition between extra/starburst light and the outer light distribution. In a parametric sense, if we fit a Sersic or Nuker-law profile to the central regions (specifically, we consider radii between 100 pc – within which the core structure is important – and  $\sim 0.5$ –2 times the radius at which our two component fit determines that the two components are equal; the exact range is not important), we find that the substantial curvature of the inner profile leads to a fit which falls short of the shoulder, and fails to reproduce the outer profile dominated (in our two-component model) by an outer, violently relaxed population.

Figure 9 compares three galaxies with relatively weak features, in Virgo. These are systems where presumably the scattering of stars in re-mergers, discussed in § 4 has smoothed any strong break to the extra light that might have been prominent in the progenitors. Despite not being obvious on visual inspection, however, the first and second derivatives of the profile show similar signatures, and in fact the deviations from a single profile fit (a Sersic or Nuker law) extrapolated outward from the central region (interior to the shoulder) are significant. Moreover, we find here (and in Figures 2-5) that although the formal uncertainties may be larger when the profiles are smoothed in this manner, our two-component model is able to successfully fit them: § 4 demonstrates that even in systems with smoother profiles than these, our applied decompositions are robust.

Together with the arguments in § 4, this gives us reasonable confidence that we can extend our analysis to the compilation of observed ellipticals described in § 3. Figures 10-14 show surface brightness profiles of objects in the Virgo core elliptical sample of Kormendy et al. (2008), in order of most massive to least massive<sup>10</sup>. For each object, we plot the surface brightness profile with the best-fit two component model, and the corresponding fitted outer Sersic index and extra light fraction. We refer to Paper I for the same comparisons with local observed gas-rich merger remnants from Rothberg & Joseph (2004), and Paper II for the comparisons with the cusp ellipticals in Virgo from Kormendy et al. (2008). A complete list of fit parameters and compiled galaxy properties is included in Table 1.

We also compare each observed system with our library of re-merger simulations, in a non-parametric fashion. We do this by allowing the normalization of the simulated light profile to vary (within  $\pm 0.5$  dex), and quantifying the  $\chi^2$  (variance of the observed points with respect to the simulated light curve at  $> 1$  gravitational softening length) of each simulation. We allow the normalization to vary because we have a finite number of simulations and therefore do not sample a continuum in e.g. total brightness, but instead discretely sample at factor  $\sim 2$  intervals (we do not allow the simulated profiles to vary by more than this amount, to avoid an unphysical match to a simulation with very different total mass). We do not allow any other parameters to vary – i.e. we allow limited rescaling in the surface brightness of the simulated galaxies, but *not* their radii or other properties. Despite the allowed surface brightness rescaling, the best-fit simulations almost always have similar total luminosities to the observed system, because they must have a similar effective radius in order to be a good match. Considering  $\sim 100$  sightlines to each of

our simulations (although, as noted in Paper I, the observed surface brightness profile varies by a small amount sightline-to-sightline), we find the best fit to each observed system.

We show in Figures 10-14 the three simulations which most closely match the observed light profile. For the best-fit simulation, we also show the profile of the stars formed in the original, central, merger-driven starburst, as described in § 1. We show in the figures the outer Sersic indices fitted to these simulations, along with the typical range both across sightlines and across the best-fitting simulations (which together give some rough approximation to the range of  $n_s$  which might be observed for these galaxies along different sightlines). We also show the best-fit starburst mass fraction, along with the range across the best-fitting simulations (described below), and the rms residuals of the observed points with respect to the best fit<sup>11</sup>. In nearly every case, we easily find simulations which provide an excellent match to the observed profiles, with variance  $\sigma_\mu$  often less than even a multi-component parameterized fit. The fits are good over the entire dynamic range from the largest observed radii ( $\sim 100$  kpc) down to our resolution limits ( $\sim 50$  pc)<sup>12</sup>.

In addition, for these simulations we show the isophotal shape and ellipticity as a function of major axis radius, compared to that observed. Note that we do *not* fit these quantities, only the surface brightness profile. We show, for each simulation, the range across sightlines in these quantities – it is clear that these depend much more strongly on sightline than the surface brightness profile (this is primarily why we do not fit these quantities). In every case, there is a significant fraction of sightlines with shape and ellipticity profiles roughly consistent with those observed, but the simulations highlight the range of profile shapes for similar spheroids to those observed.

Our simulations are also consistent with the observed kinematic ( $V$ ,  $\sigma$ ) profiles of these systems, but we do not show an explicit comparison for individual objects because sightline-to-sightline variations are sufficiently large (see § 8) as to yield only weak constraints. For more robust quantities, such as e.g. the weighted rotation  $\lambda_R$  defined in Emsellem et al. (2007), we find that our re-merger remnants yield good agreement with the (nearly universal) radial  $\lambda_R(R)$  profile of “slow rotators” in the SAURON sample (see their Figure 2). The distribution of global rotation properties (e.g.  $V/\sigma$ ) and correlations with isophotal shapes can be constraining (for a population): we consider this in § 8. There is, however, a great deal more kinematic information than just a radial mean velocity profile: more detailed constraints for individual objects can, in principle, be obtained by comparison of simulations and high-resolution two dimensional velocity field maps (with higher-order velocity moments such as  $h_3$  and  $h_4$ ). Such a comparison is clearly warranted, but is outside the scope of this paper and will be the topic of future work (Cox et al. 2009).

Figures 15-17 again show the observed and best-fit simulated surface brightness profiles, for a subset of confirmed core ellipticals in the sample of Lauer et al. (2007a), in order of V-band magnitude from brightest to faintest. For each sim-

<sup>10</sup> NGC 4261 is technically in the Virgo W cloud, but we show it because it is included in the Virgo samples from Ferrarese et al. (2006) and Kormendy et al. (2008).

<sup>11</sup> The values shown in Figures 10-14 are based on comparison only to the profiles shown, from Kormendy et al. (2008). In Table 1, the values represent the results from all available data sets, including multiple different observations of the systems shown here, and so can be slightly different (however the differences are generally small).

<sup>12</sup> The dynamic range of the fits is somewhat difficult to discern in Figures 10-14 owing to the plotting versus  $r^{1/4}$ ; we therefore reproduce these figures plotting  $\mu$  versus  $r$  in Appendix A.



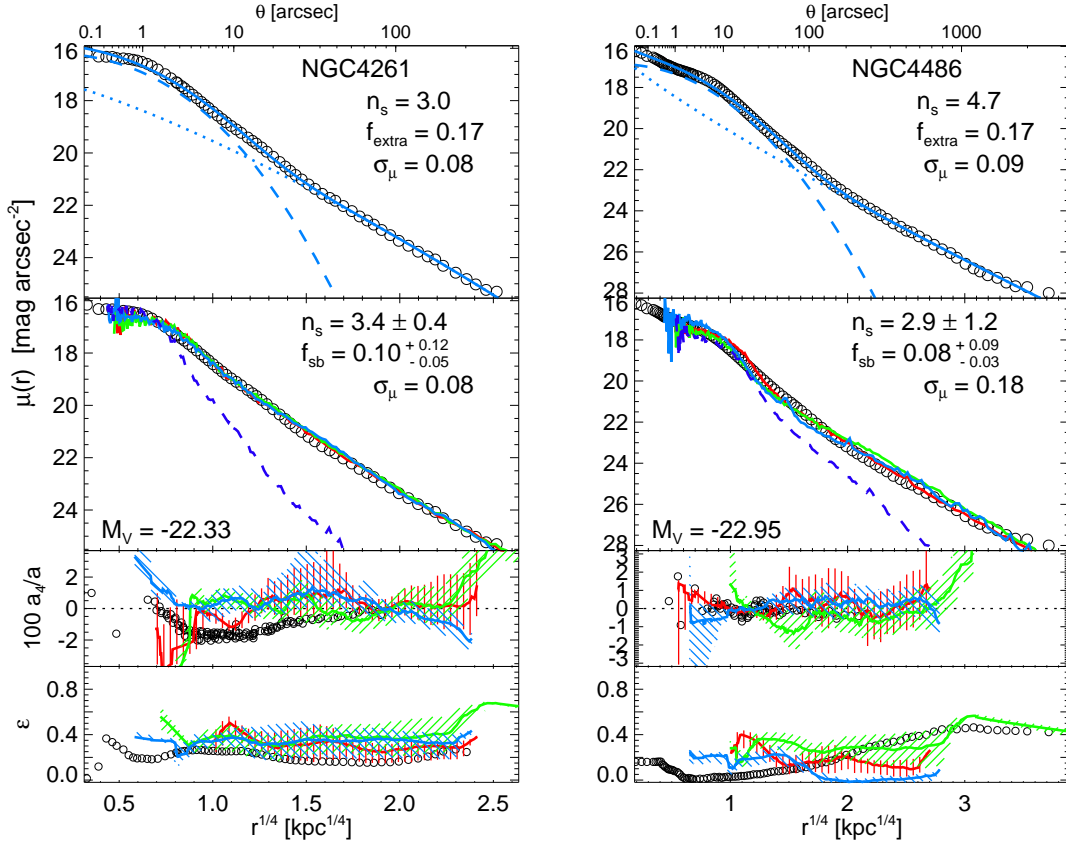


FIG. 10.— Surface brightness profiles – decomposed into dissipationless and dissipational/extra light components – are shown for core ellipticals in and around the Virgo cluster<sup>10</sup>. Open circles show the observations, from Kormendy et al. (2008). These are the highest-mass core ellipticals in Virgo ( $\sim 6-8M_*$ ). *Upper*: Observed V-band surface brightness profile with our two component best-fit model (solid, dashed, and dotted lines show the total, inner/extra light component, and outer/pre-starburst component). The best-fit outer Sersic index, extra light fraction, and rms residuals about the fit are shown. *Lower*: Colored lines show the corresponding surface brightness profiles from the three simulations in our library which correspond most closely to the observed system. Dashed line shows the profile of the starburst light in the best-matching simulation. The range of outer Sersic indices in the simulations (i.e. across sightlines for these objects) and range of starburst mass fractions which match the observed profile are shown, with the rms residuals of the observations about the best-fit simulation<sup>11</sup>. *Bottom*: Observed disk/boxy-ness ( $a_4$ ) and ellipticity profiles, with the median (solid) and 25–75% range (shaded) corresponding profile from the best-fitting simulations above. Note that these are not fitted for in any sense. Figures 11–14 show the other core ellipticals in the sample, ranked from most to least massive<sup>12</sup>.

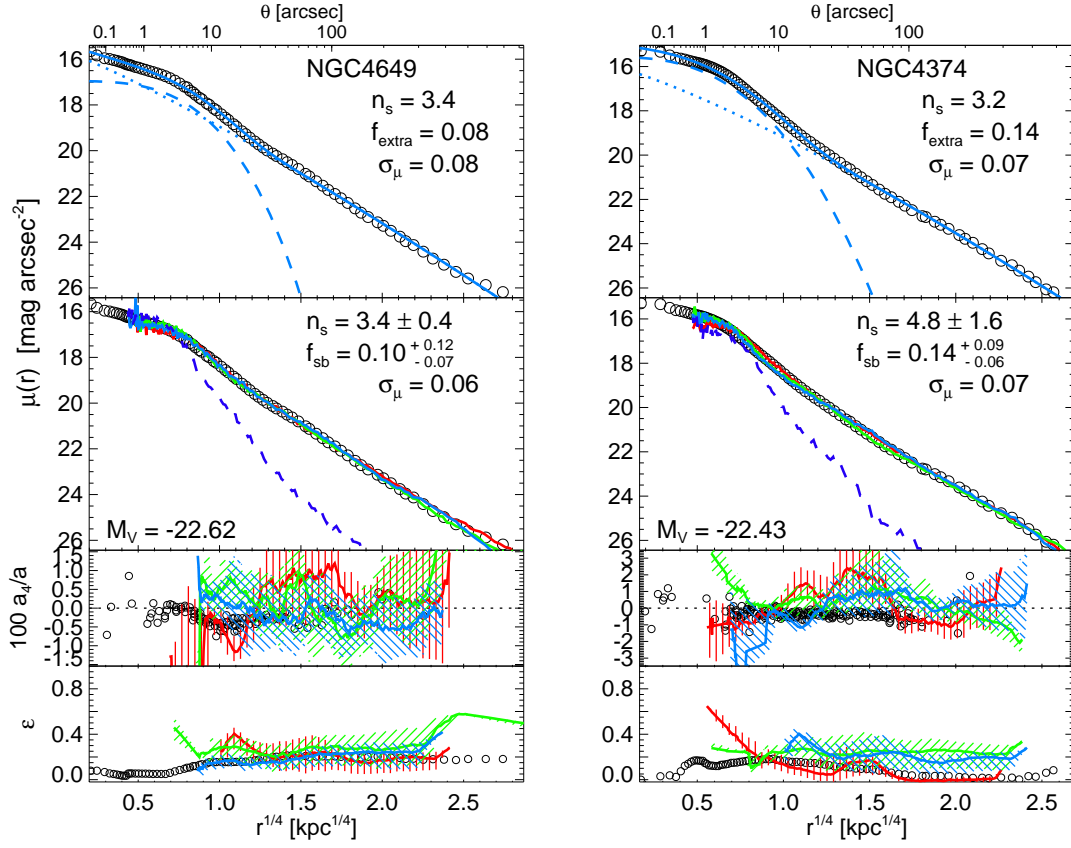
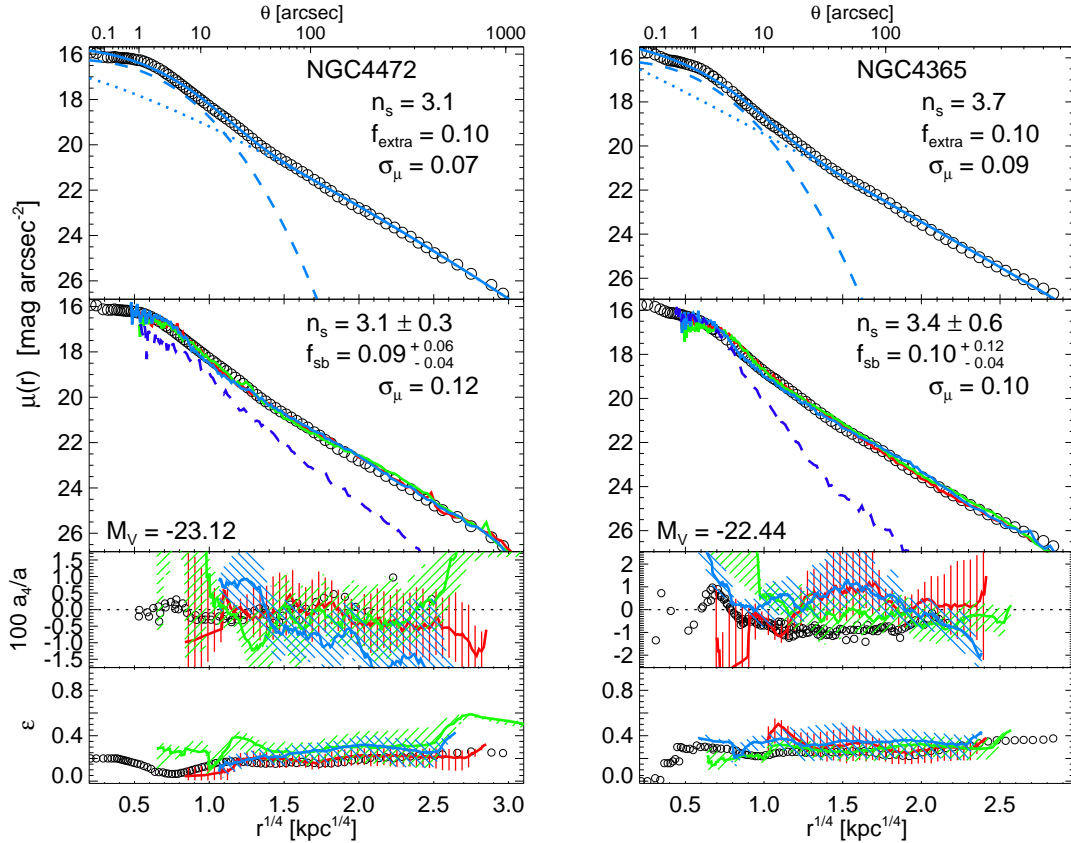
ulation in our library, we have a  $\chi^2$  corresponding to its goodness of fit to the observed profile, and the genuine physical starburst mass fraction  $f_{sb}$  from the original gas-rich merger. We can therefore construct a  $\chi^2$ -weighted distribution of  $f_{sb}$  for each observed system – essentially, the probability, across a uniform sample of initial conditions, that the observed profile was drawn from a simulation with the given starburst mass fraction. These are shown, and compared to the fitted extra light fraction for our two-component models. In general, the fitted extra light fraction corresponds well to the characteristic starburst mass fractions in simulations which produce similar light profiles.

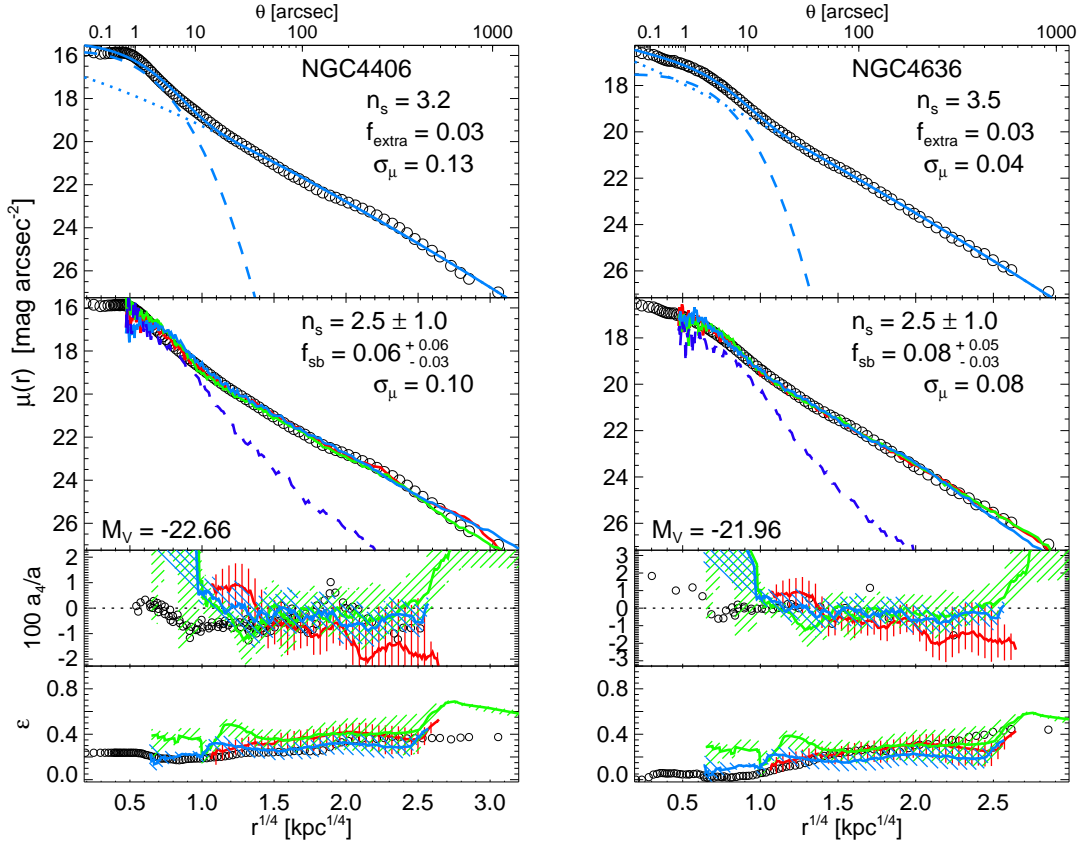
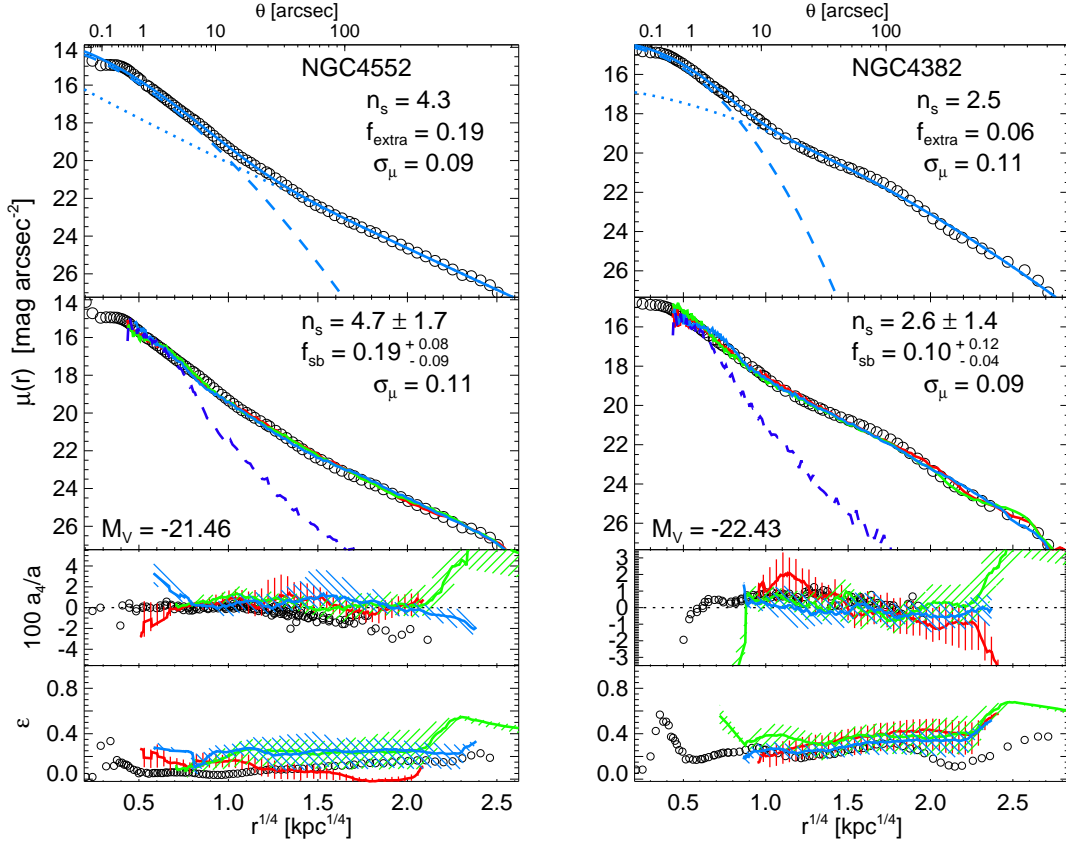
## 6.2. Independent Evidence for the Surviving Dissipational Component

Figure 18 compares our estimates of the dissipational mass fraction in the observed ellipticals: the directly fitted extra light fraction  $f_{extra}$  and inferred starburst mass fraction  $f_{sb}$  from the best-fitting simulations. For clarity we restrict to a sample where the range in  $f_{extra}$  from different sources of photometry is less than  $\sim 20\%$  (we find the same results for the entire sample, but with correspondingly larger scatter). We compare with the same quantities fit to cusp ellipticals and observed gas-rich merger remnants in Paper II and Paper I, respectively. Our fitted decomposed extra light fraction re-

liably traces the inferred starburst mass fraction, with a factor  $\sim 2$  scatter similar to that predicted from our simulations (Figure 4). This is true even for profiles without an obvious “break” or feature indicative of a transition to extra light. The starburst fraction  $f_{sb}$  itself must, in some sense, reflect the cold gas mass available in the disks just before the original gas-rich merger (and we show in Paper I that this is the case) – in this physical sense (insofar as our simulations are reasonable qualitative proxies for observed profiles), our fitted  $f_{extra}$  and inferred  $f_{sb}$  are a robust reflection of the dissipational content of the progenitors.

We can independently test these decompositions with other observations of stellar populations, shown in Figure 18. Given sufficiently detailed observations and stellar population models, observers have estimated the mass fraction which formed in a more recent, central starburst (as opposed to the more extended quiescent star formation history) – completely independent of our analysis here – for several of the observed systems (Schweizer 1996; Titus et al. 1997; Schweizer & Seitzer 1998, 2007; Reichardt et al. 2001; Michard 2006). Unfortunately, the observational expense required leaves us with samples of relatively limited size (there are only a few objects with sufficiently deep stellar population data to allow this comparison). Nevertheless, comparing our estimated  $f_{extra}$  or  $f_{sb}$  with these estimates for the mass fraction in the secondary

FIG. 11.— The next most massive core ellipticals ( $\sim 5-6M_*$ ).FIG. 12.— Similar massive core ellipticals ( $\sim 4-5M_*$ ).

FIG. 13.— The next most massive core ellipticals ( $\sim 2-3M_*$ ).FIG. 14.— The least massive core ellipticals in the Kormendy et al. (2008) Virgo sample ( $\sim 1-2M_*$ ).

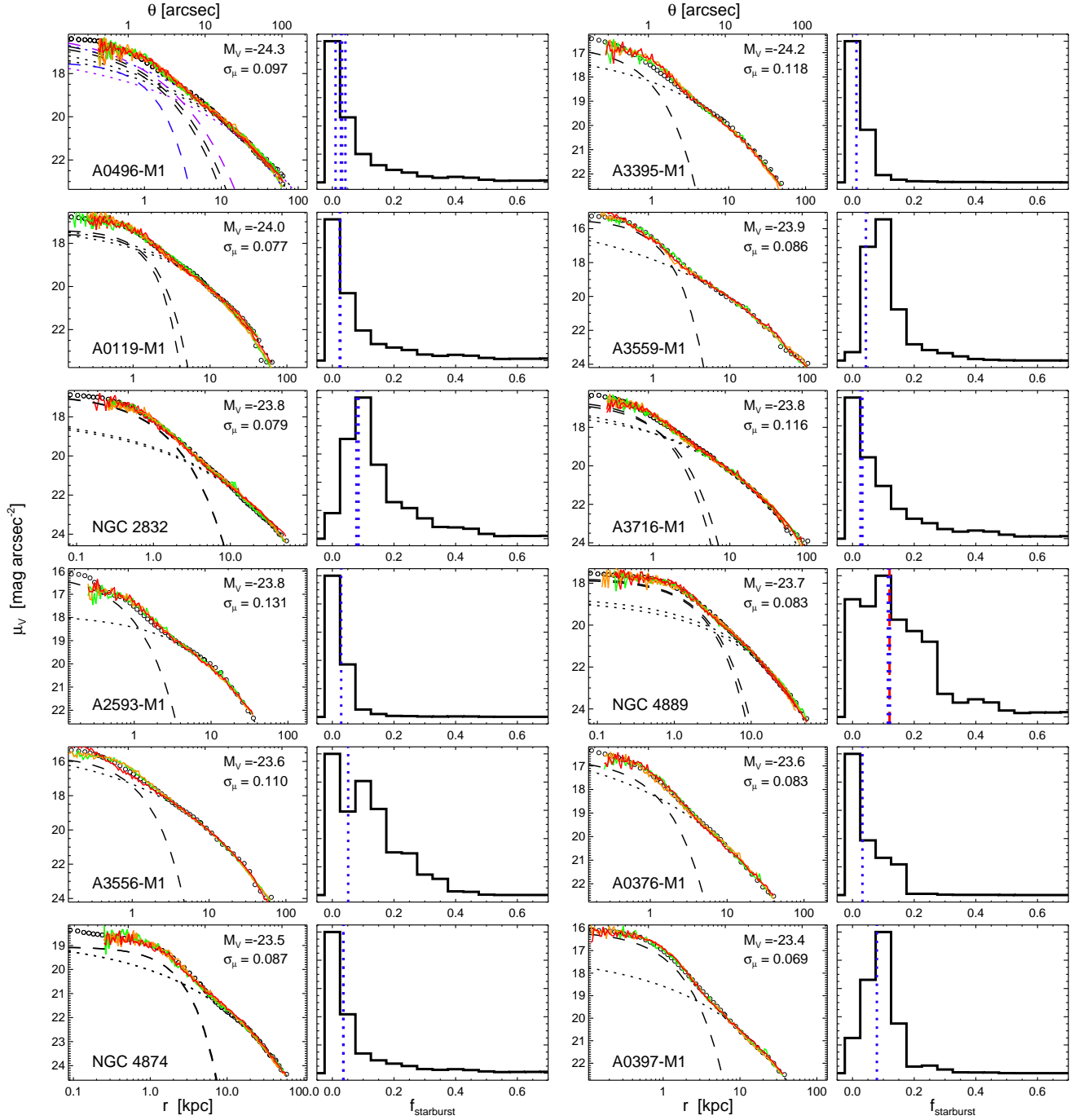


FIG. 15.— Observed surface brightness profiles of a subset of the confirmed core ellipticals from the sample of Lauer et al. (2007a), with the best-matching two component parameterized fit (dashed and dotted lines) and best-fitting simulations (red, orange, and green lines), as in Figure 10. Where multiple sources of photometry are available, independent fits to each are shown. The objects are ranked from brightest to faintest in  $V$ -band (as shown): these are among the brightest galaxies in the sample; Figures 16–17 continue to fainter luminosities. Profiles are shown over a constant angular scale (top axis; bottom axis shows physical radius in kpc). The corresponding (*right*) panel for each shows the distribution of physical starburst fractions for the simulations which provide a good fit to the observed profile (as described in the text), with the fitted (parameterized) extra light fraction (blue dotted line; one for each source of photometry) and observed secondary (recent) starburst components (red dashed, where available). Note that our simulation resolution limits do not extend within the central  $\sim 30\text{--}50\text{pc}$ , and our fits are not intended to describe these radii.

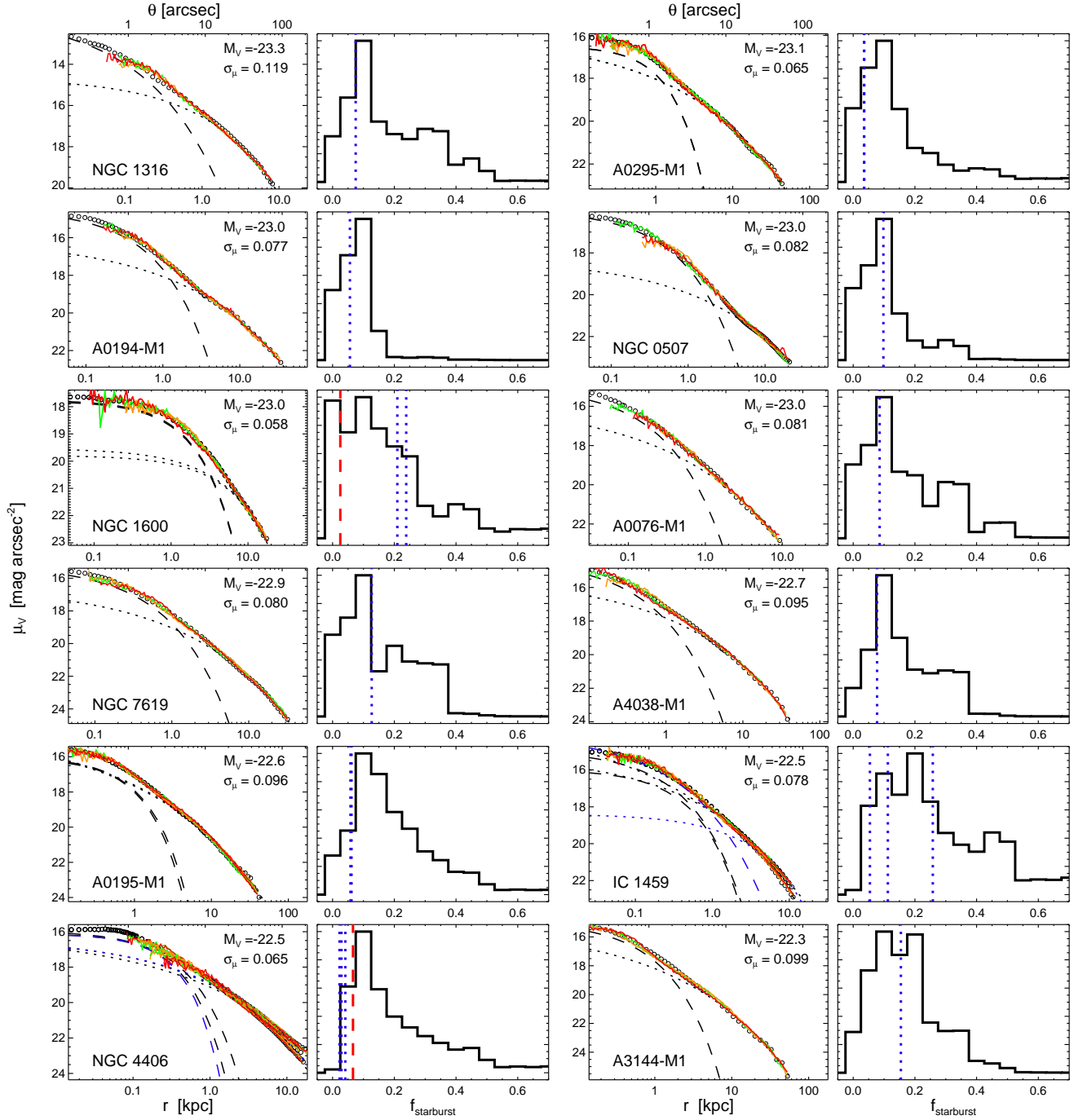


FIG. 16.— Figure 15, continued.

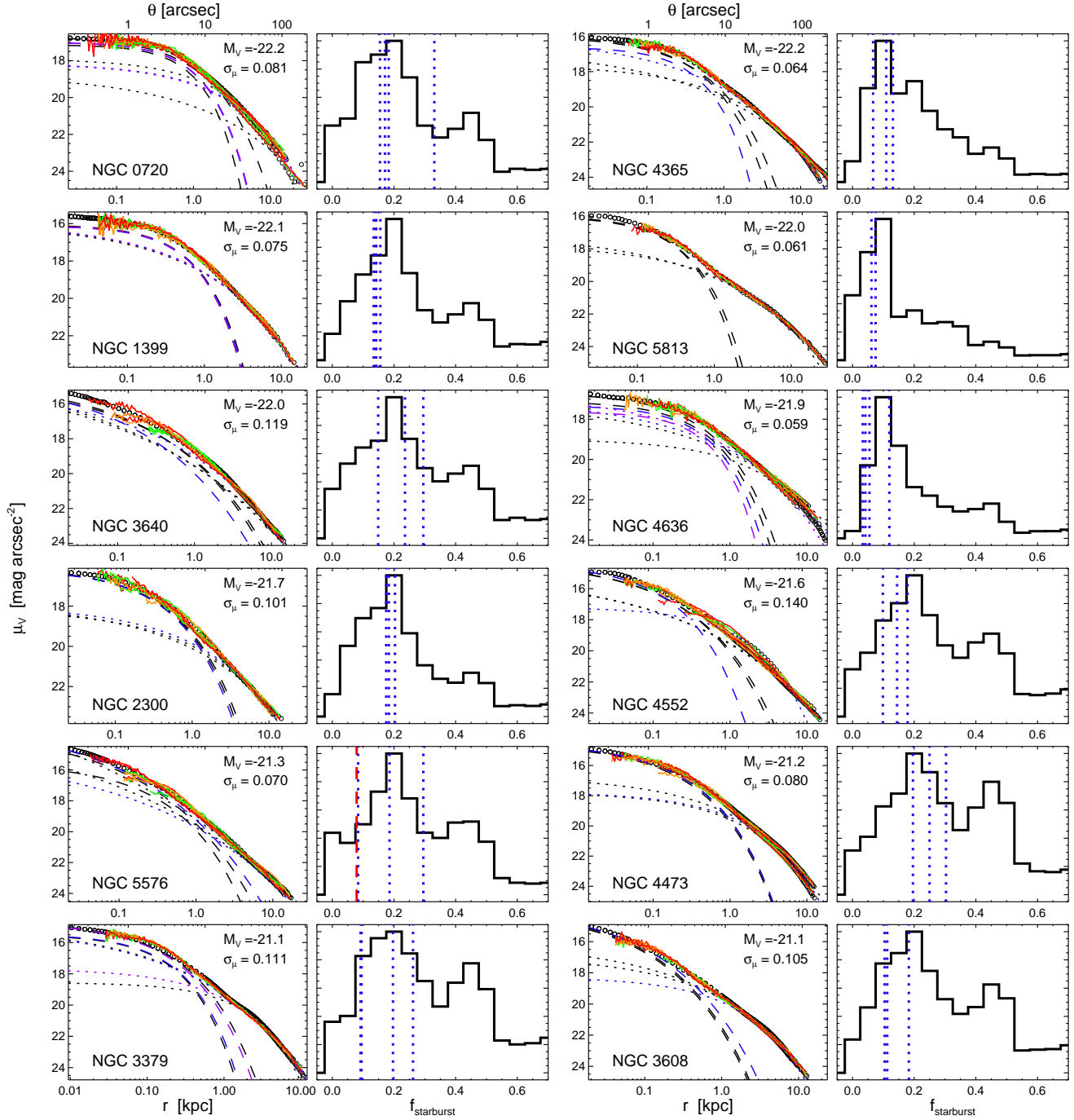


FIG. 17.— Figure 15, continued.

(newly formed/starburst) stellar populations, we find reasonable agreement. They all suggest that our fitted extra light component is indeed a good proxy for the mass fraction which was involved in the central, merger-driven starburst. We find similar good agreement in these cases for both our core ellipticals here and the cusp ellipticals considered in Paper II, and the merger remnants considered in Paper I, together constituting a sample of  $\sim 25$  objects.

Other independent lines of support further suggest that the decomposition is recovering a real physical difference in the populations. In Figures 10-14, there is often a change in isophotal shape and kinematics at the radii we associate with the dissipational remnant – systems become slightly diskier,

despite the fact that re-mergers will smooth the isophotal shapes and destroy strong transitions in features such as the kinematics that might be present in cusp ellipticals at the extra light-outer light transition. We show in § 8 that the distribution of global kinematic properties and isophotal shapes independently requires re-mergers with a relatively narrow range in starburst mass fractions, in agreement with our estimates from fitting the surface brightness profiles.

Moreover, we show in Paper I that the extra light is associated with, and indeed drives, stellar population gradients in the remnant elliptical. In particular, we argue that metallicity gradients are most robust (age gradients are very weak once the system is old, and gradients in  $\alpha$ -enhancement are much



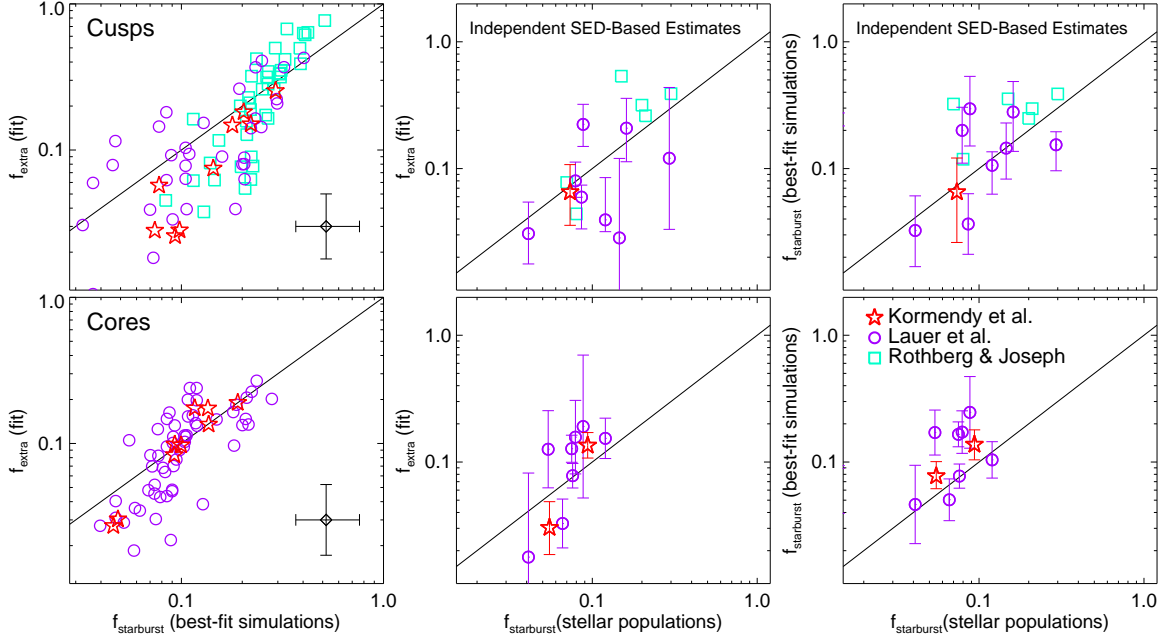


FIG. 18.— *Left*: Comparison of our estimated mass in the fitted extra light component ( $f_{\text{extra}}$ ) versus the starburst mass fraction in the best-fitting simulations ( $f_{\text{sb}}$ ; as in Figures 10-15). We show the results from the core elliptical sample studied here (*bottom*; red stars are systems from Kormendy et al. (2008), violet circles from Lauer et al. (2007a)) the observed gas-rich merger remnant and cusp elliptical samples in Paper I and Paper II (*top*; cyan squares are the merger remnants from Rothberg & Joseph (2004)). The two estimates agree well, with a factor  $\sim 2-3$  scatter in  $f_{\text{extra}}(f_{\text{sb}})$  (similar to what we expect from our simulations; see Figure 4). Open point with error bars shows the typical range in  $f_{\text{extra}}$  and  $f_{\text{sb}}$  across different sources of photometry and in different wave bands. *Center*: Fitted  $f_{\text{extra}}$  versus independent observational estimates of the mass fraction formed in a more recent starburst/star formation event, from two-component stellar population model fits to the observed SEDs (Schweizer 1996; Titus et al. 1997; Schweizer & Seitzer 1998, 2007; Reichardt et al. 2001; Michard 2006). *Right*: Same, but comparing the stellar population estimates to  $f_{\text{sb}}$  from the best-fitting simulations. More observations are needed to test our estimates, but the stellar population data independently suggest that our decompositions are reasonable.

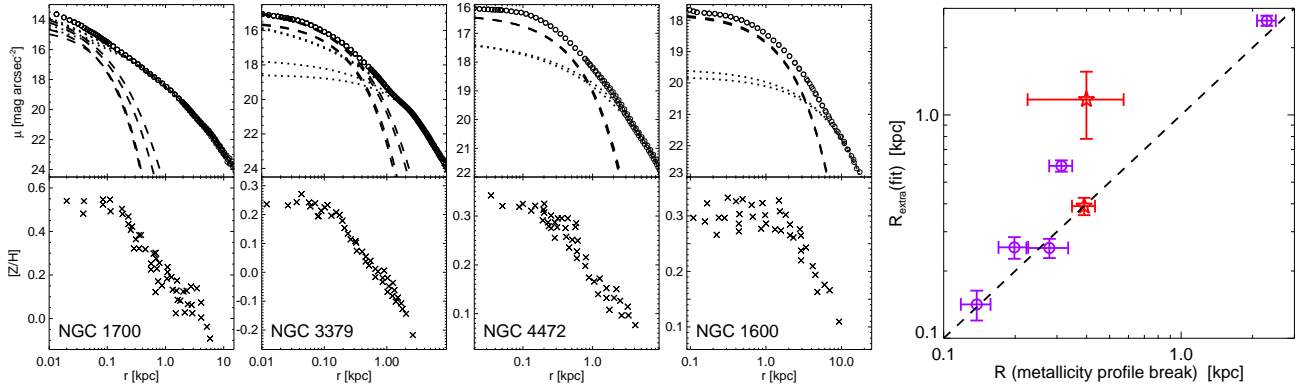


FIG. 19.— Independent tests of our two-component decompositions with observed stellar population gradients in core ellipticals. *Left*: Comparison of the surface brightness profile (*top*; points) and two-component decomposition (dashed and dotted lines show the fitted inner & outer components for each source of photometry, as Figure 15) with the observed metallicity profile (*bottom*; as discussed in text this is the most robust indicator of extra light) for the cases observed in Sánchez-Blázquez et al. (2007). The comparison agrees with our predictions in Paper II and § 5: the metallicity gradients are strong at the radii of the transition from the outer (dissipationless) stellar populations to the inner (dissipational, metal-enriched) population, and begin to flatten within the radius of the inner component (since it is a similar population). In each of these cases, we see a supporting (albeit weaker and more sensitive to age effects, see Paper II) trend towards younger stellar populations at the same radii. *Right*: Summary of these comparisons: radius interior to which the fitted inner component dominates the light profile in observed systems (points as Figure 18), versus the radius where the metallicity profile flattens below a power-law inwards extrapolation larger radii (fitting the profiles to an outer power law with an inner break to weakly changing  $[Z/H]$ ). Metallicity profiles are from Sánchez-Blázquez et al. (2007) and McDermid et al. (2006). The stellar population gradients independently support our two-component decompositions, showing a more metal-rich, younger stellar population in the center, with a characteristic radius that closely tracks our fitted radii for the extra light. More observations are needed, but with Figure 18 this lends confidence to our two-component decompositions in core ellipticals.

more sensitive to initial conditions and the exact details of e.g. the starburst timing relative to the timescale for star formation in progenitor disks). We show in § 5 that these are expected to survive re-mergers relatively intact, and therefore should provide independent indicators of the dissipational versus dissipationless decomposition.

There are a small number of systems in our observed core sample for which detailed stellar population gradients have been measured in Sánchez-Blázquez et al. (2007) or two-dimensional stellar population maps have been constructed in McDermid et al. (2006). In almost every case, we see what is predicted: a strong rise in metallicity around the radii where our fits infer the transition between the dissipational and dissipationless components, with the metallicity gradient flattening within the radius where the extra light dominates the profile. Figure 19 shows a few illustrative examples, comparing the observed metallicity gradients to our two-component surface brightness decompositions. If we attempt to quantify where the metallicity profile flattens (expected inside the radius where the extra light dominates, since the predicted gradient is largely driven by the transition from an outer, less metal-rich population into the more metal-rich dissipational population) by fitting it to an external power law with a break at some radius  $R_b$ , and compare this radius  $R_b$  to the radius at which the fitted inner/starburst component dominates the profile (the outer radius where the fitted inner component surface brightness becomes larger than that of the outer component, or similarly the effective radius of the extra light component), we find a remarkably good correlation. In every case, the age gradients (while weak and less uniform, as predicted) also confirm that the central component we identify is younger than the outer profile, as predicted (the difference is usually small,  $\sim 1$  Gyr, as expected in merger models with relatively early formation – if the central components were instead formed by e.g. dissipation of gas from stellar mass loss (Ciotti & Ostriker 2007), we might expect the central components to be much younger). More data are needed to test these decompositions and predictions over the entire dynamic range of interest, but our preliminary comparisons all lend some confidence that we are, in an average sense at least, recovering the appropriate physical separation between inner radii dominated by the remnants of extra light systems originally formed in dissipational starbursts and outer light profiles formed by violent relaxation acting on older, initially low-phase space density (disk) stars.

## 7. PROPERTIES AND SCALING LAWS OF DISSIPATIONAL COMPONENTS

### 7.1. Amount of Dissipation Versus Mass

The preceding analysis indicates that re-mergers do indeed have a “dissipational” component (the surviving remnant of the original starburst that formed the progenitors’ extra light), and that its mass can be estimated from their surface brightness profiles. Now, we examine how this scales with other properties, specifically in reference to how the extra light<sup>13</sup> content was seen to scale with galaxy properties in cusp ellipticals in Paper II.

Figure 20 plots the inferred starburst mass fraction  $f_{\text{sb}}$  for the observed systems as a function of stellar mass. In the same

manner that we have defined a best-fit  $f_{\text{sb}}$  from the best-fit simulations, we can also define a best-fit “initial” gas fraction (roughly the gas fraction  $\sim 1$  Gyr before the final merger), and show this as well. We emphasize though that this is a much less robust quantity (for example, if we place the systems on a longer period orbit with the same initial gas fraction, then by the time they merge, more gas will have been consumed in the disks and the results will look like a shorter period orbit, lower “initial” gas fraction simulation). In either case there is a clear trend of increasing dissipation (increasing fractional mass required in a dissipational starburst component) at lower masses. We compare this with the behavior found for observed cusp ellipticals in Paper II. The significance of the correlation is unambiguous ( $> 8\sigma$ , in each of the cusp and core samples). The two trends are statistically indistinguishable: fitting them as a function of stellar mass with the form

$$\langle f_{\text{starburst}} \rangle \approx \left[ 1 + \left( \frac{M_*}{M_0} \right)^\alpha \right]^{-1}, \quad (3)$$

we obtain  $(M_0, \alpha) = (10^{9.2 \pm 0.2} M_\odot, 0.43 \pm 0.04)$  for the cusp sample and  $(10^{8.8 \pm 0.3} M_\odot, 0.35 \pm 0.04)$  for the core sample, with roughly a constant factor  $\sim 2$  intrinsic scatter at each mass in both cases. It is worth noting that if identical systems begin on the cusp correlation and re-merge, they will conserve  $f_{\text{starburst}}$  but double  $M_*$ . To the extent that there is not a large offset between the two correlations, then, this suggests that at least the typical core ellipticals have not undergone a large number of re-mergers. A single dry re-merger, especially if it is of a more typical  $\sim 1:3$  mass ratio, is however consistent with what we see, within the scatter.

In Paper II we noted that the inferred gas fractions correspond well to observed disk galaxy gas fractions as a function of mass, from  $z = 0 - 2$ . We show these observations as well, and note that they are sufficient to explain the trend and scatter in the extra light fractions of both cusp and core ellipticals. In other words, the distribution in progenitor gas fractions implied by the elliptical surface brightness profiles is, as a function of mass, exactly what would be predicted if one assumes that the original progenitors were spirals, and that most of the systems were first formed by a major merger somewhere between a redshift of  $z \sim 0 - 3$ . In fact, this is exactly what is inferred for the formation times of the ellipticals in our sample and those of similar mass ( $\lesssim$  a few  $L_*$ ) from both observations of the early-type or red galaxy mass functions (Bundy et al. 2006; Borch et al. 2006; Fontana et al. 2006; Hopkins et al. 2006b, 2007a, 2008c), from direct stellar population synthesis studies (Trager et al. 2000; Thomas et al. 2005; Gallazzi et al. 2005), and by association of elliptical galaxy formation with the triggering of quasar activity (e.g. Hopkins et al. 2006a, 2007b, 2008e).

There may be an interesting suggestion that the extremely massive, BCG tail of the core population (for which the various caveats described in § 4 apply) might asymptote to  $\sim$  constant values of  $f_{\text{sb}} \sim 0.05 - 0.1$  at  $M_* \gtrsim 10^{12} M_*$ . This would be expected if these systems all “began” at lower masses (where this gas fraction is typical of disks) and moved up by a large number of dry re-mergers. Unfortunately, the data here are limited, but we stress that these systems do not significantly alter our comparison, and are not the systems we intend our modeling (applicable to those core ellipticals with a moderate re-merger history) to describe.

The inference of  $f_{\text{sb}}$  requires some comparison with our simulations, but  $f_{\text{extra}}$  is a purely empirical quantity. We there-

<sup>13</sup> In what follows, we use the phrase “extra light” for the core ellipticals in the physically pertinent sense, to refer to the component that traces or reflects the original starburst mass, i.e. the centrally concentrated contribution to the light profile that is the remnant of the original gas-rich merger remnant extra light.

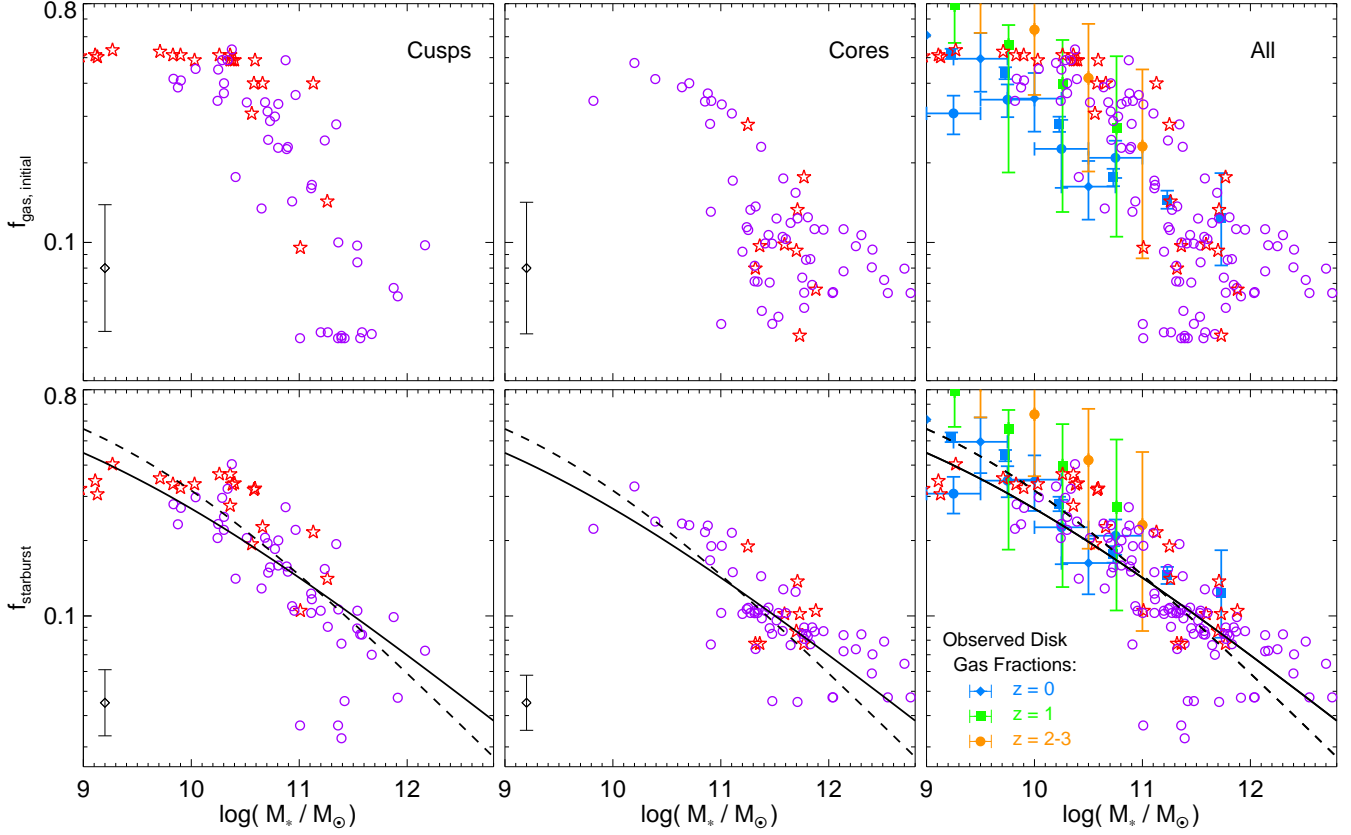


FIG. 20.— Inferred gas content (dissipational/starburst fraction) of elliptical-producing mergers as a function of stellar mass. Initial gas fraction (*top*) and physical final starburst mass fraction (*bottom*) corresponding to the best-fit simulations to each observed system in the samples of Lauer et al. (2007a) (circles) and Kormendy et al. (2008) (stars) are shown, with the typical 25–75% allowed range (error bar). We show results separately for cusp ellipticals (*left*), core ellipticals (*center*), and both together (*right*). Dashed (solid) line shows the fit to the data (Equation 3) in cusp (core) ellipticals. Colored points with error bars indicate the mean (and  $\pm 1\sigma$  range in) disk gas fractions at the same stellar mass, at  $z = 0$  (Bell & de Jong 2001; Kannappan 2004; McGaugh 2005, blue diamonds, squares, and circles, respectively),  $z = 1$  (Shapley et al. 2005, green squares), and  $z = 2$  (Erb et al. 2006, orange circles). There is a clear trend of increasing dissipation required to explain elliptical profiles at lower masses (significant at  $> 8\sigma$  in either core or cusp subsamples separately), in good agreement with the observed trend in progenitor disk gas fractions over the redshift range where cusp ellipticals are formed, and with what is invoked to explain the observed densities and fundamental plane correlations of ellipticals (e.g. Kormendy 1989; Hernquist et al. 1993). The best-fit trends in cusp and core populations are statistically identical: i.e. the dissipational/extra light component is preserved in re-mergers.

fore repeat this exercise with the empirically fitted extra light component  $f_{\text{extra}}$ , and show the results in Figure 21. The trend seen in  $f_{\text{extra}}(M_*)$  is completely consistent with that in  $f_{\text{sb}}$ , but with a scatter larger by a factor  $\sim 2$  (exactly what we expect, based on the predicted and observed scatter in  $f_{\text{extra}}(f_{\text{sb}})$ ). Moreover the trend we find in the core ellipticals is consistent with that in the cusp elliptical sample from Paper II. Considering just the data in Figure 21, even given its increased scatter, the trend of decreasing extra light fraction with mass is significant at  $> 6\sigma$  ( $> 8\sigma$ , if we include both the cusp and core ellipticals). We have experimented with alternative, non-parametric (albeit less accurate) estimators based on e.g. the concentration indices or stellar populations of our simulations and observed systems, and obtain a similar answer. In short, even without reference to our simulations, however we derive an estimate of the dissipational component, it is difficult to escape the conclusion that it is more prominent in lower-mass ellipticals, even in core ellipticals that may have experienced re-mergers. The mass range covered by the two samples is somewhat different, but where there is overlap they are similar, and at the extremes the two populations appear to be continuous extensions of the same trends.

### 7.2. Sizes of the Extra Light/Dissipational Region

The inferred dissipational components in simulations, cusp ellipticals, and core ellipticals also appear to follow a similar size-mass relation (especially if we restrict to systems with similar  $f_{\text{sb}}$ ), shown in Figure 22. In Paper I we show that the size-mass relation is driven by the condition that the gas collapsing into the central regions in the final starburst becomes self-gravitating:  $(GM_{\text{extra}}/R_{\text{extra}}) \sim (GM_*/R_e)$ . In Figure 22 we show that the observed core ellipticals also follow this constraint, with small scatter and dynamic range similar to that in our simulated mergers. This is expected even if these systems have experienced substantial re-merging, provided that re-mergers puff up the system uniformly.

To test, this, Figure 23 plots the distribution in the ratio of the effective velocity dispersion/self-gravity of the inner component to that of the outer component, for the cusp and core elliptical samples. Interestingly, there is small offset, in the sense that the effective dispersions of the core ellipticals are slightly higher than those of cusp ellipticals. This is true even if we restrict the analysis to a narrow mass bin – i.e. the extra light in core ellipticals is (on average) slightly more concentrated relative to the outer light component, compared to cusp ellipticals.

It is unlikely that this is caused by scouring or whatever process might directly give rise to the core on  $\lesssim 50\text{pc}$  scales, since the effect is seen even in the high-mass objects where the

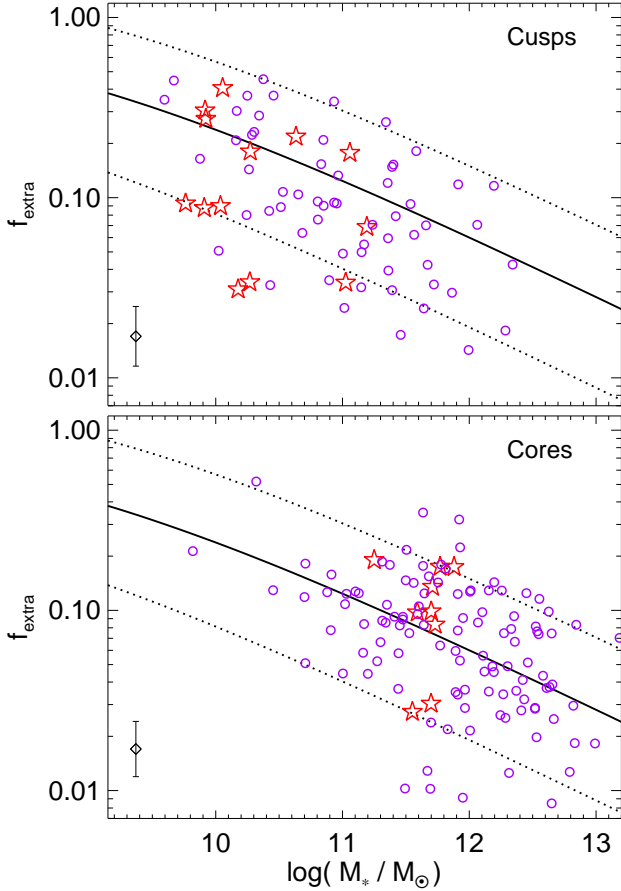


FIG. 21.— As Figure 20, but showing our empirically fitted  $f_{\text{extra}}$  as a function of stellar mass. The trend of increasing dissipation at lower masses is still clear and is consistent with that in Figure 20, but with an expected extra factor  $\sim 2-3$  scatter from the scatter in our purely empirical estimator. Solid line shows the best-fit from Figure 20, dotted lines show the  $\pm 1\sigma$  scatter expected based on the scatter in  $f_{\text{extra}}(f_{\text{sb}})$  (see Figure 18). Fitting to just these data yield trends statistically consistent with the solid line, ruling out no dependence of dissipation on mass at  $> 8\sigma$  confidence.

effective radius of the extra light component is  $\gtrsim 1$  kpc. However, it is well established in numerical simulations that, when merging collisionless systems, angular momentum and orbital energy are preferentially transferred to less bound material, expanding their orbits while allowing the central regions to remain tightly bound (see, e.g. Hernquist 1992, 1993). In practice, most of this less bound material is part of the outer halo – so the gradient in terms of energy input and expansion of material across the baryonic galaxy is weak (i.e. the profiles are stretched by a roughly constant factor in Figure 1). Nevertheless, a small effect of this nature would be expected in collisionless re-mergers. The observed offset is in fact weak, a factor  $\sim 1.5$  in  $R_{\text{extra}}/R_{\text{outer}}$  (in the most extreme case of a single major re-merger where the inner profile was not affected by the merger and the outer profile doubled in radius, we would expect a factor of two offset), and more data would be needed to demonstrate that it is robust. However, if real, it provides further support to the idea that these have re-merged, but not destroyed their extra light content.

### 7.3. Dissipation and the Sizes of Ellipticals

We demonstrated in Paper II that the effective radii of cusp ellipticals scales with their extra light content – systems with more dissipation are smaller, since more of the light comes

from the compact starburst remnant. Figure 24 extends this to the core ellipticals. Specifically, we determine  $\langle R_e(M_*) \rangle$  from the sample of Shen et al. (2003), and take the ratio of the half mass radius of each system (determined directly from the light profile, or from the fits, it does not change the comparison) to that value. Our mass bins are small enough, however, that this makes little difference compared to just e.g. considering  $R_e$  in a given bin. Again, we see a similar behavior in the cusp and core ellipticals: at a given stellar mass, systems with larger extra light have systematically smaller  $R_e$  (they also have slightly larger velocity dispersion  $\sigma$ , although the scatter is larger there in both simulations and observations). We showed that this could be predicted analytically, following Covington et al. (2008) given the impulse approximation to estimate the energy loss in the gaseous component, followed by collapse in a self-gravitating starburst. For typical conditions, this reduces to the simple approximation

$$R_e \approx \frac{R_e(f_{\text{sb}}=0)}{1 + (f_{\text{sb}}/f_0)}, \quad (4)$$

where  $f_0 \approx 0.25-0.30$  and  $R_e(f_{\text{sb}}=0)$  is the radius expected for a gas-free remnant. In each case, the simulations and observed systems occupy a similar locus to that predicted in this simple dissipational model. We can also construct this plot with the starburst mass fraction  $f_{\text{sb}}$  of the best-fitting simulation as the independent variable, and find an even tighter correlation of the same nature. Core elliptical sizes depend on the relative strength of dissipation (evident in their profile shapes) in the same manner as in cusp ellipticals.

This is expected: even if the systems with cores have expanded via re-mergers, they should (so long as there is not a wide range in number of re-mergers or systematic dependence of the number of re-mergers on starburst fraction at fixed mass) grow uniformly, and preserve these trends. We might expect some normalization offset: if the mean size-mass relation after a gas-rich merger is a power law  $R_e \propto M_*^\alpha$ , and two such systems with mass ratio  $f$  (where  $f$  is the mass ratio of the secondary to the primary) have a parabolic dry merger (and preserve profile shape), then the remnant will increase in radius by a factor  $(1+f)^2/(1+f^{2-\alpha})$  relative to the primary. However, it has also increased in mass, so compared to ellipticals of the same (final) mass, its relative increase in size is only  $(1+f)^{2-\alpha}/(1+f^{2-\alpha})$ . For observationally suggested values  $\alpha = 0.56$  (Shen et al. 2003), this yields only a 30% ( $\sim 0.1$  dex) relative size increase for mass ratios of 1:3 through 1:1. This is easily dwarfed by the effects of dissipation seen in Figure 24, which can change the sizes of systems by nearly an order of magnitude. That there is not a substantial normalization offset between the trends for cusp and core ellipticals in Figure 24 therefore suggests that the number of major re-mergers for typical core ellipticals has been relatively moderate, but it is not a strong constraint. Our simulations and the observations plotted suggest that the dominant factor regulating the size of an elliptical is the amount of dissipation, even for systems which have undergone re-mergers.

## 8. DISSIPATION AND RE-MERGER KINEMATICS/SHAPES

In Paper II we showed that the existence and mass fraction in a dissipational component is related to the kinematics and shapes of cusp ellipticals. In particular, we confirmed what has been recognized in a growing number of simulations (see e.g. Naab et al. 2006a; Cox et al. 2006b; Jesseit et al. 2007; Burkert et al. 2008), that disk-disk mergers without signif-

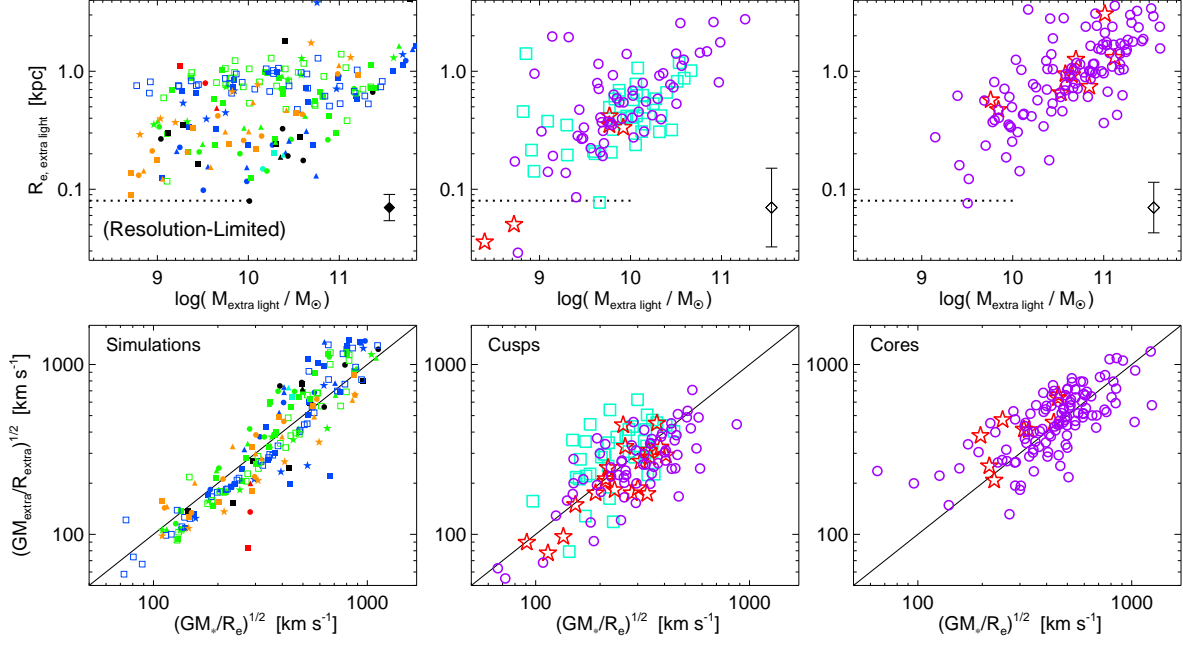


FIG. 22.— *Top*: Effective radius of the extra light component (*not* equivalent to the radius where it breaks from the outer Sersic fit) as a function of extra light mass (points as in Figure 18). Simulations (*left*) and observed cusp (*middle*) and core (*right*) ellipticals are similar, especially if we restrict to simulations with initial gas fractions  $\sim 0.2$ – $0.4$ . Resolution limits (see Paper II) prevent us from simulating systems with  $R_{\text{extra}} \ll 100$  pc, but this is only important for the few very lowest-mass ellipticals ( $L \lesssim 0.01 L_*$ ). Filled diamond is typical sightline-to-sightline variance in the simulations, open diamond the source-to-source (or band-to-band) scatter in observed profile fits. *Bottom*: Effective velocity dispersion of the extra light component vs. that for the whole galaxy. Solid line shows  $(GM_{\text{extra}}/R_{\text{extra}}) = (GM_*/R_e)$  – the extra light collapses to the point where it is self-gravitating. The observed systems follow a trend which agrees well with the simulations.

icant dissipational components (whether this component is created in the merger, as a gas-rich merger, or “inherited” from the progenitor disk bulges – which formed it dissipationally in some earlier encounter/dissipational event) do not resemble any observed spheroids: they are slowly rotating and boxy, but highly elliptical. However, systems with the appropriate dissipational content for their stellar mass (as in e.g. Figure 20) agree well with observed distributions in cusp ellipticals in all of these properties (and the same is true for more sophisticated kinematic and shape measures, including their orbital isotropy, rotation, triaxiality, kinematic misalignments, and higher-order velocity moments  $h_3$  and  $h_4$ ; Cox et al. 2006b; Jesseit et al. 2007). This is related to two aspects of the gas content in the mergers. First, the dissipational stellar component itself, by creating a dense central stellar mass concentration, acts for stars at  $R_e$  almost as a central point mass with large stellar mass fraction  $\sim 10$ – $20\%$  – directly making the galaxy potential more spherical (less elliptical) and reducing the portion of phase space available to box orbits (Barnes & Hernquist 1991, 1996). Second, if more gas is available to form the starburst, more is likely to survive the merger. This gas will quickly re-form a disk (albeit often a very small, nuclear disk with relatively small mass fractions of order a couple percent, more often designated a nuclear subcomponent, if it can be recognized in observations), giving rise to more rapid rotation and diskier isophotal shapes.

Given the connection between the dissipational component and the shapes/kinematics of the disk-disk merger remnant, it is worth examining how this compares after dissipationless spheroid-spheroid re-mergers (and how this scales with the original starburst/dissipational mass fraction). Figure 25 shows this comparison for representative simulations with different gas fractions. We consider the rotation  $(V/\sigma)$ , where  $V$  is the maximum rotational velocity from the projected stel-

lar rotation curve and  $\sigma$  the central dispersion), ellipticity  $\epsilon$ , and isophotal shape (boxy/diskiness, quantified as  $a_4/a$  in standard fashion) for a 1:1 identical disk-disk merger and spheroid-spheroid re-merger of that remnant<sup>14</sup>.

In the case where the initial disk-disk merger is gas-poor ( $f_{\text{starburst}} \approx 0.01$ ), we recover the results in the papers described above: gas-poor disk-disk mergers yield remnants that are slow rotators with large ellipticity, without a correlation between  $\epsilon$  and  $a_4$ , and extending to very boxy isophotal shapes, in stark disagreement with the properties of *either* cusp or core ellipticals (given similar resolution and seeing). This is relatively unchanged in re-mergers, and remains so regardless of the number of “generations” of re-mergers (we have experimented with series of several such re-mergers): without dissipation to build a central mass concentration (increase the central phase-space density), dissipationless processes cannot produce such a central density as required to make the potential sufficiently round and eliminate most of the phase space available to the most extreme boxy/triaxial or-

<sup>14</sup> Specifically we show the rotation  $(V/\sigma)$  or  $(V/\sigma)^*$  measured within  $R_e$ , and boxy/diskiness  $100a_4/a$ , and ellipticity  $\epsilon$  measured for the half-mass projected ( $R_e$ ) isophotal contour, for each of  $\sim 100$  lines-of-sight to the remnant uniformly sampling the unit sphere (i.e. representing the distribution across random viewing angles). The details of the fitting for our simulations are described in Cox et al. (2006b), and for the observations in Bender et al. (1987); Bender (1988); Bender et al. (1992); Faber et al. (1989); Simien & Prugniel (1997a, 2002). We define rotation in the standard manner, relative to that of an oblate isotropic rotator, with the parameter  $(V/\sigma)^*$ , defined using the maximum circular velocity  $V_c$ , velocity dispersion within  $R_e$ , and ellipticity as (Kormendy 1982)

$$(V/\sigma)^* = (V/\sigma) / \sqrt{\epsilon/(1-\epsilon)}. \quad (5)$$

We exclude the coplanar merger simulations from our comparisons here: those simulations are idealized perfectly coplanar prograde orbits, and as such produce pathological orbit and phase structure (we do, however, include some more representative orbits below that are not far from coplanar).



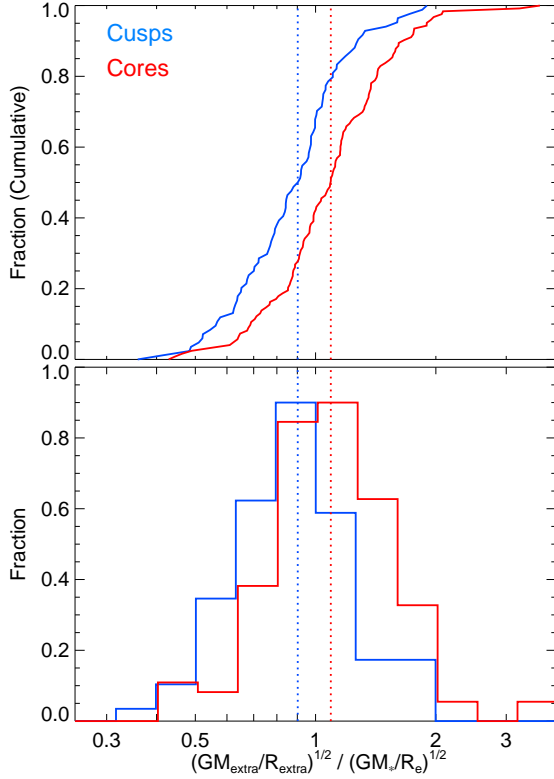


FIG. 23.— Cumulative (*top*) and differential (*bottom*) distribution of the ratio of effective velocity dispersion of the inner light component to that of the outer light component ( $(GM_{\text{extra}}/R_{\text{extra}})^{1/2}/(GM_*/R_e)^{1/2}$ ), for cusp ellipticals (blue) and core ellipticals (red). Dotted line shows the median for each. Typical values are similar, but slightly higher for core ellipticals (the difference in mean/median is significant at  $> 3\sigma$ ), suggesting that the inner component is relatively less puffed up by re-mergers than the outer component.

bital configurations (which are not observed in real systems). Regardless of re-merging, initially gas-free disk-disk mergers cannot ultimately reproduce the kinematics and shapes of core ellipticals.

If instead the initial disk-disk merger is reasonably gas-rich ( $f_{\text{starburst}} \sim 0.1$ ), in the range that we have inferred from fitting observed surface brightness profiles of  $\sim 1-5L_*$  ellipticals (and in agreement with the observed gas fractions of disks in the relevant mass and redshift range), then the remnants are more round (owing to dissipation building a central mass concentration), with kinematic subcomponents that give rise to the rotation and disky isophotes in good agreement with the observed cusp population (see e.g. Krajnović et al. 2008, who show such subcomponents are ubiquitous in cusp ellipticals and drive much of this rotation). Re-mergers of these remnants destroy these kinematic subsystems (they are small disks/subsystems, and as such are violently relaxed in re-mergers), but retain the central mass concentrations (as we have argued they must), and this leads to the formation of sufficiently round, but boxy and slowly-rotating systems with the  $\epsilon - a_4$  correlations appropriate for core ellipticals (compare the observations in e.g. Bender 1988; Bender et al. 1992; Emsellem et al. 2004, 2007). The re-merger remnants of cusp ellipticals with the starburst mass fractions we have independently inferred from profile fitting appear to agree well with observed core elliptical kinematics and isophotal shapes.

If the initial disk-disk merger is *too* gas-rich ( $f_{\text{starburst}} \sim 0.4-0.6$ ), larger than that inferred for any of the observed core

ellipticals in our sample, this presents an interesting case as well. These extremely gas-rich situations may apply to some of the most low-mass cusp ellipticals, but are clearly more gas-rich than expected at the masses of typical core ellipticals (and disk progenitors), even at high redshifts (Erb et al. 2006). In these cases, we find that the initial disk-disk merger remnant is even more round, rapidly rotating, and disky. However, with such a large dissipational component, the kinematic subsystems are often quite massive – in many cases they are more appropriately described as large surviving disks (see e.g. Hopkins et al. 2009). As a consequence, it becomes difficult to simply disrupt them in re-mergers. Moreover, conservation of the specific angular momentum in such large components makes it very difficult to achieve a slow rotator even if the subsystem is disrupted (as opposed to the case above, where the relevant subcomponents represent a small fraction of the galaxy mass); this has been seen when e.g. mock ellipticals with uniform rotation (as opposed to more realistic rotation associated with kinematic subcomponents) are re-merged (Naab et al. 2006b; Burkert et al. 2008; Jesseit et al. 2008; Cox et al. 2009). As a consequence, the re-merger remnant looks like an oblate isotropic rapid rotator, not a slow rotator, and exhibits correlations between e.g. diskiness and ellipticity (and higher-order kinematic moments) that do not resemble either the cusp or core population.

Some of the observed differences between cusp and core distributions owe to the fact that core ellipticals (because they predominate at high masses) tend towards lower  $f_{\text{sb}}$  and cusp ellipticals (dominant at low masses) towards higher  $f_{\text{sb}}$ . However, at the same mass, the two populations evidence similar  $f_{\text{sb}}$  (Figure 20), but show differences in their kinematics. Figure 25 demonstrates that at fixed  $f_{\text{sb}}$  the kinematics also depend significantly – and in a different manner – on merger history. As a consequence, the well-established observational differences between these populations (e.g. Bender et al. 1989; Faber et al. 1997) are non-trivial – there is no population with a large number of dissipationless re-mergers (at any  $f_{\text{sb}}$ ) that matches the observed kinematic/shape distributions of cusp ellipticals, and no population of disk-disk mergers (at any  $f_{\text{sb}}$ ) that matches the observed distributions of core ellipticals<sup>15</sup>.

Figures 26 & 27 show how the rotation and isophotal shapes of our simulated disk-disk and re-merger remnants compare with observed cusp and core elliptical populations. We specifically consider simulations with similar dissipational fractions to the observations (we only compare simulations that have values of  $f_{\text{sb}}$  in broad agreement with the locus we observationally infer from fitting the observed systems in Figure 20; equivalently but more strictly, we can consider only the set of simulations each of which is a best-fit match to one of the observed surface brightness profiles, as in Figure 10). Despite these simulations being constrained to match the observed systems only in their averaged surface brightness profile, they occupy a similar locus to the observations in each sense in Figures 26 & 27.

Figure 27 illustrates that the distribution in  $\epsilon$ ,  $a_4/a$  and  $(V/\sigma)^*$  for core ellipticals constrains not only their merger history, but also the dissipational content of the *original* gas-rich mergers, (even if these systems are the product of spheroid-spheroid re-mergers). This constraint agrees well with our estimates from their surface brightness profiles: sys-

<sup>15</sup> As discussed below, this statement is not true for any *single* object, but applies to the populations as a whole.



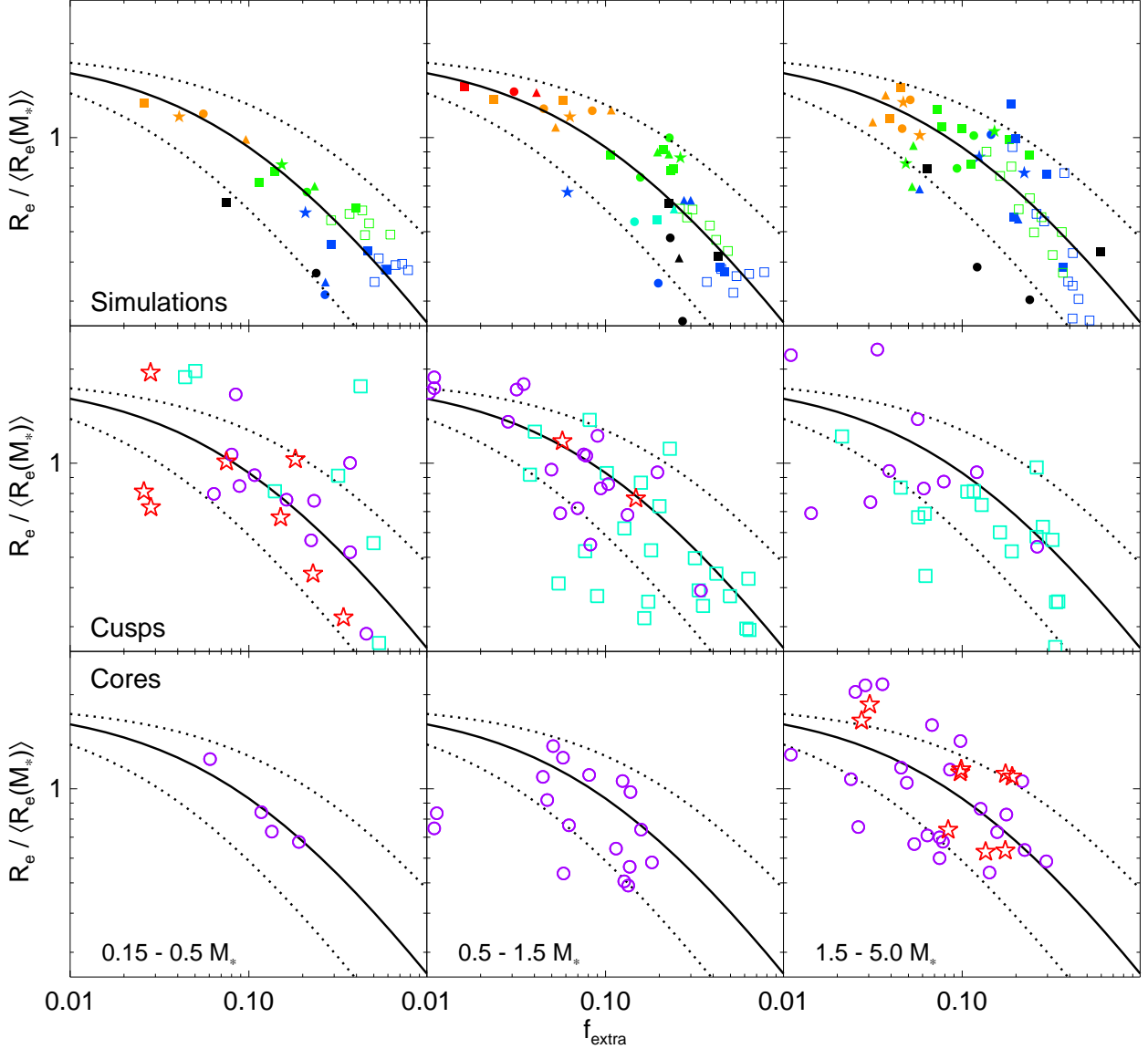


FIG. 24.— Effective radius  $R_e$  relative to the median value for all ellipticals of the same stellar mass, as a function of our fitted extra light fractions (the empirical tracer of the dissipational/starburst mass fraction). We compare simulated merger remnants (*top*) with observed cusp ellipticals and gas-rich merger remnants (*middle*) and observed core ellipticals (*bottom*), with points as in Figures 4 & 18. We show this in three bins of stellar mass (relative to  $M_* \approx 10^{11} M_\odot$ , or  $M_V^* = -21$ ). Solid (dotted) lines show the mean ( $\pm 1\sigma$ ) correlation, following the analytic solution for dissipational mergers and fits to our simulation in Covington et al. (2008). Simulations and observations exhibit the same behavior: systems with smaller  $R_e$  at fixed mass have systematically higher extra light fractions ( $> 6\sigma$  significance in the observations). This implies that, at fixed mass, systems are driven along the fundamental plane by the relative amount of dissipation involved in their formation. This behavior is true regardless of cusp/core status, suggesting that (most) core ellipticals have not had a large number of re-mergers.

tems which originally had too much or too little gas, relative to that we infer from the surface brightness profiles, fail to reproduce the observed shapes and kinematics (with or without re-mergers).

Unlike the case of surface brightness profiles, however, such a constraint can only be derived from a statistical population of ellipticals; as in Figure 25, the sightline-to-sightline scatter (even the object-to-object scatter in median properties seen in Figure 26) is sufficiently large that the isophotal shape and/or rotation of any *individual* elliptical, observed from only the single available viewing angle, does not present a strong constraint on the gas-richness of the original spheroid-forming merger (especially after allowing for the dependence on merger history in a re-merged population). However, given the distribution observed in a statistical population, it is pos-

sible to make a strong statement of independent support for typical dissipational fractions similar to that inferred from the individual surface brightness profile fits.

Finally, we note that one population that our simulations may have difficulty reproducing are the most extreme slow-rotators, with  $(V/\sigma)^* < 0.1$ . This may be a by-product of observational uncertainties or differences between our simulation versus observational fitting methodologies. At this level, both simulations and observations are sensitive to resolution and to the outer radii within which velocities are defined (with velocities, even in slow rotators, rising significantly at larger radii; see e.g. Emsellem et al. 2007); many of the observed objects in this category have  $V/\sigma$  measured within relatively small radii  $\lesssim 0.6 R_e$ . We have broadly matched the simulation resolution and radii where kinematic quantities are defined

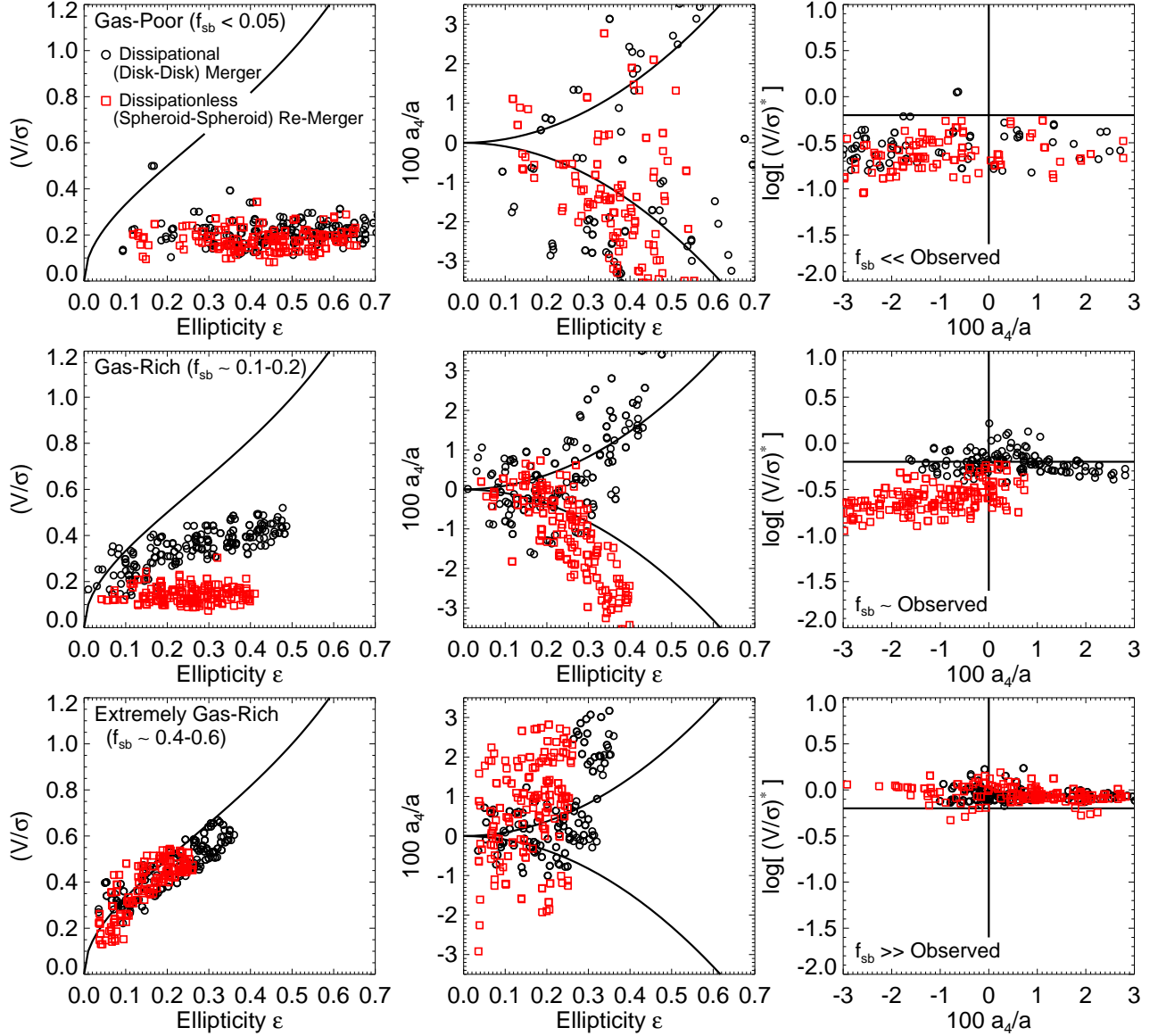


FIG. 25.— Rotation ( $V/\sigma$ ), ellipticity  $\epsilon$ , and isophotal boxy/diskiness ( $a_4/a$ ) for a 1:1 identical disk-disk merger and spheroid-spheroid re-merger of that disk-disk remnant. *Top*: Case where the initial disk-disk merger is gas-poor ( $f_{\text{starburst}} \approx 0.01$ ). *Middle*: Case where the initial disk-disk merger is gas-rich ( $f_{\text{starburst}} \sim 0.1$ , typical of  $\sim 1-5 L_*$  ellipticals). *Bottom*: Case where the initial disk-disk merger is extremely gas-rich ( $f_{\text{starburst}} \sim 0.4-0.6$ , larger than we infer for any of the observed core ellipticals in our sample). For each, we show a single merger remnant, as viewed from  $\sim 100$  independent sightlines. Gas-poor disk-disk mergers yield remnants that are slow rotators with large ellipticity, without a correlation between  $\epsilon$  and  $a_4$ , and extending to very boxy isophotal shapes. This is relatively unchanged in their re-mergers (simple energetic concerns mean they cannot get significantly “more round,” and the extension to “too boxy” isophotes and lack of  $\epsilon-a_4$  correlation is enhanced). Gas-rich disk-disk mergers are more round (owing to dissipation building a central mass concentration), with kinematic subcomponents that give rise to the rotation and disk-like isophotes observed in cusp ellipticals (and their correlations). Their re-mergers destroy these subsystems, but retain the central mass concentrations – this enables the formation of very round, but boxy and slowly-rotating systems with the  $\epsilon-a_4$  correlations appropriate for core ellipticals. But systems which are significantly more gas-rich than we infer remain disk-like and rapidly rotating even after re-mergers, in conflict with the observed core population.

( $= R_e$ ) to most of the observations shown, but a more rigorous comparison should carefully match the sampling radii for given sub-classes of objects and consider full kinematic profiles, rather than the integrated quantities here.

The difference between our simulations and these slowest rotators may also reflect a real physical difference: probably our simplification of realistic merger histories. As demonstrated in e.g. Boylan-Kolchin et al. (2005, 2006), the rotation properties of spheroid-spheroid merger remnants can be significantly dependent on orbital parameters. We do not find as strong a dependence as those authors (namely because their model ellipticals did not include a central mass concentration

as do the systems here; the presence of this component leads to more regular tube and loop orbits as opposed to the long box orbits that support the most extreme ellipticity/rotation configurations seen in that paper); however, we still expect that a systematic bias towards certain orbital parameters (for example, a preference for particularly radial orbits in the formation of the most massive ellipticals, if they accrete galaxies along filaments) can change  $(V/\sigma)^*$  in a corresponding systematic manner.

Also, the systems with such low rotation are typically the most massive systems, with early stellar formation times (see e.g. Bender et al. 1992, 1993; Ferrarese et al.

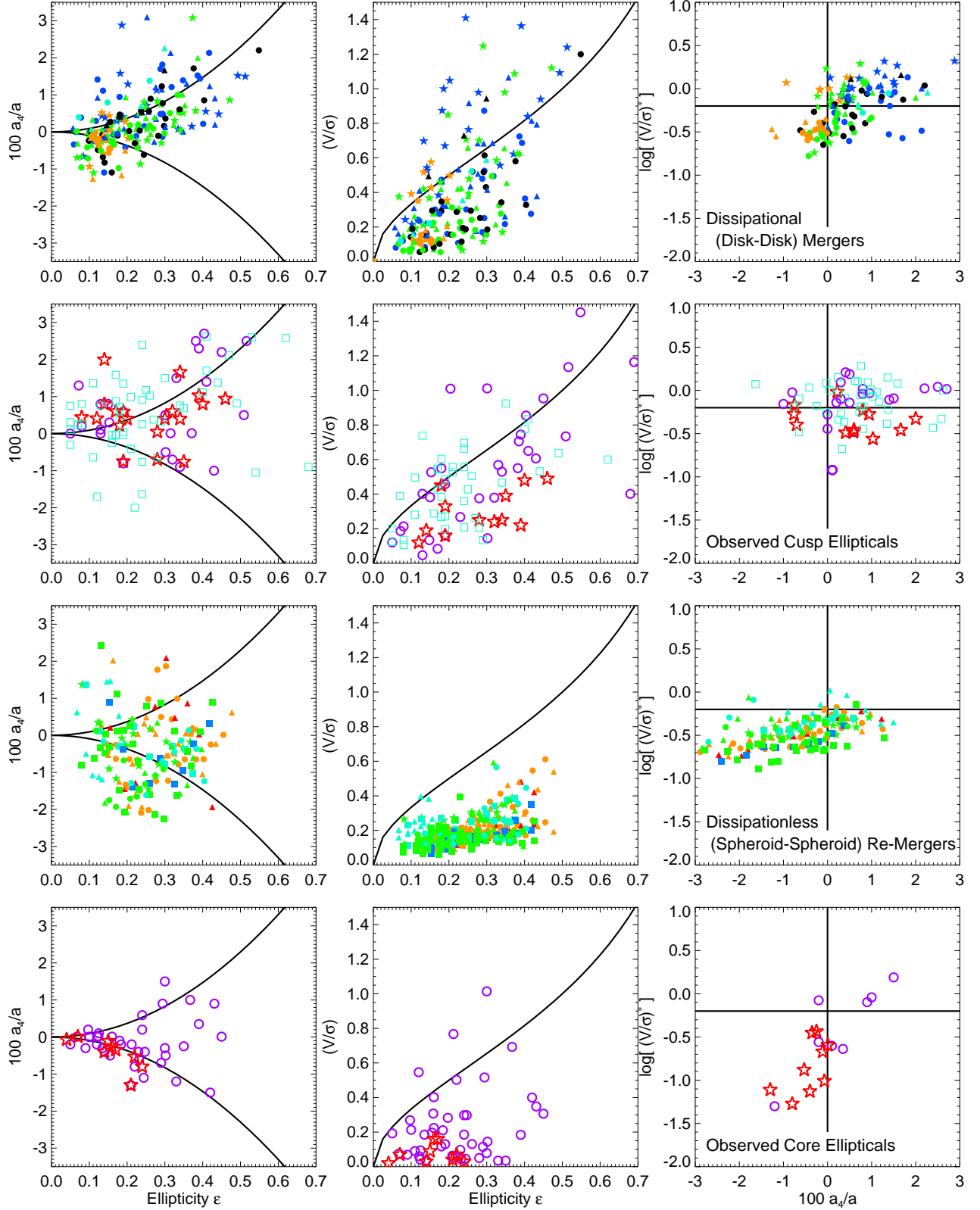


FIG. 26.— As Figure 25, but comparing our library of simulations to observed systems. *Top:* Rotation ( $V/\sigma$ ), ellipticity  $\epsilon$ , and isophotal boxy/diskiness ( $a_d/a$ ) for disk-disk merger remnants, with dissipational/starburst fractions appropriate for their mass (matched to that inferred from the observed systems; roughly  $f_{\text{starburst}} \sim 0.1$  for most of the near  $\sim L_*$  sample). Each point is the median value for a given simulation, across  $\sim 100$  sightlines. Below, we compare cusp ellipticals and gas-rich merger remnants. *Bottom:* Same, for spheroid-spheroid re-mergers of the original disk-disk merger remnants, and observed core ellipticals. The simulated and observed loci agree for both populations (despite being distinct from one another). Comparing to Figure 25, it is clear that mergers and re-mergers of systems without sufficient dissipation (less than that inferred from our surface brightness profile fitting) do *not* agree with the observed cusp and core populations – significantly different dissipational fractions from our estimates are ruled out by the kinematic data.

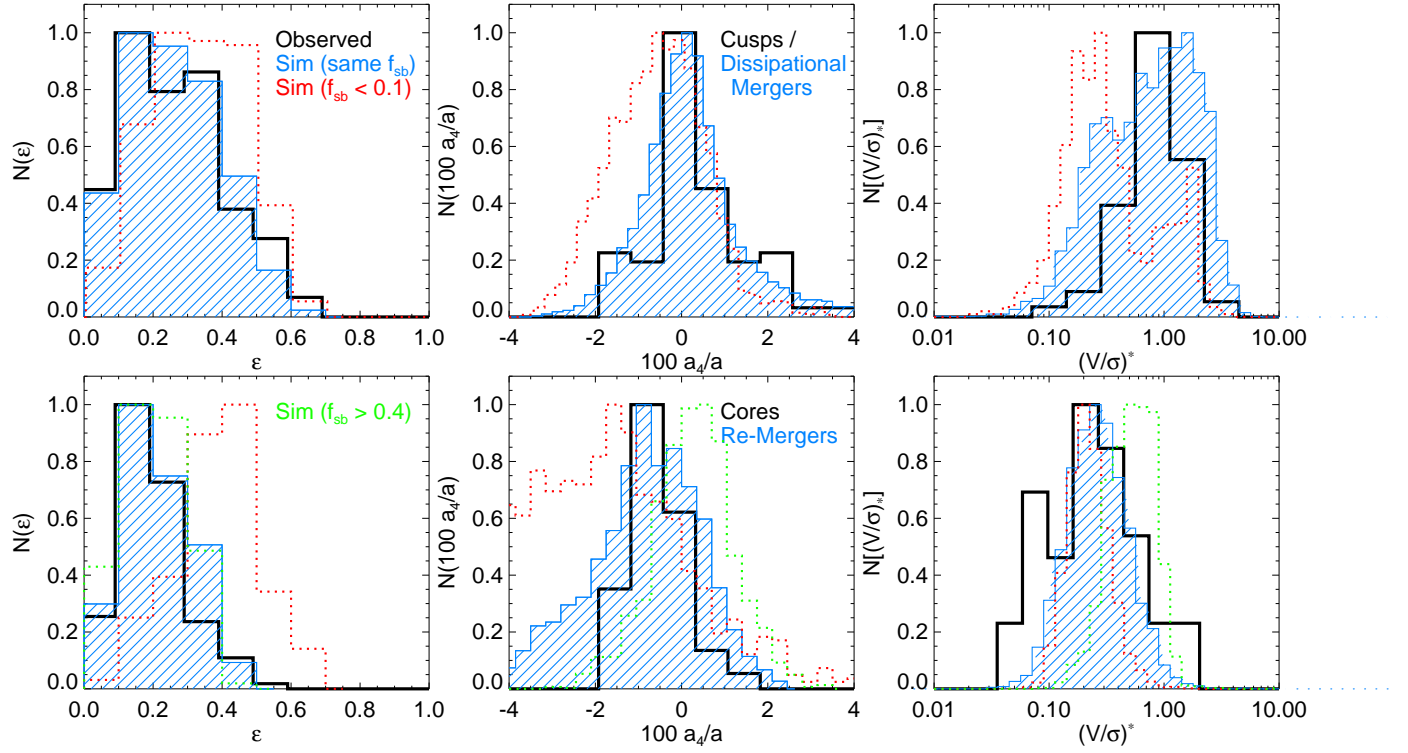


FIG. 27.— Histograms show the distribution in each property from Figure 26 (ellipticity  $\epsilon$ , isophotal shape boxy/diskiness  $a_4/a$ , and rotation  $(V/\sigma)^*$ ), for observed systems and simulations. *Top:* Observed cusp ellipticals (black line) compared to simulated disk-disk merger remnants which have similar moderate extra light fractions (blue shaded), and gas-poor (nearly dissipationless) disk-disk mergers ( $f_{sb} < 0.1$ ; red dotted). The simulation distributions uniformly sample each simulation in solid angle over  $\sim 100$  lines-of-sight – sightline-to-sightline and object-to-object differences contribute comparably to the scatter. *Bottom:* Same, for observed core ellipticals (black line) compared to simulated re-mergers of the disk-disk merger remnants with appropriate extra light fractions (dissipational fractions in the original disk-disk merger; blue shaded) and with much lower (red dotted) or higher (green dotted) dissipational content. The simulations, when they have the appropriate extra light/dissipational content, agree with the observed distributions. There is some “memory” of the amount of dissipation retained in the kinematics: systems without sufficient extra light are too elliptical and have a much broader  $a_4$  distribution extending to extremely boxy isophotal shapes; systems with too much extra light remain too disk-like and rapidly rotating even after re-mergers.

1994; Kuntschner et al. 2006; Emsellem et al. 2007; Cappellari et al. 2007; Kormendy et al. 2008); these are most likely to have undergone a mix of major and minor mergers, with e.g. five 1:5 mergers becoming a more likely channel for mass doubling in dry mergers than a single 1:1 merger for the most massive systems  $L \gg L_*$ . Although this will not change our analysis of the extra light components in the surface brightness profiles (provided these are as robust to minor mergers as they are to major mergers), it has long been proposed as a means to yield systems with low net angular momentum and such little rotation (Gallagher & Ostriker 1972; Ostriker & Tremaine 1975; Hausman & Ostriker 1978; Weil & Hernquist 1994, 1996; Naab et al. 2007). The formation of these objects, therefore, requires further study, with more cosmologically representative accretion and merger histories.

#### 9. OUTER SERSIC INDICES OF ELLIPTICALS WITH CORES

Given the issues surrounding profile fitting described in § 4, we have to be somewhat careful when we attempt to describe the typical outer Sersic indices of core ellipticals. We can (and do) obtain different answers depending on how we approach our fits, even for data sets of excellent quality and large dynamic range. However, we still find that the distribution of Sersic indices in core ellipticals is relatively narrow, with a characteristic value somewhat higher than those in cusp galaxies (as expected if they are indeed re-merger remnants).

Figure 28 compares the Sersic indices of the outer component in our standard two-component decompositions fitted to our gas-rich merger simulations, cusp and core ellipticals. Here, the same fitting procedure has been applied over a self-consistent dynamic range, regardless of the cusp or core status (profile at  $\lesssim 50$  pc) of the system (for a detailed discussion of the dynamic range requirements for reliable Sersic index fits, see Kormendy et al. 2008). As we demonstrated in Paper II, for cusp ellipticals and gas-rich merger remnants considered in this fashion, there is no dependence of outer Sersic index on stellar mass or other galaxy properties. The cusps and gas-rich mergers have a relatively narrow Sersic index distribution centered around  $n_s \sim 2.6-2.7$  with a width of  $\pm 0.75$ .

Applying our two-component models to the core ellipticals, we obtain a similar result. There is no evidence for a significant dependence of the fitted outer Sersic index on mass or any other property within the core elliptical sample. There is an offset between the Sersic index distribution of this sample and that of the cusp ellipticals, roughly corresponding to an increase in Sersic index of  $\Delta n_s \approx 1$  (i.e. a median  $n_s \sim 3.6$  and dispersion  $\pm 1.0$ ).

As described in § 4, the change in the outer profile shape from cusp to core ellipticals is expected to be a real consequence of re-mergers. Figure 29 illustrates the difference between typical profiles before and after a re-merger. To lowest order, the profile is simply puffed out by a uniform factor (which has no effect on the Sersic index). However, there is significant scatter in final radii at fixed initial radii – in other words, more stellar light will be scattered to large radii with a re-merger (and, roughly speaking, this fraction will increase weakly as the amount of violence, in terms of the orbital energy, of the re-mergers is increased; see e.g. Boylan-Kolchin et al. 2006). This will slightly raise the outer Sersic index, and help build up the extended envelopes seen around many massive galaxies and BCGs. Exactly how much this outer profile is raised depends somewhat on how we define our profile fits – in a more robust physical sense, it reflects

a lognormal scattering of stars by  $\sim 0.4$  dex (Figure 1).

Since there was no strong dependence on mass in the cusp population, we expect no strong dependence in the core population, so long as there is not a dramatic dependence of merger history (within this sub-population) on mass. To the extent that we see these effects and no substantial mass dependence, it implies that most of our core ellipticals have undergone a relatively small number of re-mergers, and are therefore reasonable analogs of our re-merger simulations (where we see this change – where we see large envelopes that imply very high Sersic indices for the outer components – is at the extreme masses of  $\gtrsim$  a few  $L_*$  BCGs, where we have emphasized our models should not be extrapolated without caution).

This relatively modest increase in Sersic index may seem surprising, as are the (still relatively low) Sersic indices fitted in this manner, given that massive ellipticals are often fitted to high Sersic indices  $n_s \gtrsim 6$ . However, we caution that those results are based on fitting those profiles to either single Sersic or core-Sersic type laws (or similarly an outer Sersic law allowing for some inner “deficit” or core), and are *not* directly comparable to the results fitting the two-component models adopted here. For comparison, we therefore consider the results obtained with these fitting functions and how they relate to the galactic components inferred from our two-component decompositions.

Figures 29 & 30 compare the results of our two-component fits with those obtained fitting our simulated re-mergers to a “core-Sersic” law of the form

$$I = I' \left[ 1 + \left( \frac{r_b}{r} \right)^\alpha \right]^{\gamma/\alpha} \exp \left[ -b_n \left( \frac{r^\alpha + r_b^\alpha}{r_e^\alpha} \right)^{1/(\alpha n)} \right] \quad (6)$$

(e.g. Graham et al. 2003), where  $r_b$  is the core break radius within which the profile shifts to a power law of slope  $\gamma$ ,  $r_e$  is the effective radius and  $n$  the Sersic index of the outer light profile, and  $\alpha$  a parameter describing how rapidly the break occurs. Whether we free  $\alpha$  or set  $\alpha \rightarrow \infty$  (the limit of a sharp break into the profile core) we obtain similar results (although the fit quality  $\chi^2/\nu$  is slightly improved with a free  $\alpha$ ).

We also consider fitting a single Sersic index to the outer profile, i.e. the profile outside of the central core (following the methodology of Kormendy et al. 2008). In practice, we fit a core-Sersic law to identify the radius where the inner profile breaks from the outer Sersic law, and then re-fit the radii larger than  $\sim 1-2$  times this radius to a single Sersic law (we can also in more detail fit steadily inwards from larger radii until the fit residuals begin to rapidly grow, which yields similar results).

In the case of the direct gas-rich merger remnants, where the breaks between the inner and outer components are sharp (and where the outer component Sersic indices are relatively low), the results are more or less similar. The two-component fits not only match the physical decompositions in the simulations, but they also happen to be excellent fits in a formal statistical sense. The functional form of the Sersic distribution is such that fitting just the outer profiles to a Sersic function – in this case giving low  $n_s$  – yields a shallow inwards extrapolation, similar to that in the progenitor ( $n_s \sim 1$ ) disks and therefore the dissipationless component; so the extra light again appears as a characteristic central excess (although the nature of fitting inwards “as far as possible” yields a mild bias towards some underestimation of the extra light content). The core-Sersic distribution (or equivalently, forcing a single Sersic function to fit the entire profile, inner and outer), designed

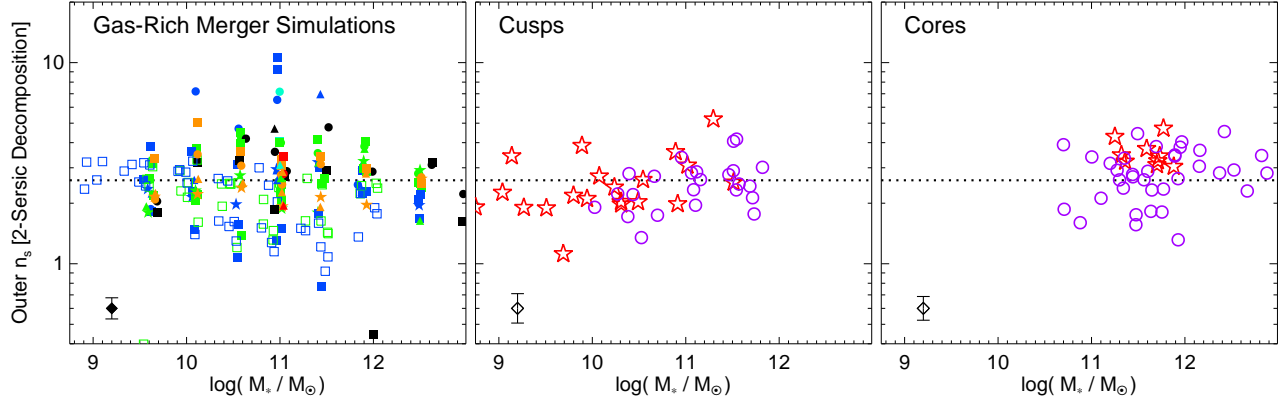


FIG. 28.— Outer Sersic indices (from our two-component decomposition) in ellipticals and simulated gas-rich merger remnants (point style as in Figure 18). Filled diamond is typical sightline-to-sightline variation in the simulations, open diamond the source-to-source (or band-to-band) scatter in observed profile fits. Gas-rich merger remnants and cusp ellipticals have characteristic  $n_s \sim 2-3$ , without a strong systematic dependence on mass or other properties (dotted line is the median for cusp ellipticals and gas-rich merger remnants,  $n_s = 2.7$ ); core ellipticals are the same, but with slightly higher characteristic  $n_s \sim 3-5$ .

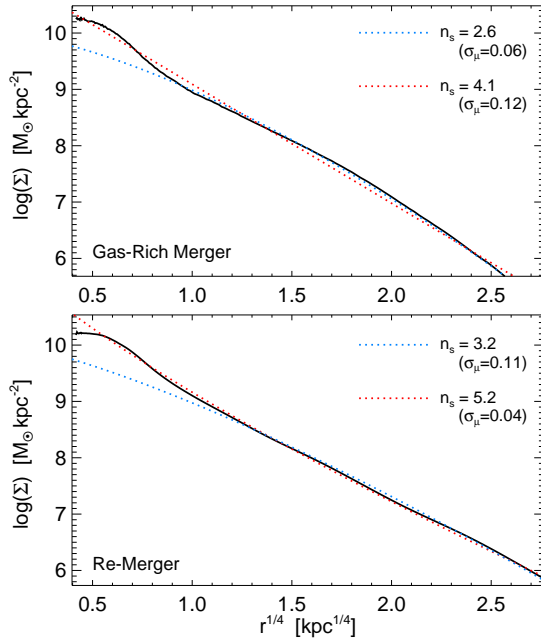


FIG. 29.— Illustration of how profile shapes change in a re-merger, as a consequence of the scattering of stars. *Top*: Gas-rich merger remnant. Dotted blue line shows the outer Sersic index from our typical two-component fits ( $n_s = 2.6$ ; concave down in this projection) with the rms deviations of the profile from the best-fit two-component model (the rise above this curve accurately traces the physical starburst component). Dotted red line shows the result of fitting the entire profile to a core-Sersic profile (or a Sersic profile with some downward break at small radii;  $n_s = 4.1$ ). Both methods yield reasonably good fits, but the meaning and values of  $n_s$  are different (the  $n_s$  obtained fitting the profile in the latter manner reflects some combination of the dissipational and dissipationless components). For gas-rich merger remnants, the sharper “break” in the profile also yields significant residuals about the cored-Sersic fit. *Bottom*: Same, after a gas-poor re-merger. The two-component decomposition is just as successful at recovering the physical dissipational and dissipationless components. However, the scattering of stars to larger radii and smoothing of the transition to the starburst component yields a situation where other possible fitting functions – in this case a core-Sersic fit, with a higher outer index ( $n_s = 5.2$ ; concave up here) and central deficit – can be excellent fits in a formal statistical sense.

to describe ellipticals with higher outer  $n_s$  and a downward break at small radii, performs reasonably well fitting a higher  $n_s$  Sersic distribution to the entire profile (including the extra light), but the relatively sharp break between the components yields noticeably larger residuals.

If re-mergers exactly preserved profile shape, the behavior

would, of course, be identical. In reality however, a re-merger scatters stars out to large radii (in addition to the overall “puffing up” of the profile; Figure 1), which raises the characteristic Sersic index  $n_s$  describing the outer profile shape, and smooths any sharp breaks in the inner profile. As a consequence, we obtain rather different results applying alternative fitting functions to re-merger remnants. In Figure 29, for example, fitting from the outer radii inwards yields a high outer Sersic index  $n_s \sim 5$ ; the nature of the Sersic distribution is such that higher- $n_s$  outer profiles extrapolate to relatively large central densities, so the fitted distribution maps onto or attaches smoothly to the high central density that is the extra light component. Eventually, the inward extrapolation of the high- $n_s$  profiles rises above the light profile (and this will be even more pronounced in the presence of black hole scouring flattening the nuclear profile slope), so the profile appears to “break downwards” relative to the outer Sersic fit. Together with the smoothing of sharp features near the transition between the dissipational and dissipationless components, this means that one can – after a re-merger – obtain very good statistical profile fits with simple cored-Sersic models ( $\sigma_\mu \lesssim 0.04 \text{ mag arcsec}^{-2}$ ), with considerably higher outer  $n_s$ .

Figure 30 demonstrates this in a more rigorous manner: we compare the results of these different fitting methods with the known physical decompositions in the simulations. This emphasizes an important point: the good fits obtained with e.g. cored Sersic models (that do not include an explicit “extra” component) do *not* necessarily mean that the extra light (as we physically define it: stars formed originally in a dissipational starburst) is not still manifest in the light profile. This stellar material survives the dry spheroidal re-mergers we simulate, and the rank order of particles in radius is sufficiently preserved that it still contributes a substantial component of the light within  $\sim \text{kpc}$  scales in Figure 30. In fact, the high *central* densities implied by the large Sersic indices of the fitted cored Sersic models (typical  $n_s \sim 6-8$  in observed cored systems; see e.g. Prugniel & Simien 1997; Trujillo et al. 2002; Ferrarese et al. 2006; Kormendy et al. 2008) can only be part of the fit if the extra light is included – scattering of stars cannot, by Louisville’s theorem, raise the central density of the elliptical. If there were no dissipational component in core ellipticals, then their outer portions would resemble a high- $n_s$  envelope, but their inner portions ( $\lesssim 2-3 R_e$ ) would resemble a low- $n_s$ ,



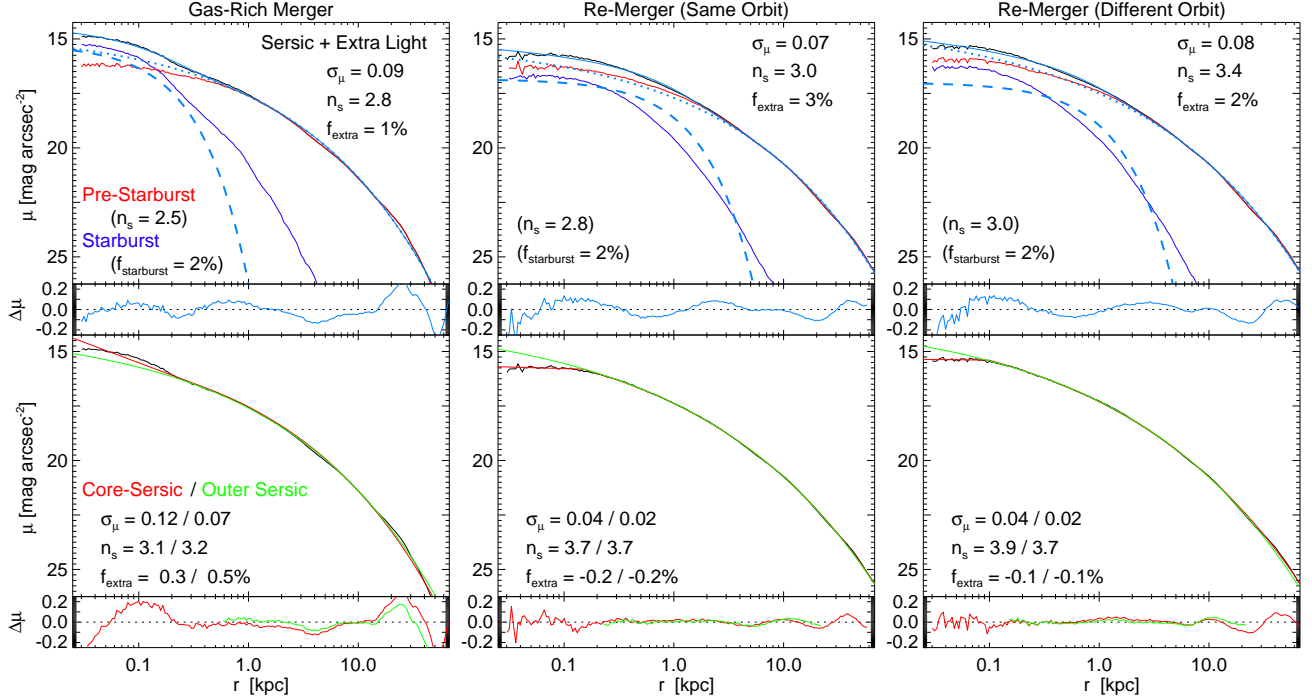


FIG. 30.— *Top*: Surface brightness profiles from the smooth extra light simulations shown in Figure 2, including the original gas-rich merger remnant (*left*), a major re-merger remnant (*center*) and another re-merger with different orbital parameters (*right*). We show the physical decomposition into pre-starburst and starburst stars (tracking the starburst component after re-mergers), with the mass fraction in the starburst and Sersic index directly fitted to the pre-starburst component. We compare with our two-component fit, with corresponding extra light mass fraction, outer Sersic index, and rms residuals  $\sigma_\mu$  (in  $\text{mag arcsec}^{-2}$ ), and show the fit residuals ( $\Delta\mu$ ). As before, the two-component decomposition reliably recovers the physical decomposition of the light. *Bottom*: Same, but fitted with a core-Sersic law profile (red) or a single Sersic law fitted only to radii outside of where the central profile begins to deviate from the Sersic law (green). In the original gas-rich merger remnant, these methods all show some extra light, and the core-Sersic model performs poorly. After a re-merger, the core-Sersic model formally fits the profile well with a higher Sersic index that reflects the *combination* of the outer profile and the inner extra light profile. If we were to simply take  $f_{\text{extra}}$  as the integrated light relative to that from extrapolation of the Sersic fit to all radii (instead of using our calibrated two-component decomposition), we would infer much less “extra” light in the gas-rich remnant and some “deficit” (*missing* light) in the re-merger remnants – the starburst component is still there (with the mass fraction correctly inferred by our two-component fits), but these parameterized fits reflect it only indirectly (with their higher Sersic indices) – inferring the “extra” or dissipational component mass from these alternative fitting functions is not physically motivated, even if they are better statistical fits to the light profile.

low density disk (which would mean, among other things, that they could not be well-fit over a significant dynamic range by *any* Sersic function). Note that the apparent “deficit” seen in these simulations (i.e. shortfall of the inner light profile relative to the inwards extrapolation of the outer Sersic fit) does not reflect a physical deficit (since the high- $n_s$  outer profile is much steeper in the central regions than the profiles of the actual progenitors); this lends some caution to the approach of using such comparisons to infer the mass “scoured” by a nuclear binary black hole (which we discuss further in § 10).

This general behavior is quite common; Figure 31 summarizes these results for our library of simulations – we plot the distribution of relative fit quality (for which we adopt the proxy of the difference in  $\sigma_\mu$  between a core-Sersic fit and our two-component decomposition), for both single gas-rich merger remnants and re-merger remnants. These examples illustrate the importance of combining models and observations in interpreting the parameters obtained from galaxy surface brightness profile fits: these different functions are fitting the same profiles, with broadly similar quality (and with varying relative quality in populations with different merger histories), but the Sersic indices and other parameters obtained from the fits have different physical interpretations in the context of our simulations. Our proposed decompositions, although physically motivated, are not required by the observations: in a purely statistical sense, the two-component decomposition is not only non-unique as a parameterization, it is not even necessarily the best-fitting choice in all cases. Our intention here

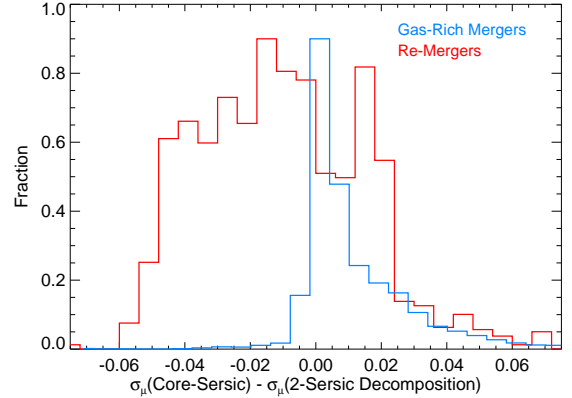


FIG. 31.— Summary of the difference in fitting single gas-rich merger remnants (blue) and re-merger remnants (red). We show the distribution for both samples of simulations in relative fit quality of a core-Sersic law and our two-component decomposition – i.e. the difference in  $\sigma_\mu$  (in  $\text{mag arcsec}^{-2}$ ) between the best-fit core-Sersic law and our two-component fit (note the two forms have the same number of degrees of freedom). Negative values mean the core-Sersic law is formally a better fit. The gas-rich mergers are poorly fitted by a core-Sersic law – they almost all prefer the two-component decomposition, or little difference (that being in cases where there is only a small fraction of extra light). A large fraction of re-merger remnants are better fit by a core-Sersic law.

is not to argue that the proposed decomposition is a better fit in a formal sense to observed profiles, but rather that it is useful because it tends, when adopted in numerical experiments, to recover the correct physical decomposition between

the dense inner (high surface-brightness) component of the galaxy originally formed by dissipation of gas into the central regions of the system, and the less dense outer component originally formed by violent relaxation of stellar disks. If we were to interpret the extra or excess light to be that light in the real profile above the prediction of the best-fit single Sersic or core-Sersic model, in the same manner that we do relative to the outer components in our two-component fits, we would (incorrectly) infer effectively no extra light in most of our simulated re-merger remnants. Clearly, calibrating a given method against simulations and models is important for assigning it a specific physical meaning.

Interestingly, we find that only our re-merger remnants are better fit (in a purely formal sense) by a core-Sersic law, as opposed to a two component model, and we find this in general becomes more true as we repeatedly re-merge systems. As a consequence, although the parameters of the core-Sersic or single Sersic fit may not be directly analogous to those obtained from our two-component fits, the fact that a galaxy can be formally better fit by one of those functions is predicted to be a consequence of dry re-mergers which will smooth the profile in the manner described above. Indeed, a tight association is observed between galaxies with nuclear cores and galaxies better fit by a single Sersic or core-Sersic law, despite differences in the spatial scales where the two are determined (Ferrarese et al. 2006; Kormendy et al. 2008). Our models provide a natural explanation for this, which not only reconciles such profile fits with the survival of dissipational/extra light components from cusp elliptical progenitors, but in fact requires such components to explain the highest observed Sersic indices from single Sersic or core-Sersic fits. This lends further confidence to our modeling of profile shapes, even at the level of smooth profiles apparently better fit by functional forms different from the convenient two-component decomposition we adopt in this paper.

Given these different choices that can be made when estimating an observational Sersic index, we compare in Figure 32 the distribution of Sersic indices for cusp and core ellipticals, obtained with different methods. First, we show the distribution of Sersic indices measured from our two-component decomposition, in both the observed samples and our simulations. We compare the distribution extracted from our gas-rich merger simulations to the distribution fitted to the observed cusp elliptical profiles from Kormendy et al. (2008) and Lauer et al. (2007a), and compare the distribution extracted from our re-merger simulations to that fitted to the observed core ellipticals from the same samples (with the same method applied). Because (as demonstrated in Paper II) the fitted outer Sersic indices can be quite sensitive to the photometric depth and systematics between different observations, we restrict ourselves to a robust subsample described in Paper II: specifically, those ellipticals for which we have  $> 3$  independent sources of photometry that agree to within  $\sim 20\%$  on the fitted value of  $n_s$ . We note that we obtain identical results (but with larger scatter) if we consider our entire samples.

We compare these distributions with what we would obtain using two other methods to estimate the outer Sersic index. First, we follow Kormendy et al. (2008) and fit a single outer Sersic profile inwards from large radii until the central profile begins to break upwards or downwards from this extrapolation, as described above (the comparison in the core ellipticals is similar if we fit the entire profile with a core-Sersic distribution). Second, we attempt to directly fit just the outer radii

– we first fit a single  $r^{1/4}$  law to estimate the effective radius, then consider only the profile at radii larger than  $\sim 0.5\text{--}2.0 R_e$  (within this range, our results are not dramatically sensitive to the exact cut). We then fit a single Sersic law just to these points. This limits our observational samples to only those systems with a large number of observed points at  $r \gg R_e$  (where such a fit is possible).

Applied to the cusp ellipticals, these methods yield similar distributions, all with median  $n_s \sim 2.5$  and similar scatter ( $\pm 0.7\text{--}0.9$ ), as expected from our previous comparisons. Applied to core ellipticals, the Sersic index distribution is, as expected, more sensitive to the method adopted. Fitting directly only to large radii yields a roughly similar distribution in  $n_s$  to our two-component model, with typical  $n_s \sim 3\text{--}4$  (perhaps somewhat larger). There is more scatter (dispersion  $\Delta n_s \sim 1\text{--}1.5$ ) – this relates to two effects. First, our restriction to radii  $r \gtrsim R_e$  limits the number of data points and dynamic range of the fits, increasing the associated uncertainties. Second, the fact (as noted above) that the rise in outer  $n_s$  (in our two-component model) in a re-merger is primarily driven at large radii from scattered stars, not by any increased density at small radii (which still behaves like a lower- $n_s$  system). Fitting only the large radii is therefore not restrained by the curvature and lack of sharply rising density at small  $r$ , and is more sensitive to the increased scattering of stars into the envelope at large radii. Adopting the method of fitting a single Sersic profile with a downward break from Kormendy et al. (2008) or fitting core-Sersic models (Graham et al. 2003; Ferrarese et al. 2006) gives a higher typical  $n_s \sim 4\text{--}5$  and scatter  $\Delta n_s \sim 2\text{--}3$ , reflecting the physical behavior outlined above.

In any case, our simulated distributions and the observed Sersic index distributions match well when the same methods are applied to determine  $n_s$ . There is a significant (albeit not dramatic) and physically meaningful offset in the Sersic indices of gas-rich merger remnants and re-merger remnants (again, regardless of methodology used to estimate  $n_s$ ), which appears to be reflected in the Sersic index distributions of cusp and core ellipticals. This supports the notion that there is some difference in the populations, in the sense expected for a relatively small number of major dry re-mergers.

#### 10. THE APPEARANCE OF “MISSING” LIGHT: A CAUTION

As we discussed in § 4 and § 9, core ellipticals are sometimes referred to as having “missing light” or “mass deficits” at small radii (generally below the size scales of the extra light of interest to us here), which has been associated with the action of black hole “scouring” scattering stars from the nucleus. We have argued that such scouring should not make a difference to the scales of interest for our inferences of the dissipational content in these objects. Having said that, however, the co-existence of “extra” and “missing” light (i.e. the presence of cores in the central profiles of ellipticals dominated, at their center, by the dense remnants of dissipational star formation) can mean that some additional care is needed when observers attempt to estimate the amount of “missing” light (i.e. how much stellar mass has been kicked out from small radii in order to form the central core). The problem is that one desires a method to empirically determine where (and by how much) the profile has been modified by scouring. Of course, any such estimate requires some knowledge of what the profile shape was *before* the scouring took place (roughly, the pre-“dry merger” profile of the galaxy). If the galaxy profile were simply one-component, then provided some physi-

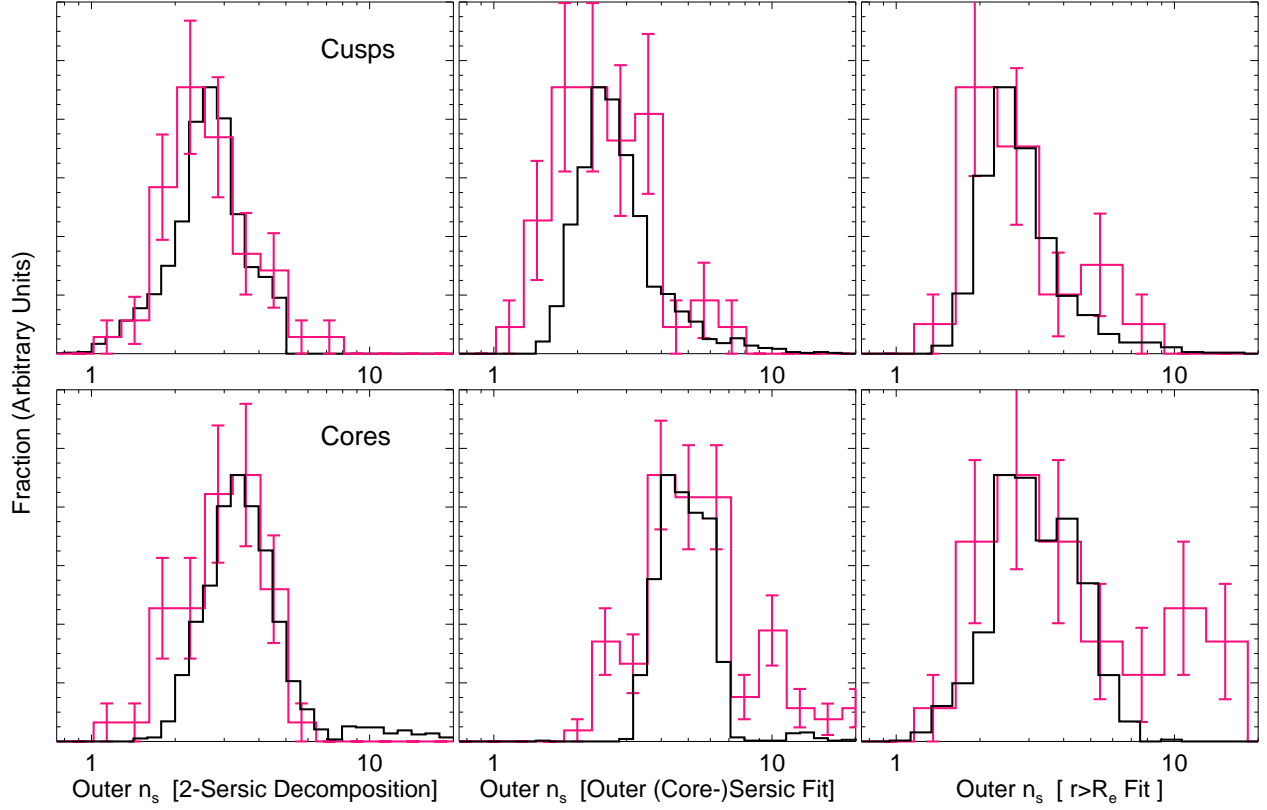


FIG. 32.— Distribution of outer Sersic indices in ellipticals, using different methods for determining  $n_s$ , for cusp ellipticals and gas-rich merger remnant simulations (*top*) and core ellipticals and spheroid-spheroid re-merger simulations (*bottom*). Solid black lines show the results for our entire sample of simulations (each across  $\sim 100$  sightlines). Colored lines show the results for the combined observed samples of Lauer et al. (2007a) and Kormendy et al. (2008), with Poisson error bars. *Left*: Outer Sersic index determined using our standard two-component decomposition. *Center*: Outer Sersic index determined following Kormendy et al. (2008) or Ferrarese et al. (2006) (fitting an “outer” Sersic index inwards, including an extra component if there is some small-scale rise above it or allowing a deficit or core-Sersic fit when there is a core or high outer  $n_s$ ). *Right*: Outer Sersic index determined by re-fitting only the observed profile data at  $r > R_e$  to a Sersic law. Cuspy ellipticals have a fairly narrow range of  $n_s \sim 2.7 \pm 0.8$ , in good agreement with gas-rich merger simulations, and relatively insensitive to the parameterization. Core ellipticals also have a narrow range with a higher  $n \sim 3.5 - 4 \pm 1.0$ , in good agreement with re-merger simulations, when parameterized with our two component fit or fitted directly at large radii – however, the issues in the choice of fitting function described in § 10 make the estimated  $n_s$  distribution more sensitive to the parameterization.

cal model for the profile or robust constraints on the profile shapes of progenitor (non-scoured) galaxies, this would be straightforward. But the profile of the progenitors is in fact multi-component – so the question arises, can (and if so, by how much does) the amount of “extra light” or dissipation in the galaxy bias the estimators of scoured/“missing” light?

Our comparisons in § 9 should lend some insight to this discussion. In Figure 30, for example, we consider the profiles of re-merger remnants fit to both our two-component decomposition and to (instead) a core-Sersic distribution or an outer single Sersic distribution down to radii including the outer portions of the dissipational/extra light component. If we were to assume that the true “pre dry-merger” profile of the galaxies was given by the inwards extrapolation of whatever fitting law we chose (or, in the case of the core-Sersic law, by the inwards extrapolation of the “Sersic” part of the law, without the central flattening implied by the “core”), then the application of the core-Sersic law to the simulations in Figure 30 yields some apparent “missing light” in their nuclei (i.e. they fall below the inward extrapolation of the outer Sersic indices from these particular fitting functions). This happens not because of scouring in our simulations (recall, we do not resolve the scales where initial cusps would be transformed into cores), but because the outer Sersic indices of the core-Sersic (or limited single Sersic) fits are quite large, and large Sersic indices extrapolate (as  $r \rightarrow 0$ ) to very high central

densities – even above the true densities of the dissipational central components (which themselves drive the fits towards high  $n_s$  values, as described in § 9). In short, the estimate of the “pre-merger” (or “un-cored”) profile at small radii is biased to higher values than the true “pre-merger” profile.

Physically, two things contribute to this bias (see § 9): the re-merger smooths the difference between the extra light (which rises to higher surface densities at  $r < R_e$ ) and dissipationless/outer component, leading to some of it (potentially) being included in the fit; also, the re-merger scatters more stars out to large radii (by  $\sim 0.4$  dex), broadening the overall profile and raising the outer  $n_s$ .

This can yield a bias because of the nature of the Sersic profile – if we fix the profile normalization at  $R_e$ , then changing  $n_s$  from, for example,  $n_s = 3$  to  $n_s = 6$  yields relatively little change at moderate radii (amounting to a factor  $\sim 2 - 3$  higher surface brightness at  $r = 0.1 R_e$  and  $r = 5 R_e$ ), but as  $r \rightarrow 0$  the profiles diverge strongly. An  $n_s = 3$  profile contains  $\sim 0.1 - 0.2\%$  of its mass within  $0.01 R_e$ , but an  $n_s = 6$  profile contains  $\sim 1 - 2\%$ , an order of magnitude difference. If the nuclear profile shape within  $\sim 0.01 R_e$  were flat in both cases, one would therefore infer an order of magnitude more “missing light” in the higher- $n_s$  case. In fact, all the observed cases where the “missing light” fraction is estimated to be as high as  $\gtrsim 1\%$  ( $\sim 10 - 100 M_{\text{BH}}$ ) have high outer Sersic indices  $n_s \sim 6 - 10$  (see Ferrarese et al. 2006; Côté et al. 2006;

Kormendy et al. 2008). The physical concern is that these Sersic indices are much higher than those of typical “cusp” ellipticals (with slopes corresponding to  $n_s \sim 2-4$  in their central regions) – in other words, the assumed “pre-scouring” profile in these cases is rising much more steeply as  $r \rightarrow 0$  than is actually observed in the presumed progenitors of core ellipticals.

This is not to say that the presence of central light deficits is meaningless – simply that, with this methodology, the inferred amount of missing light at small scales ( $\sim R_{\text{BH}}$ ) can be biased (generally towards higher values) by features on large scales ( $\sim R_e$ ). A more robust null hypothesis (i.e. estimator of what the nuclear profile would be in the absence of scouring) may be obtained if we assume the “pre-merger” nuclear profile rises about as steeply as observed in typical cusp ellipticals.

For example, if we examine the profile of just the inner dominant component (the “extra light”) in cusp ellipticals, we expect that the median non-scoured distribution would rise about as steeply as an  $n_s \sim 3.6$  profile (or a Nuker profile with inner logarithmic slope  $\gamma \sim 0.7-0.8$ ) once well interior to the effective radius of the extra light. In core ellipticals, the observed nuclear profile at  $r \ll R_{\text{extra}}$  is flatter, more like median  $n_s \sim 1.6$  (or Nuker slope  $\gamma \sim 0.2$ ) – this, of course, is why they are cores. Taking the typical nuclear shape in cusp ellipticals as our null hypothesis, we obtain characteristic missing light fractions  $\sim 0.5-3 \times 10^{-3} M_{\text{gal}}$ , comparable to the black hole mass and expectations from scouring models. Alternatively, Lauer et al. (2007b) estimate the scoured mass as that within  $r_\gamma$  (defined as the radius where the logarithmic slope  $\gamma = 1/2$ , which is reasonably representative of the radius in which scouring has significantly flattened the profile), giving a median value  $\sim 2.4 M_{\text{BH}}$ .

This is important because the high values sometimes inferred for the scoured mass fraction or “missing light” ( $\gtrsim 0.01 M_{\text{gal}}$ ) would actually present a challenge to the black hole scouring models – those models predict a scoured core mass  $\sim M_{\text{BH}}$ , but in some cases these empirical estimators yield scoured masses  $\sim 10-100 M_{\text{BH}}$ . Our simulations demonstrate that these extreme observational estimates can probably be explained as artifacts of the fitting functions chosen, in cases where the outer  $n_s$  is large. Qualitatively, this is not expected to alter the classification of cusp and core ellipticals; but if a robust *quantitative* estimate of the scoured or core mass is desired, then care is needed in empirically evaluating these cases. We find that if we adopt estimators less sensitive to the profile at large radii, these high values come down, more in line with the expectations from scouring models.

## 11. DISCUSSION

In Paper I and Paper II, we demonstrated that “extra light,” in the sense of stellar populations formed from dissipation in e.g. a gas-rich merger induced starburst, is ubiquitous in cusp ellipticals and gas-rich merger remnants, and studied how its properties are related to and (in some cases) drive those of the galaxy. Here, we show that this dissipational component is expected to survive subsequent re-mergers of those ellipticals, even major gas-poor spheroid-spheroid mergers, in the sense that it will continue to contribute substantially to the central light profile and can be empirically recovered. We apply this to a large observed sample of ellipticals with central cores (i.e. flattening of their light profiles within the central  $\sim 30-50$  pc), and show that they are consistent with a surviving dissipational “relic extra light” component which

our adopted empirical fitting machinery and comparison with simulations allow us to recover and interpret.

### 11.1. Comparing Simulations and Observations: Empirical Decomposition of Light Profiles

In Paper II, we argued that stars in cuspy ellipticals/gas-rich merger remnants should be separated into at least two distinct populations. First, stars which are formed in the disks (or otherwise in extended distributions in progenitor galaxies) before the final merger and coalescence of the progenitors. The final merger scatters these stellar orbits and they undergo violent relaxation. They dominate the light, even in highly gas-rich merger remnants, outside of  $\sim 0.5-1$  kpc, and form a Sersic-law profile owing to their partial violent relaxation. Second, the starburst or dissipational population, formed in the central gas concentration in the final merger. This component is compact, and dominates the light inside a small radius  $\lesssim 0.5-1$  kpc. These stars *do not* undergo significant violent relaxation, but form in a nearly fixed background potential set by the dissipationless component of the galaxy.<sup>16</sup> We developed, tested, and studied in detail in Paper I a two-component fit decomposition that, in simulations, could reliably extract the properties of these two physically distinct components.

Here, we demonstrate that, to lowest order, the two primary components structuring the surface brightness profile are expected to survive in dissipationless spheroid-spheroid re-mergers, in the sense that the physical starburst component still forms a more compact distribution that dominates or contributes significantly to the profile at small radii. Re-mergers will generally expand or puff up the system by a factor  $\sim 2$  in size, and smooth out the profile by mixing stellar populations and scattering stars by a typical factor  $\sim 0.4$  dex in radius (see Figure 1) – this can make fitting the profile more sensitive to the prescription adopted, and may smooth an obvious break in the profile around the transition from dissipational to dissipationless components (Figures 29-30), but does not fundamentally remove the extra light in a physical sense.

We apply our same fitting procedure to simulated re-merger remnants, and find that, despite the re-merger, it is still able to statistically recover the physically meaningful components of the original, spheroid-forming gas-rich merger (i.e. the original dissipational or starburst component and the original dissipationless or pre-starburst component; see Figures 2-4). In other words, even after a re-merger, the surface brightness profiles of ellipticals retain information about the gas fractions and starburst mass fractions of their original gas-rich mergers. Our parametric fitting form is simple. We consider the sum of two Sersic laws: an inner extra light component, for which a fixed  $n_s = 1$  works best in a mean sense when the data are not especially constraining in the central regions, but for which  $n_s$  can be freed if the data are of sufficient quality; and an outer component with a free Sersic index. We explicitly demonstrate that this approach is successful even when (as is common in re-merger remnants) the profile is smoothed by re-mergers and obvious breaks might not be present in the profile (Figures 29-31).

We apply this to a large sample of “core” ellipticals, which (it is often argued) have been modified by re-mergers, and

<sup>16</sup> There is also a third component present in simulations and important for observed kinematics but not prominent in light profile fitting: gas moved to large radii temporarily either by feedback or tidal effects, which settles into the relaxed remnant and re-forms small rotationally supported components (embedded disks, kinematically decoupled cores, etc.; e.g. Hernquist & Barnes 1991; Hopkins et al. 2009).

find that it is reliable and implies significant “extra light” (by which we mean the remains of the original gas-rich component) in almost all cases (Figures 8-17). We also match each of the observed profiles to our library of simulations (of both gas-rich mergers and re-mergers) – i.e. directly find the simulation mass profile which most closely resembles that observed, and consider non-parametric estimators of the mass in a central starburst component. We find that in all cases we have simulations which provide good matches to the observed systems, comparable to the typical point-to-point variance inherent in the simulation surface brightness profiles ( $\sigma_\mu \lesssim 0.1$ ). The physical starburst components in these best-fitting simulations are closely related to those that we fit directly to the observed profiles, lending further support to our attempt to physically decompose the profiles (Figure 18). Where available, stellar population models including extended star formation and a subsequent burst independently support our inferred starburst mass fractions (Figure 18). Likewise, metallicity, age, and abundance gradients, where available, support our decompositions, typically demonstrating a smooth transition to a younger, more metal rich population at the radii where the dissipational component begins to dominate the profile, as predicted in Paper II (Figure 19). A complete list of fit parameters and compiled galaxy properties is included in Table 1.

### 11.2. Predictions and Observations

Fundamentally, we argue that *all ellipticals – including those with central cores – are “extra light” ellipticals (dissipational systems)*, insofar as “extra light” refers to a component originally formed dissipationally on top of a background of dissipationlessly scattered envelope (a physical two-component nature). Ellipticals with cores show just as much dissipation, at a given mass, as cuspy or power-law ellipticals. Over the core population, the mass contributed by a central starburst or dissipational population can vary substantially, but in a physical sense, it always exists in addition to the pre-starburst or violently relaxed stellar populations. In terms of their dissipational or starburst population properties, we demonstrate that core ellipticals appear to be, for the most part, a continuous extension of the cusp population. The correlations obeyed by the inferred dissipational component itself are continuous and agree where there is overlap in galaxy properties between the cusp and core populations, as expected in physical models where core ellipticals are formed by re-mergers of cusp elliptical progenitors.

Specifically, we find:

(1) *The mass fraction in the dissipational or starburst component of both cusp and core ellipticals is a strongly decreasing function of mass* (Figures 20-21). In detail, the mean starburst mass fractions can be approximated as Equation (3):

$$\langle f_{\text{starburst}} \rangle \sim \left[ 1 + \left( \frac{M_*}{10^{9.15} M_\odot} \right)^{0.4} \right]^{-1},$$

with a factor  $\sim 2$  scatter at each mass. The trend is similar for both cusp and core ellipticals, and the gas fractions needed span a range bracketed by the typical observed gas fractions of spiral galaxies at the same mass, at  $z = 0$  (bracketing the low end of the required gas fractions) and  $z \sim 2 - 3$  (bracketing the high end). Core ellipticals have not only preserved their dissipational content, but its fraction reflects that of their ultimate progenitor disks.

(2) At each mass, the degree of dissipation strongly affects the sizes of the remnants. In both observations and simulations we *demonstrate a tight correlation between effective (half-light) radius at a given stellar mass and the inferred dissipational/extra light fraction* (Figure 24). This owes to the compact nature of the central dissipational component – increasing the mass fraction in this component means that the half-light radius must be smaller. The correlations obeyed between dissipational content and size at fixed mass are similar for cusp and core ellipticals.

Despite the fact that re-mergers puff up remnants by a factor  $\sim 2$ , their masses also double, so this only moves them by about  $\sim 0.1$  dex off the mean size-stellar mass relation obeyed by gas-rich merger remnants (which has an intrinsic scatter  $\sim 0.3$  dex). On the other hand, we demonstrate that changes in the original starburst or extra light fraction can alter the remnant size by nearly an order of magnitude at fixed mass. Thus, even if core ellipticals have undergone a moderate number of re-mergers, we expect that the degree of dissipation in their original formation should still be the most important factor setting their sizes today, and we demonstrate this in the observations.

(3) Re-mergers roughly preserve the size-mass relation of the dissipational/starburst component itself, approximately set by the radius at which the starburst component becomes self-gravitating ( $GM_{\text{extra}}/R_{\text{extra}} \approx GM_*/R_e$ ); and we do find that the core ellipticals and cusp ellipticals obey nearly the same correlation (Figure 22). If re-mergers preferentially puff out low binding energy material (i.e. material at large initial radii), then we might expect that the quantity ( $GM_{\text{extra}}/R_{\text{extra}} \approx GM_*/R_e$ ) should increase slightly in a re-merger (by a maximum factor  $\sim 2$  in a 1:1 merger, if the inner component is not expanded at all, and the outer component expands by a factor of 2). We see tentative evidence for such an offset, but it is small (a factor  $\sim 1.4 - 1.5$ ; Figure 23).

(4) In Paper II we demonstrated that the extra light component gives rise to stellar population gradients in the remnant. We show here that these gradients are only weakly affected by re-mergers, in agreement with observations which find that cusp and core ellipticals do not show significant differences (at fixed galaxy properties) in their gradient strengths (Figure 6-7). To the extent that both radius and gradient strength scale with the contribution of the original dissipational component at fixed mass, we find that our prediction from Paper II should also hold for core ellipticals (namely that at fixed mass, smaller ellipticals should, on average, exhibit stronger metallicity gradients), and early observational evidence appears to support this (e.g. Mehlert et al. 2003; Sánchez-Blázquez et al. 2007; Reda et al. 2007, see also Figure 19). There are other lines of evidence for the survival of extra light: Lauer et al. (2005) find that nuclear color gradients, ellipticities, and isophotal twists in the centers of cusp and core galaxies are continuous and trace similar distributions as a function of mass and luminosity. Analogous correlations should hold with integrated stellar populations, which we discuss in Paper II, provided that these are correlated with the gas fractions of the pre-merger disks.

(5) Given the appropriate dissipational mass fraction inferred from fits to the observed surface brightness profiles, simulated re-merger remnants reproduce the global kine-



matics and isophotal shape distributions of core ellipticals (specifically rotation  $V/\sigma$ , ellipticity, and boxyness  $a_4/a$ ), and their mutual correlations (Figures 26-27). These distributions are *only* reproduced by simulations with matched dissipational mass fractions: systems with too little dissipation (lacking a high central density to make the potential more round and disrupt box orbits) are too elliptical, and systems with too much dissipation remain too disky and rapidly rotating even after several re-mergers (Figures 25 & 27). More detailed comparison of simulations with full two-dimensional velocity fields, along with higher-order measures of the velocity field at a given point, are needed to robustly discern whether scenarios as simple as a single re-merger are viable formation mechanisms for slowly-rotating, boxy ellipticals, but similar dissipational content appears to be a basic prerequisite.

(6) We predict and find that the outer Sersic indices of ellipticals with cores (in our two-component decompositions) trace a roughly constant distribution with median  $n_s \sim 3-4$  and scatter  $\Delta n_s \sim 1$ , without a strong dependence on galaxy mass, effective radius, or other properties (Figure 28). We found similar results in Paper II for the cusp elliptical population, but with a lower median  $n_s \sim 2-3$ . The difference arises naturally in our re-merger simulations, as the scattering of stars in subsequent mergers will tend to broaden the outer regions of the light profile, leaving a less steep falloff and giving rise to a higher Sersic index. That there is an offset in the outer Sersic index distribution of these populations suggests that indeed some sizable fraction of core ellipticals have experienced a re-merger, but that the offset is relatively small suggests that there have not been a large number of such re-mergers.

We emphasize that these Sersic indices are not directly comparable to those in previous studies, which fit different functional forms to the light profile or fit e.g. a Sersic profile to the entire light profile (including the extra light). If we fit our simulations to a single Sersic index or core-Sersic profile where it is the formal best fit, we recover a stronger dependence of Sersic index on galaxy mass, luminosity, or effective radius, similar to earlier claims (Caon et al. 1993; Prugniel & Simien 1997; Graham 2001; Trujillo et al. 2002; Ferrarese et al. 2006): our models are consistent with the results derived using these methods, however this does not strictly trace the physical dissipationless component of the galaxy. In fact, we show in § 9 (Figures 29-31) that re-merger remnants are often formally well-fit by core-Sersic laws (Sersic profiles with a central deficit), in agreement with observations of core ellipticals. These cases obtain high Sersic indices, driven in part by the presence of a dissipational component at small radii, raising the central surface brightness (Figure 29). These functional forms are a precise formal parameterization of the light profile, but the best-fit parameters determined in this manner reflect the combination of the dissipational and dissipationless outer components, and do not trivially translate to physical descriptions of the components of the galaxy.

Indeed, as demonstrated in Paper II, many of the results in studies using these fitting approaches are actually driven by a dependence of extra light on galaxy properties. The meaningful dependence of outer Sersic index as we quantify it (tracing the dissipationless component) on mass owes to the dependence of typical merger history on mass (dwarf spheroidals and pseudobulges will have lower typical  $n_s$ ,

than gas-rich merger remnants, which themselves have lower typical  $n_s$  than re-merger remnants, and these populations, on average form an increasing sequence in mass). For a broadly similar merger history (in terms of e.g. number of major mergers), the profile of the true dissipationless component is expected to be self-similar, as we recover (for both the cusp and core populations), since it is determined purely by gravity.

These and other correlations argue that core ellipticals should be properly thought of as containing “extra” or dissipational components in the same physical (although not necessarily observational) manner as cusp ellipticals; their central, high density regions formed via dissipational processes. We therefore refer to Paper II for a number of other proposed observational tests of the models herein, which should hold for core ellipticals as well. This is a critical test of the merger hypothesis and supports the notion that even massive, slowly rotating, boxy ellipticals with cores were originally formed in gas-rich major mergers, albeit potentially modified by subsequent re-mergers.

Points (1) and (2) emphasize that, even if a system has experienced re-mergers, and even in observed massive core ellipticals, dissipation is the key driver of galaxies along the fundamental plane (in terms of galaxy stellar mass). The degree of dissipation in the original gas-rich merger is the most important factor determining the size of the object and the ratio of baryonic to dark matter within the effective radius of the stellar light, and the correlations obeyed by the observed systems agree well with our simulations.

We show that this degree of dissipation is a systematic function of mass, without a significant offset between cusp and core elliptical populations (as expected if it is set by the gas fractions of the progenitor disks, and there have not been a large number of re-mergers of individual objects). In other words, we are able to demonstrate that the amount of dissipation expected based on known disk gas fractions as a function of mass is precisely that needed to explain the extra light in the surface brightness profiles and to reconcile the densities and radii of disks and ellipticals as a function of mass. We investigate this further in Hopkins et al. (2008b), and show how it gives rise to the fundamental plane scalings and “tilt.” Once on the fundamental plane, our simulations and other experiments (Boylan-Kolchin et al. 2005; Robertson et al. 2006a) find that re-mergers typically move more or less parallel to the fundamental plane, emphasizing that the tilt must arise in the initial, gas-rich spheroid-forming merger.

Although some of these effects will become increasingly scattered or smeared out by a large number of re-mergers, multiple lines of evidence above suggest that the typical core elliptical has undergone relatively limited dry re-merging. If re-mergers are indeed the mechanism by which cores are formed, our comparisons suggest a small number  $\sim 1$  major re-mergers per object since its formation in a gas-rich merger.

This is in line with other observational indications from e.g. the mass function evolution of ellipticals and red galaxies (e.g. Bundy et al. 2005; Borch et al. 2006; Pannella et al. 2006; Franceschini et al. 2006; Fontana et al. 2006) and direct observational estimates of the dry merger rate (Lin et al. 2004, 2008; van Dokkum 2005; Bell et al. 2006). It is also generally expected in cosmological models (De Lucia et al. 2006; Zheng et al. 2007; Hopkins et al. 2008c), where only the most massive BCGs with  $M_* \gg 10^{12} M_\odot$  or so are expected to have a large number of major re-mergers. Even in these cases,

it is not clear whether such mergers actually proceed efficiently, or whether the secondary is tidally destroyed before the merger and added as part of an extended envelope or inter-cluster light (Gallagher & Ostriker 1972; Monaco et al. 2006; Conroy et al. 2007; Purcell et al. 2007). At these masses, the growth of the system may also be dominated by a large number of minor mergers, rather than a few major mergers (major mergers being the dominant “dry” growth mode at  $\lesssim$  a few  $L_*$ ; see Maller et al. 2006; Masjedi et al. 2008).

Our constraints on this extreme of the population are, unfortunately, much weaker. Moreover, we do not intend our modeling to be extrapolated to this regime. Such systems formed, for the most part, at early times from potentially very different progenitors than those we model, with more complex subsequent merger histories our simulations do not capture (see, e.g. Li et al. 2007). More detailed analysis of individual objects, and more detailed models incorporating a fully cosmological context are called for to study the formation history of galaxies in this regime. However, such systems constitute only a small fraction ( $\lesssim 10\text{--}20\%$ ) of the mass density in even the core elliptical population (and just  $\sim 3\text{--}5\%$  of the total mass density in ellipticals), so the vast majority of the stellar populations of spheroids should be reasonably represented by our modeling.

### 11.3. Profile Fitting and Tests of Core Creation Models

The existence of nuclear cores in these ellipticals is commonly attributed to “scouring” by a binary black hole in gas-poor re-mergers. This will eject stars in close encounters with the binary, flattening the initial steeply-rising power-law cusps into the observed shallow cores. To the extent that the stars in this initial cusp are ejected to larger orbits, leaving a core, these remnants can be thought of as having “missing” light in their centers. We emphasize that this is completely consistent with there also being “extra light,” as we define it, in these galaxies. The “extra light” we refer to is the remnant of stars formed in dissipational central star formation events, and dominates the profile within rather large radii  $\sim \text{kpc}$ , blending smoothly onto the outer dissipationless profile. Scouring will flatten the nuclear peak or cusp of this dissipational remnant, but will not be likely to remove the  $\sim 10\%$  of the stellar mass that constitutes the dissipational starburst relic. Despite the terminology, “extra” and “missing” light are not mutually exclusive. In a strict physical sense, all ellipticals are dissipational/“extra light” ellipticals – they have all experienced some dissipational star formation. Of these dissipational ellipticals, there are “un-cored” or “un-scoured” (“power-law,” “cusp,” or “cuspy core”) ellipticals (presumably objects whose last major merger was gas-rich, allowing the black holes to merge quickly, and forming the central cusp via new star formation) and “cored” or “scoured” ellipticals (presumably the remnants of subsequent spheroid-spheroid “dry” re-mergers). The “missing light” is a core – a flattened nuclear profile as opposed to a continued steeply rising cusp – within the very center of the dense dissipational component.

Our methodology is robust to re-mergers and scouring: our two-component profiles still recover the dissipational component in simulations allowing for any reasonable model of nuclear scouring. However, we demonstrate that the same profile can be well-fitted by different assumed functional forms, and the parameters obtained from these fits – particularly in regards to the “extra” and “missing” light – are not trivially related and require careful interpretation. In particular, obser-

vations find that core ellipticals can be reasonably well-fit in a formal statistical sense by cored Sersic laws (an outer Sersic profile with an inner “flattening” or deficit), generally with high Sersic indices  $n_s \gtrsim 5$ , and we obtain consistent results fitting our re-merger simulations with these methods. There is no explicit “extra” component in these fits: rather, in our simulations, we find that the high  $n_s$  values – which extrapolate to high central densities before the flattening or deficit – implicitly reflect the extra light (that being the central, dense component that enables the high- $n_s$  fit; otherwise the system would have a high outer  $n_s$  but a low central density, not resembling any Sersic profile). Because the re-merger has smeared out the light profile, removing characteristic features (or kinematic subsystems) that might have (in the original gas-rich merger remnant) been a more obvious indication of the transition to radii where stars formed dissipationally dominate the profile, the physical breakdown of these systems is not obvious from a strictly empirical standpoint. By calibrating different fitting methods with our simulations, we have attempting to provide an interpretive context and physical motivation for specific interpretations of these fits.

In a related manner, this raises some cautions regarding the purely empirical methods sometimes used to estimate how a profile has been modified by core scouring – i.e. how much mass is “missing” from the nuclear region (relative to the steep nuclear rise of the progenitor cusps). This is a subtle issue. There may of course be no light actually missing after scouring – rather, stars are scattered from small radii to large, flattening the central profile (what is really desired is an estimate of how much stellar mass has been scattered – i.e. how much stellar mass must be moved from the nuclear region to larger radii to explain the difference in profiles). So any such estimate is sensitive to the model for the nuclear profiles of the progenitors – equivalently, what the profile would be in the absence of scouring.

We explicitly consider one such (commonly adopted) model, where the implicitly assumed progenitor profile is based on the inwards extrapolation of an outer Sersic law (as in e.g. core-Sersic fits). In these fits, the effects described above (effects on the profile at larger radii than the core itself) can lead to a very large outer Sersic index in the formal best fit; in the high- $n_s$  regime ( $n_s \gtrsim 6$ ), the nature of the Sersic profile is such that these profiles then rise steeply at small radii (more steeply even than the power-law nuclear profiles of cusp ellipticals), and a small change in the outer profile (raising  $n_s$ ) can substantially raise the extrapolated (and assumed “pre-merger”) inner profile. This can bias the estimate of the “missing light” fraction towards very high values ( $\sim 1\text{--}5\%$ ) and literally interpreted can make it appear as if the “core” extends to radii  $\sim \text{kpc}$ . In fact, we find that adopting this methodology in such cases, we would infer “missing light” at this level even in simulations where there is no physical scouring (i.e. there is no actual “missing light”). Moreover, if real, these values would imply scoured masses  $\sim 10\text{--}50 M_{\text{BH}}$ , in troubling disagreement with models of scouring which predict scoured mass deficits  $\sim 0.1\text{--}1 M_{\text{BH}}$  per major re-merger (see e.g. Milosavljević et al. 2002; Merritt 2006; Sesana et al. 2007). If stars from centrophilic orbits in tri-axial potentials allow the binary to coalesce rapidly (providing stars from near  $\sim R_e$ , where the loss of even  $\sim 10 M_{\text{BH}}$  makes no difference to the profile, to harden the binary), as suggested in some idealized calculations (Berczik et al. 2006; Holley-Bockelmann & Sigurdsson 2006) and merger remnant simulations (Hoffman et al. 2009), the difficulty for the mod-

els in explaining such large “missing masses” grows.

Given the steep dependence of the implicitly assumed central progenitor profile on Sersic index in this regime, and the appearance of “missing light” even in simulations without scouring given a literal interpretation of this fitting methodology, it is likely that the “problems” for the scouring models in these extreme cases reflect more the observational uncertainty regarding the appropriate “un-scoured” profile, rather than fundamental uncertainties in the physics of scouring. Future work, as observations and models improve, should attempt to carefully model the progenitor profiles and develop estimators that are less sensitive to the profile shape at radii much larger than the core itself. An important test for any such estimators should be that re-merged progenitors with initially cuspy profiles (down to the desired resolution limits), without scouring included, should typically yield little or no “missing light.” We briefly consider a couple of possibilities for such estimators of the scoured mass (less sensitive to the large scale radii), and obtain (re-analyzing the observations) typical scoured mass estimates of  $\sim 0.5 - 3 M_{\text{BH}}$ , in better agreement with scouring models.

Further study, in particular observation of the nuclear regions  $\sim R_{\text{BH}}$  is needed to test models of scouring and test the accuracy of different estimators for the scoured stellar mass. For example, scouring is expected to preferentially eliminate stars on radial orbits and leave a bias for tangential orbits within the radius affected (e.g. Quinlan & Hernquist 1997). Gebhardt et al. (2003) see tentative evidence for this in a limited sample of ellipticals; the major-axis radii within which the effect appears are generally  $\sim 0.5 - 3 R_{\text{BH}}$ , as expected in scouring theories and our revised inferences from core profiles. A preliminary comparison supports our conclusions (and caveats) here, but the number of relevant ellipticals is small. If similar observations can be obtained for a sample of ellipticals with alternative estimates of the missing mass fraction, it can be determined whether some estimators are biased towards putting too much or too little of the profile into the scoured component.

#### 11.4. Summary

We have developed a paradigm to understand the structure of both cusp and core ellipticals, in which there are fundamentally two stellar components: a dissipational central starburst component and a more extended violently relaxed component. We have shown that the separation between these components can be inferred with observations of sufficient quality, and used to understand the formation history of ellipticals as a function of a wide range of properties. This allows us to demonstrate that dissipation is critical to understanding the properties of ellipticals, including (but not limited to) the structure of their surface brightness profiles, their sizes, ellipticities, isophotal shapes and rotation, age, color, and metallicity gradients (and their evolution), and the gas content and properties of their progenitors.

In particular, we argue here that this remains true for ellipticals with cores and re-merger remnants – in other words, *all ellipticals, including core ellipticals, are fundamentally “extra light” ellipticals*. The core ellipticals form a continuous family with the cusp ellipticals in terms of their dissipational content, as expected if these cusp ellipticals are their progenitors and if the number of re-mergers (if important) has not been large ( $\sim 1 - 3$  major re-mergers) for the typical core elliptical. We demonstrate that, despite the possibility that these systems have expanded via re-mergers, the degree of dissipa-

tion in the original gas-rich merger (the memory of which is retained in the surface brightness profile) remains the most important factor determining the size, gradient strength, and other properties of the remnant.

We have studied the properties and identified robust trends of dissipational stellar remnants in the nuclei of elliptical galaxies with cores and remnants of gas-poor, spheroid-spheroid re-mergers, across a large set of simulations, in which we vary e.g. the galaxy masses, initial gas fractions, concentrations, halo masses, presence or absence of bulges, presence or absence of black holes, feedback parameters from supernovae and stellar winds, orbital parameters and disk inclinations, and mass ratios of the merging galaxies. This range of parameters allows us to identify the most important physics.

As we found in Paper I and Paper II, the most important factor determining the structure of the remnant (insofar as the properties we consider are concerned) is how much mass is in the original (in the original or last spheroid forming, gas-rich merger) dissipationless (violently relaxed) component, versus the mass fraction in the dissipational (starburst) component. Orbital parameters and initial galaxy structure can, in principle, affect the remnant surface brightness profile significantly, but only indirectly, insofar as these help to set the amount of gas which will be available at the time of the final coalescence of the galaxy nuclei (i.e. how much mass ends up in the starburst component, as opposed to being violently relaxed in this final merger).

Re-mergers will expand the original gas-rich merger remnants, and smooth the profile (scattering stars substantially about their mean final radii), but, as it is well established that dissipationless mergers conserve (in a mean sense) particle rank order in binding energy and therefore radius (Barnes 1988), they will preserve these components. In other words, the product of a re-merger is, to lowest order, the sum of the two progenitor spheroid dissipationless components (constituting the nearly self-similar outer violently relaxed component) and their inner dissipational/starburst components (constituting the central dissipational/starburst remnant component of the final re-merger remnant, despite the fact that there might be little or no new dissipation in the re-merger).

We have demonstrated that this makes predictions for how fundamental plane scalings arise, which we study further in Hopkins et al. (2008b). We make a wide range of new predictions for the distributions of these properties and how they scale with the degree of dissipation, and how they should scale with each other and various other observational proxies for this degree of dissipation (which we define herein). We have predicted and shown (given these proxies) that dissipation is indeed more important (contributing a larger mass fraction) in low-mass ellipticals, in line with expectations based on how gas fractions are known to scale with disk mass. Testing all of these with better observations should be possible in the near future, with well-defined samples of ellipticals and continued improvements in mapping e.g. the surface brightness profiles, stellar populations and their gradients, and structural properties of ellipticals over a wide dynamic range.

Given our decompositions, we observationally confirm the long-standing prediction of the merger hypothesis, that sufficient dissipation should have occurred in the inner regions of ellipticals to explain the discrepancy between their central densities and those of their progenitor spirals, a confirmation that fits well in line with what is now well-established in gas-rich merger simulations and is also directly seen in progress

in ongoing/recent mergers, which have (through clear recent central star formation) raised their phase space densities to be comparable to ellipticals (Kormendy & Sanders 1992; Doyon et al. 1994; Genzel et al. 2001; Rothberg & Joseph 2006; Tacconi et al. 2002; Dasyra et al. 2007). We show that this is true for the core elliptical population just as we demonstrated it for merger remnants in Paper I and cusp ellipticals in Paper II. In other words, the *same* mechanism can explain the central densities in both cusp and core ellipticals – while core ellipticals may be modified by subsequent re-mergers, no alternative formation mechanism for them (in the sense of formation of their spheroid progenitors) is required.

We demonstrate some important caveats in observational studies of core ellipticals. These ellipticals are multi-component (dissipational plus dissipationless, in the physical sense above) galaxies, but they have shallow nuclear profiles (central cores) instead of steeply rising central cusps, and can therefore be thought of as “missing light” galaxies in the sense that some process (e.g. scattering of stars from a black hole binary) has flattened the nuclear profile slope to create the core. This is fundamentally different from the processes involved in the evolution of the “extra light” (by which we mean the remnant of the starburst/dissipational star formation) and they should not be confused – whatever process forms cores likely acts on small scales and involves a relatively small fraction of the galaxy mass, much less than the  $\sim$ kpc scales and  $\sim$  10% of the galaxy mass that are characteristic of the dissipational component. Owing to the smoothing of the outer profile in a re-merger, re-merger remnants can often be better fit (in a purely formal sense) by e.g. single Sersic profiles with central deficits or core-Sersic laws: where observed, we argue that this is an indication of such re-mergers, but we stress that it does not mean the galaxies are not, in fact, two-component objects in a physical sense (simply that the fitted function reflects some combination of the two components). For this reason, the two-component profiles adopted here lend themselves to more direct physical interpretation and comparison with galaxy formation models. Furthermore, we demonstrate that care is needed when using such core-Sersic fits as an estimator of the “scoured” nuclear mass – when the outer Sersic index is large, the inferred “missing mass” can be quite sensitive to the details of the profile at large radii. This may explain estimates of scoured masses which are much larger than those predicted by models of core creation.

There are, of course, other changes to galaxy properties in re-mergers. As discussed in Paper I and Paper II, gas which survives the original spheroid-forming gas-rich merger will quiescently settle into the galaxy and form kinematic sub-components (in particular, embedded disks and kinematically decoupled nuclear components). We demonstrated that these do not contribute significantly to the surface brightness profile, and therefore they are not evident in our analysis. However, Cox et al. (2006b) and other numerical studies of

gas-rich mergers (Naab et al. 2006a; Burkert et al. 2008) have demonstrated that these subsystems can contribute strongly to the isophotal shapes (in particular driving the diskyness of the remnant) and kinematics, yielding distributions of shape and kinematic properties (including ellipticity, isophotal shape  $a_4/a$ , rotation  $(v/\sigma)^*$ , anisotropy, triaxiality, and kinematic misalignments) in good agreement with observed cusp or disk, rapidly rotating  $\sim L_*$  ellipticals.

The evolution of these sub-systems in re-mergers is not readily apparent in the surface brightness profiles of the remnants – their contribution to the profile is much less than the smoothing effects and variations introduced by the re-merger (shown in § 4). However, their evolution in re-mergers is briefly discussed in § 8 and will be studied in detail in Cox et al. (2009), who show that they are generically destroyed by major spheroid-spheroid re-mergers. This explains the significant effects on the global kinematic properties of re-merged ellipticals shown in § 8 – making them rounder, boxier, and more slowly rotating, in agreement with the observed properties of massive core or boxy, slowly rotating ellipticals. But effects on the velocity field in detail (as a function of radius, at higher order in the velocity moments, and in spatial distribution rather than just azimuthal average) will be more pronounced, and present opportunities not just to test whether or not re-mergers are good analogs to boxy/slowly-rotating ellipticals, but to distinguish the extent to which substructure and kinematic subcomponents contribute to these rotation/isophotal shape properties, as opposed to e.g. global angular momentum content or features of the spheroid potential. Kinematic misalignments, kinematically decoupled sub-systems, triaxiality, and trends of isotropy with radius are also more sensitive to orbital parameters (see e.g. Cox et al. 2006b; Boylan-Kolchin et al. 2006; Jesseit et al. 2007) and may distinguish merger histories with preferences for certain orbital configurations (possible if e.g. massive galaxies accrete minor companions preferentially along filaments). These more detailed, “second-order” structural parameters may therefore represent a more sensitive probe of the re-merger history (i.e. the history of subsequent mergers after the original, spheroid forming gas-rich merger), while the “first-order” parameter (the light profile) retains a memory of the degree of dissipation imprinted in the *original* gas-rich merger.

We thank Marijn Franx, Josh Younger, and Barry Rothberg for helpful discussions and contributed data sets used in this paper. We also thank the anonymous referee for helpful advice on the content herein. This work was supported in part by NSF grants ACI 96-19019, AST 00-71019, AST 02-06299, and AST 03-07690, and NASA ATP grants NAG5-12140, NAG5-13292, and NAG5-13381. Support for TJC was provided by the W. M. Keck Foundation. JK’s work was supported in part by NSF grant AST 06-07490.

## REFERENCES

- Baldry, I. K., Glazebrook, K., Brinkmann, J., Ivezić, Ž., Lupton, R. H., Nichol, R. C., & Szalay, A. S. 2004, *ApJ*, 600, 681  
 Barbon, R., Benacchio, L., Capaccioli, M., & Rampazzo, R. 1984, *A&A*, 137, 166  
 Barnes, J. E. 1988, *ApJ*, 331, 699  
 Barnes, J. E., & Hernquist, L. 1996, *ApJ*, 471, 115  
 Barnes, J. E., & Hernquist, L. E. 1991, *ApJ*, 370, L65  
 Begelman, M. C., Blandford, R. D., & Rees, M. J. 1980, *Nature*, 287, 307  
 Bell, E. F., & de Jong, R. S. 2001, *ApJ*, 550, 212  
 Bell, E. F., et al. 2006, *ApJ*, 640, 241  
 Bender, R. 1988, *A&A*, 193, L7  
 Bender, R., Burstein, D., & Faber, S. M. 1992, *ApJ*, 399, 462  
 —. 1993, *ApJ*, 411, 153  
 Bender, R., Doebereiner, S., & Moellenhoff, C. 1987, *A&A*, 177, L53  
 —. 1988, *A&AS*, 74, 385  
 Bender, R., Saglia, R. P., & Gerhard, O. E. 1994, *MNRAS*, 269, 785  
 Bender, R., Surma, P., Doebereiner, S., Moellenhoff, C., & Madejsky, R. 1989, *A&A*, 217, 35  
 Bender, R., et al. 2007, *ApJ*, in preparation  
 Berczik, P., Merritt, D., Spurzem, R., & Bischof, H.-P. 2006, *ApJ*, 642, L21

- Binggeli, B., Sandage, A., & Tammann, G. A. 1985, *AJ*, 90, 1681  
 Binney, J., & Tremaine, S. 1987, *Galactic dynamics* (Princeton, NJ, Princeton University Press, 1987)  
 Blanton, M. R., Eisenstein, D., Hogg, D. W., Schlegel, D. J., & Brinkmann, J. 2005, *ApJ*, 629, 143  
 Böker, T., Sarzi, M., McLaughlin, D. E., van der Marel, R. P., Rix, H.-W., Ho, L. C., & Shields, J. C. 2004, *AJ*, 127, 105  
 Bolton, A. S., Treu, T., Koopmans, L. V. E., Gavazzi, R., Moustakas, L. A., Burles, S., Schlegel, D. J., & Wayth, R. 2008, *ApJ*, 684, 248  
 Borch, A., et al. 2006, *A&A*, 453, 869  
 Boylan-Kolchin, M., Ma, C.-P., & Quataert, E. 2005, *MNRAS*, 362, 184  
 —. 2006, *MNRAS*, 369, 1081  
 Bundy, K., Ellis, R. S., & Conselice, C. J. 2005, *ApJ*, 625, 621  
 Bundy, K., et al. 2006, *ApJ*, 651, 120  
 Burkert, A., Naab, T., Johansson, P. H., & Jesseit, R. 2008, *ApJ*, 685, 897  
 Byun, Y.-I., et al. 1996, *AJ*, 111, 1889  
 Caon, N., Capaccioli, M., & D’Onofrio, M. 1993, *MNRAS*, 265, 1013  
 —. 1994, *A&AS*, 106, 199  
 Caon, N., Capaccioli, M., & Rampazzo, R. 1990, *A&AS*, 86, 429  
 Cappellari, M., et al. 2006, *MNRAS*, 366, 1126  
 —. 2007, *MNRAS*, 379, 418  
 Carlberg, R. G. 1986, *ApJ*, 310, 593  
 Carollo, C. M. 1999, *ApJ*, 523, 566  
 Chabrier, G. 2003, *PASP*, 115, 763  
 Ciotti, L., & Ostriker, J. P. 2007, *ApJ*, 665, 1038  
 Conroy, C., Wechsler, R. H., & Kravtsov, A. V. 2007, *ApJ*, 668, 826  
 Côté, P., et al. 2006, *ApJS*, 165, 57  
 —. 2007, *ApJ*, 671, 1456  
 Covington, M., Dekel, A., Cox, T. J., Jonsson, P., & Primack, J. R. 2008, *MNRAS*, 384, 94  
 Cox, T., et al. 2009, *ApJ*, in preparation  
 Cox, T. J., Di Matteo, T., Hernquist, L., Hopkins, P. F., Robertson, B., & Springel, V. 2006a, *ApJ*, 643, 692  
 Cox, T. J., Dutta, S. N., Di Matteo, T., Hernquist, L., Hopkins, P. F., Robertson, B., & Springel, V. 2006b, *ApJ*, 650, 791  
 Crane, P., et al. 1993, *AJ*, 106, 1371  
 Dasyra, K. M., et al. 2007, *ApJ*, 657, 102  
 Davies, R. L., Efstathiou, G., Fall, S. M., Illingworth, G., & Schechter, P. L. 1983, *ApJ*, 266, 41  
 Davis, L. E., Cawson, M., Davies, R. L., & Illingworth, G. 1985, *AJ*, 90, 169  
 De Lorenzi, F. o. 2008, *MNRAS*, in press, arXiv: 0804.3350 [astro-ph], 804  
 De Lucia, G., Springel, V., White, S. D. M., Croton, D., & Kauffmann, G. 2006, *MNRAS*, 366, 499  
 de Vaucouleurs, G. 1948, *Annales d’Astrophysique*, 11, 247  
 de Zeeuw, T. 1985, *MNRAS*, 216, 273  
 Djorgovski, S., & Davis, M. 1987, *ApJ*, 313, 59  
 Doyon, R., Wells, M., Wright, G. S., Joseph, R. D., Nadeau, D., & James, P. A. 1994, *ApJ*, 437, L23  
 Dressler, A., Lynden-Bell, D., Burstein, D., Davies, R. L., Faber, S. M., Terlevich, R., & Wegner, G. 1987, *ApJ*, 313, 42  
 Emsellem, E., et al. 2004, *MNRAS*, 352, 721  
 —. 2007, *MNRAS*, 379, 401  
 Erb, D. K., Steidel, C. C., Shapley, A. E., Pettini, M., Reddy, N. A., & Adelberger, K. L. 2006, *ApJ*, 646, 107  
 Faber, S. M., Tremaine, S., Ajhar, E. A., Byun, Y.-I., Dressler, A., Gebhardt, K., Grillmair, C., Kormendy, J., Lauer, T. R., & Richstone, D. 1997, *AJ*, 114, 1771  
 Faber, S. M., Wegner, G., Burstein, D., Davies, R. L., Dressler, A., Lynden-Bell, D., & Terlevich, R. J. 1989, *ApJS*, 69, 763  
 Ferrarese, L., van den Bosch, F. C., Ford, H. C., Jaffe, W., & O’Connell, R. W. 1994, *AJ*, 108, 1598  
 Ferrarese, L., et al. 2006, *ApJS*, 164, 334  
 Fontana, A., et al. 2006, *A&A*, 459, 745  
 Franceschini, A., et al. 2006, *A&A*, 453, 397  
 Gallagher, III, J. S., & Ostriker, J. P. 1972, *AJ*, 77, 288  
 Gallazzi, A., Charlot, S., Brinchmann, J., & White, S. D. M. 2006, *MNRAS*, 370, 1106  
 Gallazzi, A., Charlot, S., Brinchmann, J., White, S. D. M., & Tremonti, C. A. 2005, *MNRAS*, 362, 41  
 Gebhardt, K., et al. 1996, *AJ*, 112, 105  
 —. 2003, *ApJ*, 583, 92  
 Genzel, R., Tacconi, L. J., Rigopoulou, D., Lutz, D., & Tecza, M. 2001, *ApJ*, 563, 527  
 Graham, A. W. 2001, *AJ*, 121, 820  
 Graham, A. W., Erwin, P., Trujillo, I., & Asensio Ramos, A. 2003, *AJ*, 125, 2951  
 Gualandris, A., & Merritt, D. 2007, in *Black Holes*, ed. M. Livio & A. M. Koekemoer, STScI Spring Symposium [arXiv:0708.3083]  
 Gunn, J. E. 1987, in *Nearly Normal Galaxies. From the Planck Time to the Present* (New York: Springer-Verlag), ed. S. M. Faber, 455–464  
 Hausman, M. A., & Ostriker, J. P. 1978, *ApJ*, 224, 320  
 Hernquist, L. 1990, *ApJ*, 356, 359  
 —. 1992, *ApJ*, 400, 460  
 —. 1993, *ApJ*, 409, 548  
 Hernquist, L., & Barnes, J. E. 1991, *Nature*, 354, 210  
 Hernquist, L., Spergel, D. N., & Heyl, J. S. 1993, *ApJ*, 416, 415  
 Hoffman, L., et al. 2009, *ApJ*, in preparation  
 Holley-Bockelmann, K., & Sigurdsson, S. 2006, *ArXiv Astrophysics e-prints*  
 Hopkins, P. F., Cox, T. J., Dutta, S. N., Hernquist, L., Kormendy, J., & Lauer, T. R. 2008a, *ApJ*, accepted, arXiv:0805.3533 [astro-ph], 805  
 Hopkins, P. F., Cox, T. J., & Hernquist, L. 2008b, *ApJ*, 689, 17  
 Hopkins, P. F., Cox, T. J., Kereš, D., & Hernquist, L. 2008c, *ApJS*, 175, 390  
 Hopkins, P. F., Cox, T. J., Younger, J. D., & Hernquist, L. 2009, *ApJ*, 691, 1168  
 Hopkins, P. F., Hernquist, L., Cox, T. J., Di Matteo, T., Robertson, B., & Springel, V. 2006a, *ApJS*, 163, 1  
 Hopkins, P. F., Hernquist, L., Cox, T. J., Dutta, S. N., & Rothberg, B. 2008d, *ApJ*, 679, 156  
 Hopkins, P. F., Hernquist, L., Cox, T. J., & Kereš, D. 2008e, *ApJS*, 175, 356  
 Hopkins, P. F., Hernquist, L., Cox, T. J., Robertson, B., & Springel, V. 2006b, *ApJS*, 163, 50  
 Hopkins, P. F., Hernquist, L., Cox, T. J., Younger, J. D., & Besla, G. 2008f, *ApJ*, 688, 757  
 Hopkins, P. F., Lidz, A., Hernquist, L., Coil, A. L., Myers, A. D., Cox, T. J., & Spergel, D. N. 2007a, *ApJ*, 662, 110  
 Hopkins, P. F., Richards, G. T., & Hernquist, L. 2007b, *ApJ*, 654, 731  
 Hyde, J. B., & Bernardi, M. 2008, *MNRAS*, in press, arXiv:0810.4924 [astro-ph]  
 Jedrzejewski, R. I., Davies, R. L., & Illingworth, G. D. 1987, *AJ*, 94, 1508  
 Jesseit, R., Cappellari, M., Naab, T., Emsellem, E., & Burkert, A. 2008, *MNRAS*, in press, arXiv:0810.0137 [astro-ph]  
 Jesseit, R., Naab, T., Peletier, R. F., & Burkert, A. 2007, *MNRAS*, 376, 997  
 Joseph, R. D., & Wright, G. S. 1985, *MNRAS*, 214, 87  
 Kannappan, S. J. 2004, *ApJ*, 611, L89  
 King, I. R. 1978, *ApJ*, 222, 1  
 Kormendy, J. 1982, in *Saas-Fee Advanced Course 12: Morphology and Dynamics of Galaxies* (Observatoire de Geneve), ed. L. Martinet & M. Mayor, 113–288  
 Kormendy, J. 1985a, *ApJ*, 292, L9  
 —. 1985b, *ApJ*, 295, 73  
 Kormendy, J. 1987a, in *IAU Symposium, Vol. 127, Structure and Dynamics of Elliptical Galaxies*, ed. P. T. de Zeeuw, 17–34  
 Kormendy, J. 1987b, in *Nearly Normal Galaxies. From the Planck Time to the Present* (New York: Springer-Verlag), ed. S. M. Faber, 163–174  
 —. 1989, *ApJ*, 342, L63  
 Kormendy, J. 1999, in *Astronomical Society of the Pacific Conference Series, Vol. 182, Galaxy Dynamics - A Rutgers Symposium*, ed. D. R. Merritt, M. Valluri, & J. A. Sellwood, 124+  
 Kormendy, J., & Bender, R. 1996, *ApJ*, 464, L119+  
 Kormendy, J., Dressler, A., Byun, Y.-I., Faber, S. M., Grillmair, C., Lauer, T. R., Richstone, D., & Tremaine, S. 1994, in *Dwarf Galaxies*, ed. G. Meylan & P. Prugniel, 147+  
 Kormendy, J., Fisher, D. B., Cornell, M. E., & Bender, R. 2008, *ApJ*, in press, arXiv:0810.1681 [astro-ph]  
 Kormendy, J., Gebhardt, K., Fisher, D. B., Drory, N., Macchetto, F. D., & Sparks, W. B. 2005, *AJ*, 129, 2636  
 Kormendy, J., & Illingworth, G. 1982, *ApJ*, 256, 460  
 Kormendy, J., & Sanders, D. B. 1992, *ApJ*, 390, L53  
 Krajnović, D., et al. 2008, *MNRAS*, 390, 93  
 Kuntschner, H., et al. 2006, *MNRAS*, 369, 497  
 Laine, S., van der Marel, R. P., Lauer, T. R., Postman, M., O’Dea, C. P., & Owen, F. N. 2003, *AJ*, 125, 478  
 Lauer, T. R. 1985a, *ApJS*, 57, 473  
 —. 1985b, *ApJ*, 292, 104  
 Lauer, T. R., Ajhar, E. A., Byun, Y.-I., Dressler, A., Faber, S. M., Grillmair, C., Kormendy, J., Richstone, D., & Tremaine, S. 1995, *AJ*, 110, 2622  
 Lauer, T. R., et al. 1991, *ApJ*, 369, L41  
 —. 1992a, *AJ*, 104, 552  
 —. 1992b, *AJ*, 103, 703  
 —. 2005, *AJ*, 129, 2138  
 —. 2007a, *ApJ*, 664, 226  
 —. 2007b, *ApJ*, 662, 808



- Li, Y., Hernquist, L., Robertson, B., Cox, T. J., Hopkins, P. F., Springel, V., Gao, L., Di Matteo, T., Zentner, A. R., Jenkins, A., & Yoshida, N. 2007, *ApJ*, 665, 187
- Lin, L., et al. 2004, *ApJ*, 617, L9
- 2008, *ApJ*, 681, 232
- Liu, Y., Zhou, X., Ma, J., Wu, H., Yang, Y., Li, J., & Chen, J. 2005, *AJ*, 129, 2628
- Maller, A. H., Katz, N., Kereš, D., Davé, R., & Weinberg, D. H. 2006, *ApJ*, 647, 763
- Masjedi, M., Hogg, D. W., & Blanton, M. R. 2008, *ApJ*, 679, 260
- Masjedi, M., et al. 2006, *ApJ*, 644, 54
- McDermid, R. M., et al. 2006, *MNRAS*, 373, 906
- McGaugh, S. S. 2005, *ApJ*, 632, 859
- Mehlert, D., Thomas, D., Saglia, R. P., Bender, R., & Wegner, G. 2003, *A&A*, 407, 423
- Merritt, D. 2006, *ApJ*, 648, 976
- Michard, R. 2006, *A&A*, 449, 519
- Mihos, J. C., & Hernquist, L. 1994a, *ApJ*, 437, L47
- 1994b, *ApJ*, 427, 112
- 1994c, *ApJ*, 431, L9
- Milosavljević, M., Merritt, D., Rest, A., & van den Bosch, F. C. 2002, *MNRAS*, 331, L51
- Monaco, P., Murante, G., Borgani, S., & Fontanot, F. 2006, *ApJ*, 652, L89
- Naab, T., Jesseit, R., & Burkert, A. 2006a, *MNRAS*, 372, 839
- Naab, T., Johansson, P. H., Ostriker, J. P., & Efstathiou, G. 2007, *ApJ*, 658, 710
- Naab, T., Khochfar, S., & Burkert, A. 2006b, *ApJ*, 636, L81
- Navarro, J. F., Frenk, C. S., & White, S. D. M. 1996, *ApJ*, 462, 563
- Nelan, J. E., et al. 2005, *ApJ*, 632, 137
- Ostriker, J. P. 1980, *Comments on Astrophysics*, 8, 177
- Ostriker, J. P., & Tremaine, S. D. 1975, *ApJ*, 202, L113
- Pannella, M., Hopp, U., Saglia, R. P., Bender, R., Drory, N., Salvato, M., Gabasch, A., & Feulner, G. 2006, *ApJ*, 639, L1
- Peletier, R. F., Davies, R. L., Illingworth, G. D., Davis, L. E., & Cawson, M. 1990, *AJ*, 100, 1091
- Postman, M., & Lauer, T. R. 1995, *ApJ*, 440, 28
- Prugniel, P., & Simien, F. 1997, *A&A*, 321, 111
- Purcell, C. W., Bullock, J. S., & Zentner, A. R. 2007, *ApJ*, 666, 20
- Quillen, A. C., Bower, G. A., & Stritzinger, M. 2000, *ApJS*, 128, 85
- Quinlan, G. D., & Hernquist, L. 1997, *New Astronomy*, 2, 533
- Ratcliff, S. J., & Burstein, D. 1982, *AJ*, 87, 1648
- Ravindranath, S., Ho, L. C., Peng, C. Y., Filippenko, A. V., & Sargent, W. L. W. 2001, *AJ*, 122, 653
- Reda, F. M., Proctor, R. N., Forbes, D. A., Hau, G. K. T., & Larsen, S. S. 2007, *MNRAS*, 377, 1772
- Reichardt, C., Jimenez, R., & Heavens, A. F. 2001, *MNRAS*, 327, 849
- Rest, A., van den Bosch, F. C., Jaffe, W., Tran, H., Tsvetanov, Z., Ford, H. C., Davies, J., & Schafer, J. 2001, *AJ*, 121, 2431
- Robertson, B., Cox, T. J., Hernquist, L., Franx, M., Hopkins, P. F., Martini, P., & Springel, V. 2006a, *ApJ*, 641, 21
- Robertson, B., Hernquist, L., Cox, T. J., Di Matteo, T., Hopkins, P. F., Martini, P., & Springel, V. 2006b, *ApJ*, 641, 90
- Rothberg, B., & Joseph, R. D. 2004, *AJ*, 128, 2098
- 2006, *AJ*, 131, 185
- Sánchez-Blázquez, P., Forbes, D. A., Strader, J., Brodie, J., & Proctor, R. 2007, *MNRAS*, 377, 759
- Schwarzschild, M. 1979, *ApJ*, 232, 236
- Schweizer, F. 1996, *AJ*, 111, 109
- Schweizer, F., & Seitzer, P. 1998, *AJ*, 116, 2206
- 2007, *AJ*, 133, 2132
- Sersic, J. L. 1968, *Atlas de galaxias australes* (Cordoba, Argentina: Observatorio Astronomico, 1968)
- Sesana, A., Haardt, F., & Madau, P. 2007, *ApJ*, 660, 546
- Shapley, A. E., Coil, A. L., Ma, C.-P., & Bundy, K. 2005, *ApJ*, 635, 1006
- Shen, S., Mo, H. J., White, S. D. M., Blanton, M. R., Kauffmann, G., Voges, W., Brinkmann, J., & Csabai, I. 2003, *MNRAS*, 343, 978
- Simien, F., & Prugniel, P. 1997a, *A&AS*, 122, 521
- 1997b, *A&AS*, 126, 15
- 1997c, *A&AS*, 126, 519
- 2002, *A&A*, 384, 371
- Somerville, R. S., Hopkins, P. F., Cox, T. J., Robertson, B. E., & Hernquist, L. 2008, *MNRAS*, in press, arXiv:0808.1227 [astro-ph]
- Springel, V. 2005, *MNRAS*, 364, 1105
- Springel, V., Di Matteo, T., & Hernquist, L. 2005, *MNRAS*, 361, 776
- Springel, V., & Hernquist, L. 2002, *MNRAS*, 333, 649
- 2003, *MNRAS*, 339, 289
- Strateva, I., et al. 2001, *AJ*, 122, 1861
- Tacconi, L. J., Genzel, R., Lutz, D., Rigopoulou, D., Baker, A. J., Iserlohe, C., & Tecza, M. 2002, *ApJ*, 580, 73
- Thomas, D., Maraston, C., Bender, R., & Mendes de Oliveira, C. 2005, *ApJ*, 621, 673
- Titus, T. N., Spillar, E. J., & Johnson, P. 1997, *AJ*, 114, 958
- Trager, S. C., Faber, S. M., Worthey, G., & González, J. J. 2000, *AJ*, 119, 1645
- Trujillo, I., Asensio Ramos, A., Rubiño-Martín, J. A., Graham, A. W., Aguerri, J. A. L., Cepa, J., & Gutiérrez, C. M. 2002, *MNRAS*, 333, 510
- van Dokkum, P. G. 2005, *AJ*, 130, 2647
- Walcher, C. J., Böker, T., Charlot, S., Ho, L. C., Rix, H.-W., Rossa, J., Shields, J. C., & van der Marel, R. P. 2006, *ApJ*, 649, 692
- Wang, L., Li, C., Kauffmann, G., & de Lucia, G. 2006, *MNRAS*, 371, 537
- Weil, M. L., & Hernquist, L. 1994, *ApJ*, 431, L79
- 1996, *ApJ*, 460, 101
- Young, P. J., Westphal, J. A., Kristian, J., Wilson, C. P., & Landauer, F. P. 1978, *ApJ*, 221, 721
- Younger, J. D., Hopkins, P. F., Cox, T. J., & Hernquist, L. 2008, *ApJ*, 686, 815
- Zheng, Z., Coil, A. L., & Zehavi, I. 2007, *ApJ*, 667, 760

TABLE 1  
FITS TO CORE ELLIPTICALS

Name (1)	Ref. (2)	N <sub>phot</sub> (3)	M <sub>*</sub> (4)	M <sub>V</sub> (5)	σ (6)	R <sub>e</sub> (7)	ε (8)	100a <sub>4</sub> /a (9)	(v/σ)* (10)	n <sub>s</sub> (fit) (11)	n <sub>s</sub> (sim) (12)	f <sub>e</sub> (fit) (13)	f <sub>sb</sub> (sim) (14)
NGC 0584	2,3	5	11.27	-21.91	217	3.39	0.30	1.50	1.55	2.92 <sup>+0.05</sup> <sub>-0.19</sub>	2.77 <sup>+0.45</sup> <sub>-0.20</sub>	0.052 <sup>+0.004</sup> <sub>-0.019</sub>	0.103 <sup>+0.191</sup> <sub>-0.066</sub>
NGC 0720	2	4	11.64	-22.20	247	6.31	0.39	0.35	0.23	1.82 <sup>+0.81</sup> <sub>-0.20</sub>	2.39 <sup>+1.07</sup> <sub>-0.34</sub>	0.177 <sup>+0.043</sup> <sub>-0.010</sub>	0.096 <sup>+0.131</sup> <sub>-0.061</sub>
NGC 0741	2	1	12.25	-23.27	293	13.18	0.15	—	—	3.10	2.41 <sup>+0.69</sup> <sub>-0.08</sub>	0.026	0.076 <sup>+0.030</sup> <sub>-0.040</sub>
NGC 0777	3	3	11.65	-22.92	348	7.17	—	-0.20	0.28	2.33 <sup>+0.16</sup> <sub>-0.16</sub>	2.98 <sup>+1.94</sup> <sub>-0.82</sub>	0.118 <sup>+0.006</sup> <sub>-0.006</sub>	0.076 <sup>+0.105</sup> <sub>-0.047</sub>
NGC 1316	2	1	12.27	-23.32	250	7.24	0.37	1.00	0.91	2.11	2.48 <sup>+0.79</sup> <sub>-0.76</sub>	0.075	0.105 <sup>+0.114</sup> <sub>-0.035</sub>
NGC 1374	2	1	10.71	-20.57	207	2.57	0.11	—	—	4.37	1.95 <sup>+1.32</sup> <sub>-0.35</sub>	0.051	0.194 <sup>+0.115</sup> <sub>-0.092</sub>
NGC 1399	2	4	11.56	-22.07	359	4.17	0.12	0.10	0.25	2.61 <sup>+0.08</sup> <sub>-0.11</sub>	3.07 <sup>+0.26</sup> <sub>-0.26</sub>	0.142 <sup>+0.004</sup> <sub>-0.002</sub>	0.108 <sup>+0.127</sup> <sub>-0.048</sub>
NGC 1407	3	2	11.31	-22.20	285	3.32	0.05	-0.20	0.84	1.22 <sup>+0.26</sup> <sub>-0.26</sub>	2.53 <sup>+0.71</sup> <sub>-0.36</sub>	0.189 <sup>+0.033</sup> <sub>-0.033</sub>	0.103 <sup>+0.123</sup> <sub>-0.071</sub>
NGC 1600	2,3	4	11.93	-23.21	321	12.96	0.33	-1.20	0.05	1.32 <sup>+0.26</sup> <sub>-0.31</sub>	3.50 <sup>+0.49</sup> <sub>-0.76</sub>	0.224 <sup>+0.023</sup> <sub>-0.022</sub>	0.087 <sup>+0.048</sup> <sub>-0.040</sub>
NGC 1700	2	4	11.49	-21.95	234	4.37	0.29	0.90	0.80	4.44 <sup>+1.04</sup> <sub>-0.57</sub>	2.95 <sup>+1.98</sup> <sub>-0.79</sub>	0.011 <sup>+0.005</sup> <sub>-0.004</sub>	0.144 <sup>+0.163</sup> <sub>-0.055</sub>
NGC 2832	2	2	12.52	-23.76	330	31.62	0.30	-0.30	0.12	2.93 <sup>+0.04</sup> <sub>-0.04</sub>	3.19 <sup>+1.48</sup> <sub>-0.55</sub>	0.081 <sup>+0.004</sup> <sub>-0.004</sub>	0.070 <sup>+0.048</sup> <sub>-0.025</sub>
NGC 3379	2,3	7	11.03	-21.14	221	2.45	0.10	0.20	0.82	2.54 <sup>+0.38</sup> <sub>-0.81</sub>	3.06 <sup>+1.81</sup> <sub>-1.48</sub>	0.124 <sup>+0.018</sup> <sub>-0.018</sub>	0.190 <sup>+0.137</sup> <sub>-0.092</sub>
NGC 3607	3	3	10.88	-21.22	248	1.68	0.16	—	0.92	1.80 <sup>+0.07</sup> <sub>-0.32</sub>	3.11 <sup>+1.48</sup> <sub>-0.87</sub>	0.126 <sup>+0.016</sup> <sub>-0.000</sub>	0.229 <sup>+0.180</sup> <sub>-0.123</sub>
NGC 3608	2	3	11.02	-21.12	195	3.31	0.18	-0.20	0.44	2.68 <sup>+0.20</sup> <sub>-0.92</sub>	3.78 <sup>+1.15</sup> <sub>-1.11</sub>	0.108 <sup>+0.074</sup> <sub>-0.004</sub>	0.167 <sup>+0.152</sup> <sub>-0.072</sub>
NGC 3640	2,3	6	11.17	-21.53	180	3.75	0.21	-0.20	1.48	3.21 <sup>+1.14</sup> <sub>-0.17</sub>	2.92 <sup>+1.05</sup> <sub>-0.53</sub>	0.098 <sup>+0.016</sup> <sub>-0.060</sub>	0.154 <sup>+0.137</sup> <sub>-0.080</sub>
NGC 3842	2	1	12.19	-23.18	316	17.78	0.17	—	—	3.09	3.69 <sup>+0.37</sup> <sub>-0.65</sub>	0.045	0.085 <sup>+0.048</sup> <sub>-0.038</sub>
NGC 4168	3	3	10.91	-21.45	182	3.94	0.11	—	0.26	2.55 <sup>+0.22</sup> <sub>-0.59</sub>	2.90 <sup>+1.28</sup> <sub>-0.90</sub>	0.081 <sup>+0.000</sup> <sub>-0.006</sub>	0.077 <sup>+0.144</sup> <sub>-0.047</sub>
NGC 4261	1,3	4	11.41	-22.33	294	11.09	0.21	-1.30	0.10	2.40 <sup>+0.69</sup> <sub>-0.64</sub>	2.78 <sup>+1.47</sup> <sub>-0.38</sub>	0.105 <sup>+0.029</sup> <sub>-0.012</sub>	0.105 <sup>+0.124</sup> <sub>-0.068</sub>
NGC 4278	2,3	8	10.70	-20.52	259	2.02	0.16	—	0.71	3.91 <sup>+0.45</sup> <sub>-0.56</sub>	3.32 <sup>+1.47</sup> <sub>-1.85</sub>	0.119 <sup>+0.016</sup> <sub>-0.017</sub>	0.234 <sup>+0.112</sup> <sub>-0.121</sub>
NGC 4291	2,3	4	10.71	-20.63	259	1.60	0.25	-0.40	0.52	1.87 <sup>+1.84</sup> <sub>-0.23</sub>	2.92 <sup>+0.55</sup> <sub>-0.80</sub>	0.182 <sup>+0.008</sup> <sub>-0.008</sub>	0.230 <sup>+0.106</sup> <sub>-0.106</sub>
NGC 4365	1,2,3	7	11.59	-22.44	269	13.83	0.24	-1.10	0.08	2.61 <sup>+1.12</sup> <sub>-0.44</sub>	2.87 <sup>+1.02</sup> <sub>-0.53</sub>	0.067 <sup>+0.037</sup> <sub>-0.002</sub>	0.105 <sup>+0.147</sup> <sub>-0.053</sub>
NGC 4374	1,3	4	11.10	-22.43	287	8.29	0.14	-0.40	0.09	2.12 <sup>+1.13</sup> <sub>-0.34</sub>	2.57 <sup>+2.11</sup> <sub>-0.35</sub>	0.126 <sup>+0.011</sup> <sub>-0.010</sub>	0.215 <sup>+0.170</sup> <sub>-0.119</sub>
NGC 4382	1,2,3	4	11.26	-22.43	196	8.43	0.19	0.59	0.33	3.89 <sup>+1.11</sup> <sub>-1.35</sub>	3.11 <sup>+0.63</sup> <sub>-0.80</sub>	0.034 <sup>+0.008</sup> <sub>-0.010</sub>	0.090 <sup>+0.086</sup> <sub>-0.054</sub>
NGC 4406	1,2,3	7	11.36	-22.66	250	19.72	0.29	-0.70	0.18	2.81 <sup>+0.90</sup> <sub>-0.47</sub>	3.09 <sup>+1.11</sup> <sub>-0.91</sub>	0.033 <sup>+0.011</sup> <sub>-0.003</sub>	0.098 <sup>+0.040</sup> <sub>-0.068</sub>
NGC 4472	1,2,3	7	11.70	-23.12	287	16.34	0.16	-0.30	0.47	2.45 <sup>+0.65</sup> <sub>-0.35</sub>	3.32 <sup>+0.91</sup> <sub>-1.27</sub>	0.091 <sup>+0.010</sup> <sub>-0.042</sub>	0.045 <sup>+0.088</sup> <sub>-0.059</sub>
NGC 4473	2,3	6	10.91	-20.82	178	2.56	0.43	0.90	0.40	2.59 <sup>+0.35</sup> <sub>-0.75</sub>	3.49 <sup>+1.27</sup> <sub>-0.91</sub>	0.162 <sup>+0.036</sup> <sub>-0.036</sub>	0.216 <sup>+0.111</sup> <sub>-0.111</sub>
NGC 4486	1,2	4	11.93	-22.95	360	31.44	0.12	0.01	0.11	2.78 <sup>+1.93</sup> <sub>-0.22</sub>	2.71 <sup>+0.56</sup> <sub>-0.52</sub>	0.054 <sup>+0.031</sup> <sub>-0.001</sub>	0.083 <sup>+0.103</sup> <sub>-0.048</sub>
NGC 4489	1,3	3	9.82	-18.56	49	1.10	0.12	-0.20	1.48	1.06 <sup>+0.13</sup> <sub>-0.76</sub>	3.06 <sup>+0.43</sup> <sub>-0.43</sub>	0.214 <sup>+0.021</sup> <sub>-0.021</sub>	0.223 <sup>+0.127</sup> <sub>-0.127</sub>
NGC 4552	1,2,3	7	11.25	-21.46	261	7.74	0.07	0.01	0.28	2.58 <sup>+1.18</sup> <sub>-0.33</sub>	2.79 <sup>+1.46</sup> <sub>-0.83</sub>	0.136 <sup>+0.025</sup> <sub>-0.021</sub>	0.190 <sup>+0.214</sup> <sub>-0.092</sub>
NGC 4589	2,3	6	11.00	-21.45	215	4.38	0.20	—	0.57	3.40 <sup>+0.81</sup> <sub>-0.34</sub>	2.72 <sup>+1.74</sup> <sub>-0.74</sub>	0.045 <sup>+0.004</sup> <sub>-0.004</sub>	0.103 <sup>+0.123</sup> <sub>-0.066</sub>
NGC 4636	1,2,3	8	11.38	-21.96	191	16.28	0.18	-0.10	0.25	2.71 <sup>+0.76</sup> <sub>-0.89</sub>	2.91 <sup>+0.83</sup> <sub>-1.31</sub>	0.056 <sup>+0.007</sup> <sub>-0.017</sub>	0.076 <sup>+0.104</sup> <sub>-0.043</sub>
NGC 4649	1,2,3	7	11.73	-22.62	341	10.52	0.17	-0.50	0.46	2.77 <sup>+0.66</sup> <sub>-1.00</sub>	3.32 <sup>+1.05</sup> <sub>-0.86</sub>	0.083 <sup>+0.037</sup> <sub>-0.012</sub>	0.103 <sup>+0.116</sup> <sub>-0.070</sub>
NGC 4874	2	2	12.37	-23.49	290	61.66	0.09	-0.30	0.22	2.83 <sup>+0.01</sup> <sub>-0.01</sub>	4.22 <sup>+0.46</sup> <sub>-0.27</sub>	0.036 <sup>+0.000</sup> <sub>-0.000</sub>	0.074 <sup>+0.093</sup> <sub>-0.057</sub>
NGC 4889	2,3	4	12.20	-23.62	381	17.67	0.35	-0.25	0.05	1.58 <sup>+0.63</sup> <sub>-0.70</sub>	3.10 <sup>+0.80</sup> <sub>-0.67</sub>	0.145 <sup>+0.000</sup> <sub>-0.026</sub>	0.073 <sup>+0.052</sup> <sub>-0.028</sub>
NGC 5061	2	1	11.53	-22.01	194	3.55	0.04	—	—	3.55	3.07 <sup>+0.12</sup> <sub>-0.90</sub>	0.075	0.194 <sup>+0.143</sup> <sub>-0.103</sub>
NGC 5322	3	3	11.34	-22.21	224	4.68	—	-0.90	0.26	2.48 <sup>+0.26</sup> <sub>-0.26</sub>	1.88 <sup>+2.92</sup> <sub>-0.011</sub>	0.086 <sup>+0.011</sup> <sub>-0.011</sub>	0.103 <sup>+0.080</sup> <sub>-0.049</sub>
NGC 5419	2	1	12.30	-23.37	315	15.14	0.21	—	—	3.78	2.89 <sup>+0.33</sup> <sub>-0.32</sub>	0.049	0.087 <sup>+0.049</sup> <sub>-0.039</sub>
NGC 5490	3	3	11.35	-22.13	301	6.31	0.19	—	0.27	3.55 <sup>+0.39</sup> <sub>-0.39</sub>	2.75 <sup>+1.92</sup> <sub>-0.79</sub>	0.108 <sup>+0.005</sup> <sub>-0.006</sub>	0.106 <sup>+0.121</sup> <sub>-0.067</sub>
NGC 5557	2,3	4	11.31	-22.28	260	5.94	0.21	—	0.12	2.78 <sup>+0.61</sup> <sub>-1.41</sub>	3.01 <sup>+4.35</sup> <sub>-0.71</sub>	0.088 <sup>+0.052</sup> <sub>-0.006</sub>	0.105 <sup>+0.101</sup> <sub>-0.068</sub>
NGC 5576	2	3	11.13	-21.31	188	3.80	0.30	-0.50	0.22	4.87 <sup>+2.67</sup> <sub>-0.69</sub>	2.96 <sup>+0.38</sup> <sub>-0.43</sub>	0.240 <sup>+0.053</sup> <sub>-0.157</sub>	0.192 <sup>+0.116</sup> <sub>-0.094</sub>
NGC 5813	2,3	6	11.20	-21.68	238	9.82	0.16	0.01	0.51	3.16 <sup>+0.04</sup> <sub>-0.11</sub>	2.93 <sup>+1.32</sup> <sub>-0.84</sub>	0.044 <sup>+0.013</sup> <sub>-0.001</sub>	0.102 <sup>+0.081</sup> <sub>-0.041</sub>
NGC 5982	2	1	11.50	-21.97	250	5.01	0.27	—	—	3.02	2.77 <sup>+0.45</sup> <sub>-0.24</sub>	0.217	0.118 <sup>+0.111</sup> <sub>-0.034</sub>
NGC 6166	2	1	12.55	-23.80	300	67.61	0.28	—	0.08	2.73	3.09 <sup>+0.15</sup> <sub>-0.56</sub>	0.074	0.089 <sup>+0.137</sup> <sub>-0.042</sub>
NGC 6702	3	3	11.45	-22.26	182	6.39	0.23	-0.40	0.18	3.11 <sup>+0.57</sup> <sub>-1.85</sub>	1.85 <sup>+1.95</sup> <sub>-0.90</sub>	0.082 <sup>+0.027</sup> <sub>-0.002</sub>	0.089 <sup>+0.131</sup> <sub>-0.063</sub>
NGC 7052	3	3	11.48	-22.46	275	9.77	0.45	0.01	0.34	1.74 <sup>+0.16</sup> <sub>-0.20</sub>	3.51 <sup>+2.83</sup> <sub>-2.83</sub>	0.087 <sup>+0.002</sup> <sub>-0.009</sub>	0.085 <sup>+0.089</sup> <sub>-0.039</sub>
NGC 7385	3	3	11.95	-23.53	259	10.27	0.12	0.01	0.16	1.83 <sup>+1.04</sup> <sub>-0.37</sub>	1.55 <sup>+2.25</sup> <sub>-1.55</sub>	0.107 <sup>+0.017</sup> <sub>-0.017</sub>	0.087 <sup>+0.056</sup> <sub>-0.040</sub>
NGC 7619	2,3	4	11.60	-22.60	337	6.85	0.24	0.20	0.53	2.88 <sup>+0.39</sup> <sub>-0.34</sub>	2.67 <sup>+0.64</sup> <sub>-1.03</sub>	0.105 <sup>+0.007</sup> <sub>-0.006</sub>	0.103 <sup>+0.119</sup> <sub>-0.066</sub>
NGC 7785	2,3	4	11.48	-22.46	291	4.56	0.42	-1.50	0.47	1.75 <sup>+1.42</sup> <sub>-0.25</sub>	2.53 <sup>+3.06</sup> <sub>-2.02</sub>	0.092 <sup>+0.006</sup> <sub>-0.026</sub>	0.046 <sup>+0.109</sup> <sub>-0.016</sub>
IC 1459	2	3	11.81	-22.51	311	4.47	0.26	—	0.22	2.08 <sup>+2.39</sup> <sub>-0.56</sub>	4.67 <sup>+0.00</sup> <sub>-2.18</sub>	0.185 <sup>+0.073</sup> <sub>-0.131</sub>	0.126 <sup>+0.150</sup> <sub>-0.041</sub>
IC 4296	3	3	11.75	-23.18	323	5.86	0.10	0.00	0.64	1.81 <sup>+0.01</sup> <sub>-0.05</sub>	2.71 <sup>+0.38</sup> <sub>-0.38</sub>	0.139 <sup>+0.005</sup> <sub>-0.005</sub>	0.085 <sup>+0.031</sup> <sub>-0.031</sub>
IC 4329	2	2	12.63	-23.95	270	41.69	0.15	—	—	2.64 <sup>+0.65</sup> <sub>-0.65</sub>	3.19 <sup>+1.48</sup> <sub>-0.25</sub>	0.045 <sup>+0.024</sup> <sub>-0.024</sub>	0.079 <sup>+0.058</sup> <sub>-0.034</sub>
A0076-M1	2	1	12.07	-22.96	—	5.95	—	—	—	3.15	3.07 <sup>+0.12</sup> <sub>-0.13</sub>	0.086	0.117 <sup>+0.136</sup> <sub>-0.031</sub>
A0119-M1	2	2	12.67	-24.01	—	45.71	—	—	—	2.30 <sup>+0.03</sup> <sub>-0.03</sub>	2.91 <sup>+0.98</sup> <sub>-0.95</sub>	0.025 <sup>+0.001</sup> <sub>-0.001</sub>	0.047 <sup>+0.058</sup> <sub>-0.001</sub>
A0168-M1	2	2	12.16	-23.12	—	31.62	—	—	—	3.67 <sup>+0.22</sup> <sub>-0.22</sub>	3.18 <sup>+0.51</sup> <sub>-1.01</sub>	0.005 <sup>+0.001</sup> <sub>-0.001</sub>	0.047 <sup>+0.058</sup> <sub>-0.001</sub>
A0193-M1	2	1	12.61	-23.91	—	63.91	—	—	—	3.74	3.76 <sup>+0.91</sup> <sub>-1.16</sub>	0.037	0.076 <sup>+0.082</sup> <sub>-0.031</sub>
A0194-M1	2	1	12.11	-23.03	—	23.84	—	—	—	2.94	2.76 <sup>+0.12</sup> <sub>-0.12</sub>	0.056	0.074 <sup>+0.058</sup> <sub>-0.031</sub>
A0195-M1	2	2	11.89	-22.65	—	14.23	—	—	—	3.43 <sup>+0.06</sup> <sub>-0.06</sub>	2.91 <sup>+2.01</sup> <sub>-0.27</sub>	0.060 <sup>+0.002</sup> <sub>-0.002</sub>	0.081 <sup>+0.057</sup> <sub>-0.045</sub>
A0260-M1	2	1	12.36	-23.47	—	31.67	—	—	—	2.64	2.89 <sup>+0.33</sup> <sub>-0.36</sub>	0.067	0.060 <sup>+0.047</sup> <sub>-0.014</sub>
A0295-M1	2	2	12.15	-23.11	—	39.81	—	—	—	3.05 <sup>+0.01</sup> <sub>-0.01</sub>	3.10 <sup>+0.72</sup> <sub>-0.94</sub>	0.035 <sup>+0.000</sup> <sub>-0.000</sub>	0.047 <sup>+0.058</sup> <sub>-0.002</sub>
A0347-M1	2	1	12.01	-22.85	—	26.47	—	—	—	2.75	2.77 <sup>+0.45</sup> <sub>-0.20</sub>	0.127	0.087 <sup>+0.054</sup> <sub>-0.043</sub>
A0376-M1	2	1	12.43	-23.60	—	47.86	—	—	—	3.50	2.77 <sup>+0.45</sup> <sub>-0.20</sub>	0.032	0.047 <sup>+0.058</sup> <sub>-0.002</sub>
A0397-M1	2	1	12.33</										

TABLE 1 — *Continued*

Name (1)	Ref. (2)	$N_{\text{phot}}$ (3)	$M_*$ (4)	$M_V$ (5)	$\sigma$ (6)	$R_e$ (7)	$\epsilon$ (8)	$100a_4/a$ (9)	$(v/\sigma)^*$ (10)	$n_s$ (fit) (11)	$n_s$ (sim) (12)	$f_e$ (fit) (13)	$f_{sb}$ (sim) (14)
A0533-M1	2	4	11.91	-22.68	—	21.38	—	—	—	4.69 <sup>+1.22</sup> <sub>-1.87</sub>	2.89 <sup>+0.45</sup> <sub>-0.29</sub>	0.034 <sup>+0.002</sup> <sub>-0.003</sub>	0.085 <sup>+0.082</sup> <sub>-0.042</sub>
A0548-M1	2	4	11.95	-22.75	—	20.89	—	—	—	3.80 <sup>+2.80</sup> <sub>-0.42</sub>	2.84 <sup>+0.39</sup> <sub>-0.40</sub>	0.009 <sup>+0.025</sup> <sub>-0.002</sub>	0.077 <sup>+0.096</sup> <sub>-0.032</sub>
A0634-M1	2	1	11.92	-22.70	—	16.60	—	—	—	3.24	2.89 <sup>+0.33</sup> <sub>-0.32</sub>	0.319	0.086 <sup>+0.049</sup> <sub>-0.040</sub>
A0779-M1	2	1	12.54	-23.78	—	36.23	—	—	—	3.01	2.89 <sup>+0.33</sup> <sub>-0.32</sub>	0.076	0.074 <sup>+0.056</sup> <sub>-0.028</sub>
A0999-M1	2	1	11.78	-22.45	—	13.80	—	—	—	2.74	2.77 <sup>+0.45</sup> <sub>-0.20</sub>	0.179	0.087 <sup>+0.086</sup> <sub>-0.050</sub>
A1016-M1	2	1	11.67	-22.26	—	22.41	—	—	—	4.82	3.13 <sup>+0.66</sup> <sub>-0.96</sub>	0.013	0.089 <sup>+0.072</sup> <sub>-0.042</sub>
A1142-M1	2	1	12.01	-22.85	—	24.84	—	—	—	4.99	2.64 <sup>+0.60</sup> <sub>-0.11</sub>	0.022	0.089 <sup>+0.080</sup> <sub>-0.030</sub>
A1177-M1	2	1	12.41	-23.56	—	66.74	—	—	—	4.31	2.64 <sup>+0.60</sup> <sub>-0.11</sub>	0.028	0.074 <sup>+0.027</sup> <sub>-0.080</sub>
A1314-M1	2	1	12.27	-23.31	—	96.02	—	—	—	4.34	2.53 <sup>+0.71</sup> <sub>-0.36</sub>	0.034	0.085 <sup>+0.083</sup> <sub>-0.038</sub>
A1367-M1	2	1	12.12	-23.05	—	14.86	—	—	—	2.88	2.91 <sup>+0.30</sup> <sub>-0.30</sub>	0.046	0.078 <sup>+0.054</sup> <sub>-0.039</sub>
A1631-M1	2	1	12.29	-23.34	—	32.36	—	—	—	4.28	2.64 <sup>+0.57</sup> <sub>-0.11</sub>	0.025	0.074 <sup>+0.028</sup> <sub>-0.028</sub>
A1656-M1	2	1	12.55	-23.81	—	22.55	—	—	—	2.20	2.64 <sup>+0.57</sup> <sub>-0.11</sub>	0.116	0.059 <sup>+0.048</sup> <sub>-0.013</sub>
A2040-M1	2	1	12.35	-23.46	—	51.29	—	—	—	1.64	2.91 <sup>+0.18</sup> <sub>-0.52</sub>	0.093	0.076 <sup>+0.064</sup> <sub>-0.121</sub>
A2052-M1	2	1	12.11	-23.04	250	189.2	0.24	—	—	3.48	2.75 <sup>+0.43</sup> <sub>-0.38</sub>	0.002	0.089 <sup>+0.057</sup> <sub>-0.042</sub>
A2147-M1	2	1	12.18	-23.16	—	36.31	—	—	—	4.44	2.64 <sup>+0.57</sup> <sub>-0.11</sub>	0.049	0.059 <sup>+0.059</sup> <sub>-0.013</sub>
A2162-M1	2	1	12.15	-23.11	—	26.01	—	—	—	3.04	3.54 <sup>+0.15</sup> <sub>-1.38</sub>	0.129	0.088 <sup>+0.077</sup> <sub>-0.041</sub>
A2197-M1	2	1	12.45	-23.63	—	33.91	—	—	—	3.38	2.53 <sup>+0.71</sup> <sub>-0.36</sub>	0.125	0.074 <sup>+0.057</sup> <sub>-0.028</sub>
A2572-M1	2	1	12.31	-23.39	—	49.16	—	—	—	4.26	3.13 <sup>+0.11</sup> <sub>-0.60</sub>	0.013	0.089 <sup>+0.095</sup> <sub>-0.043</sub>
A2589-M1	2	1	12.65	-23.98	—	74.18	—	—	—	4.53	2.89 <sup>+0.33</sup> <sub>-0.36</sub>	0.008	0.084 <sup>+0.057</sup> <sub>-0.038</sub>
A2593-M1	2	1	12.52	-23.75	—	21.00	—	—	—	1.76	2.64 <sup>+0.57</sup> <sub>-0.11</sub>	0.029	0.070 <sup>+0.083</sup> <sub>-0.024</sub>
A2877-M1	2	1	12.63	-23.94	—	24.28	—	—	—	2.79	2.91 <sup>+0.33</sup> <sub>-0.75</sub>	0.098	0.087 <sup>+0.048</sup> <sub>-0.041</sub>
A3144-M1	2	1	11.68	-22.28	—	10.96	—	—	—	3.19	2.64 <sup>+0.57</sup> <sub>-0.48</sub>	0.155	0.120 <sup>+0.110</sup> <sub>-0.046</sub>
A3193-M1	2	2	11.97	-22.78	—	15.17	—	—	—	4.04 <sup>+0.00</sup> <sub>-0.00</sub>	2.64 <sup>+0.60</sup> <sub>-0.11</sub>	0.036 <sup>+0.003</sup> <sub>-0.003</sub>	0.090 <sup>+0.082</sup> <sub>-0.043</sub>
A3367-M1	2	2	11.69	-22.30	—	12.52	—	—	—	3.84 <sup>+0.31</sup> <sub>-0.24</sub>	2.77 <sup>+0.43</sup> <sub>-0.02</sub>	0.011 <sup>+0.002</sup> <sub>-0.002</sub>	0.087 <sup>+0.051</sup> <sub>-0.051</sub>
A3376-M1	2	2	12.26	-23.29	—	35.48	—	—	—	1.90 <sup>+0.36</sup> <sub>-0.36</sub>	3.17 <sup>+0.32</sup> <sub>-0.64</sub>	0.133 <sup>+0.033</sup> <sub>-0.033</sub>	0.084 <sup>+0.084</sup> <sub>-0.037</sub>
A3395-M1	2	1	12.79	-24.23	—	81.28	—	—	—	2.75	2.64 <sup>+0.60</sup> <sub>-0.10</sub>	0.013	0.074 <sup>+0.094</sup> <sub>-0.027</sub>
A3526-M1	2	2	12.88	-24.38	—	20.63	—	—	—	2.82 <sup>+0.01</sup> <sub>-0.01</sub>	2.83 <sup>+0.30</sup> <sub>-0.26</sub>	0.005 <sup>+0.000</sup> <sub>-0.000</sub>	0.047 <sup>+0.038</sup> <sub>-0.001</sub>
A3528-M1	2	1	12.83	-24.30	—	184.2	—	—	—	5.25	3.09 <sup>+0.15</sup> <sub>-0.56</sub>	0.018	0.086 <sup>+0.104</sup> <sub>-0.039</sub>
A3532-M1	2	1	12.99	-24.58	—	200.7	—	—	—	4.36	3.20 <sup>+1.73</sup> <sub>-0.71</sub>	0.018	0.085 <sup>+0.098</sup> <sub>-0.033</sub>
A3554-M1	2	1	12.66	-23.99	—	52.48	—	—	—	1.55	2.53 <sup>+0.66</sup> <sub>-0.36</sub>	0.039	0.061 <sup>+0.055</sup> <sub>-0.015</sub>
A3556-M1	2	1	12.46	-23.65	—	19.95	—	—	—	3.01	2.53 <sup>+0.66</sup> <sub>-0.36</sub>	0.051	0.078 <sup>+0.055</sup> <sub>-0.031</sub>
A3558-M1	2	1	13.19	-24.92	—	81.28	—	—	—	1.95	2.53 <sup>+0.66</sup> <sub>-0.36</sub>	0.070	0.090 <sup>+0.135</sup> <sub>-0.027</sub>
A3559-M1	2	1	12.58	-23.86	—	45.19	—	—	—	3.94	2.53 <sup>+0.66</sup> <sub>-0.36</sub>	0.043	0.074 <sup>+0.061</sup> <sub>-0.028</sub>
A3562-M1	2	1	12.84	-24.32	—	110.8	—	—	—	1.63	2.77 <sup>+0.17</sup> <sub>-0.24</sub>	0.083	0.089 <sup>+0.128</sup> <sub>-0.042</sub>
A3564-M1	2	1	11.91	-22.68	—	5.62	—	—	—	1.79	2.91 <sup>+0.18</sup> <sub>-0.38</sub>	0.123	0.102 <sup>+0.096</sup> <sub>-0.065</sub>
A3570-M1	2	1	11.83	-22.54	—	23.44	—	—	—	8.62	2.77 <sup>+0.45</sup> <sub>-0.20</sub>	0.022	0.090 <sup>+0.093</sup> <sub>-0.042</sub>
A3571-M1	2	1	13.40	-25.30	—	117.9	—	—	—	2.51	2.89 <sup>+0.33</sup> <sub>-0.32</sub>	0.004	0.105 <sup>+0.139</sup> <sub>-0.051</sub>
A3574-M1	2	1	12.53	-23.77	—	34.85	—	—	—	3.25	2.89 <sup>+0.33</sup> <sub>-0.32</sub>	0.020	0.074 <sup>+0.064</sup> <sub>-0.028</sub>
A3656-M1	2	2	12.42	-23.58	—	69.98	—	—	—	4.58 <sup>+0.60</sup> <sub>-0.60</sub>	2.77 <sup>+0.45</sup> <sub>-0.20</sub>	0.046 <sup>+0.022</sup> <sub>-0.022</sub>	0.084 <sup>+0.083</sup> <sub>-0.038</sub>
A3677-M1	2	1	11.64	-22.21	—	26.30	—	—	—	5.99	2.77 <sup>+0.45</sup> <sub>-0.20</sub>	0.083	0.103 <sup>+0.103</sup> <sub>-0.064</sub>
A3716-M1	2	2	12.52	-23.75	—	53.70	—	—	—	2.95 <sup>+0.44</sup> <sub>-0.44</sub>	2.49 <sup>+0.75</sup> <sub>-0.52</sub>	0.029 <sup>+0.003</sup> <sub>-0.003</sub>	0.060 <sup>+0.081</sup> <sub>-0.014</sub>
A3736-M1	2	1	12.65	-23.98	—	41.69	—	—	—	2.87	2.64 <sup>+0.30</sup> <sub>-0.11</sub>	0.074	0.047 <sup>+0.058</sup> <sub>-0.001</sub>
A3742-M1	2	1	11.64	-22.20	—	6.35	—	—	—	1.95	2.72 <sup>+0.17</sup> <sub>-0.75</sub>	0.349	0.117 <sup>+0.115</sup> <sub>-0.044</sub>
A3744-M1	2	1	12.01	-22.86	—	32.73	—	—	—	6.75	2.59 <sup>+0.07</sup> <sub>-0.35</sub>	0.129	0.087 <sup>+0.080</sup> <sub>-0.041</sub>
A3747-M1	2	2	11.89	-22.65	—	14.45	—	—	—	3.50 <sup>+0.46</sup> <sub>-0.46</sub>	2.81 <sup>+0.43</sup> <sub>-0.63</sub>	0.035 <sup>+0.003</sup> <sub>-0.003</sub>	0.090 <sup>+0.051</sup> <sub>-0.053</sub>
A4038-M1	2	1	11.91	-22.68	—	13.24	—	—	—	2.95	2.89 <sup>+0.33</sup> <sub>-0.36</sub>	0.077	0.090 <sup>+0.053</sup> <sub>-0.044</sub>

Compiled and fitted parameters for the confirmed core ellipticals in our observed samples. Columns show: (1) Object name. (2) Source for surface brightness profiles, where 1 =Kormendy et al. (2008), 2 =Lauer et al. (2007a), 3 =Bender et al. (1988). (3) Total number of different surface brightness profiles in our combined samples for the given object. (4) Stellar mass [ $\log M_*/M_\odot$ ]. (5) V-band absolute magnitude. (6) Velocity dispersion [km/s]. (7) Effective (half-light) radius of the *total* light profile [kpc]. (8) Ellipticity. (9) Boxy/diskyness. (10) Rotation. (11) Outer Sersic index  $n_s$  of the two-component best-fit profile. Where multiple profiles are available for the same object, we show the median and minimum/maximum range of fitted  $n_s$  values. (12) Range of outer Sersic indices fit in the same manner to the best-fit simulations, at  $t \approx 1-3$  Gyr after the merger when the system has relaxed. (13) Fraction of light in the inner or extra light component of the fits. Where multiple profiles are available for the same object, we show the median and minimum/maximum range of fitted values. (14) Fraction of light from stars produced in the central, merger-induced starburst in the best-fit simulations ( $\pm$  the approximate interquartile range allowed).

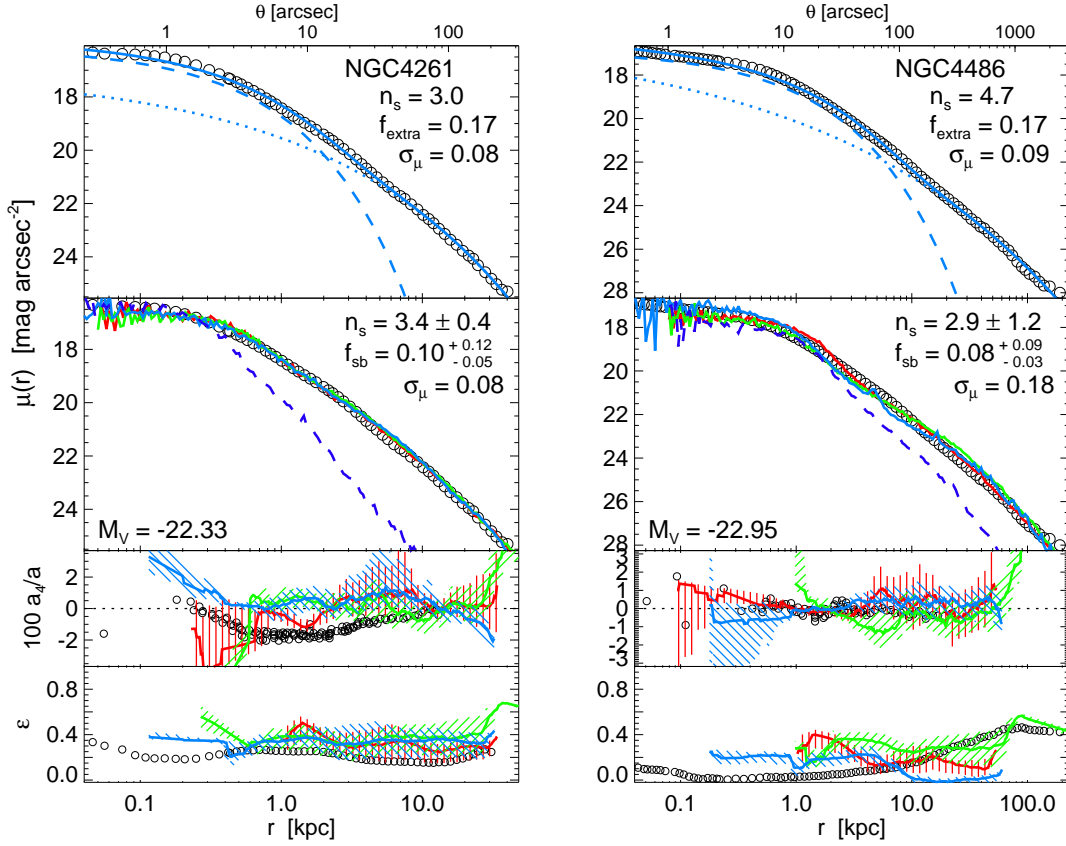
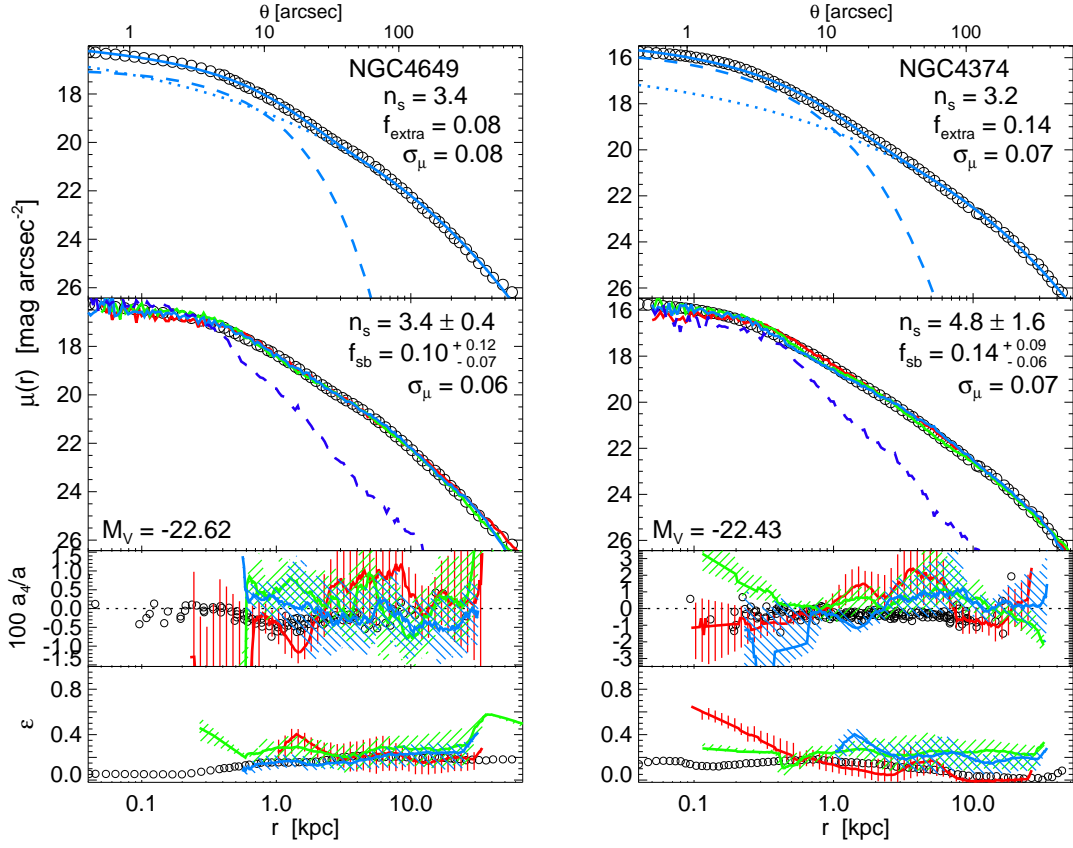
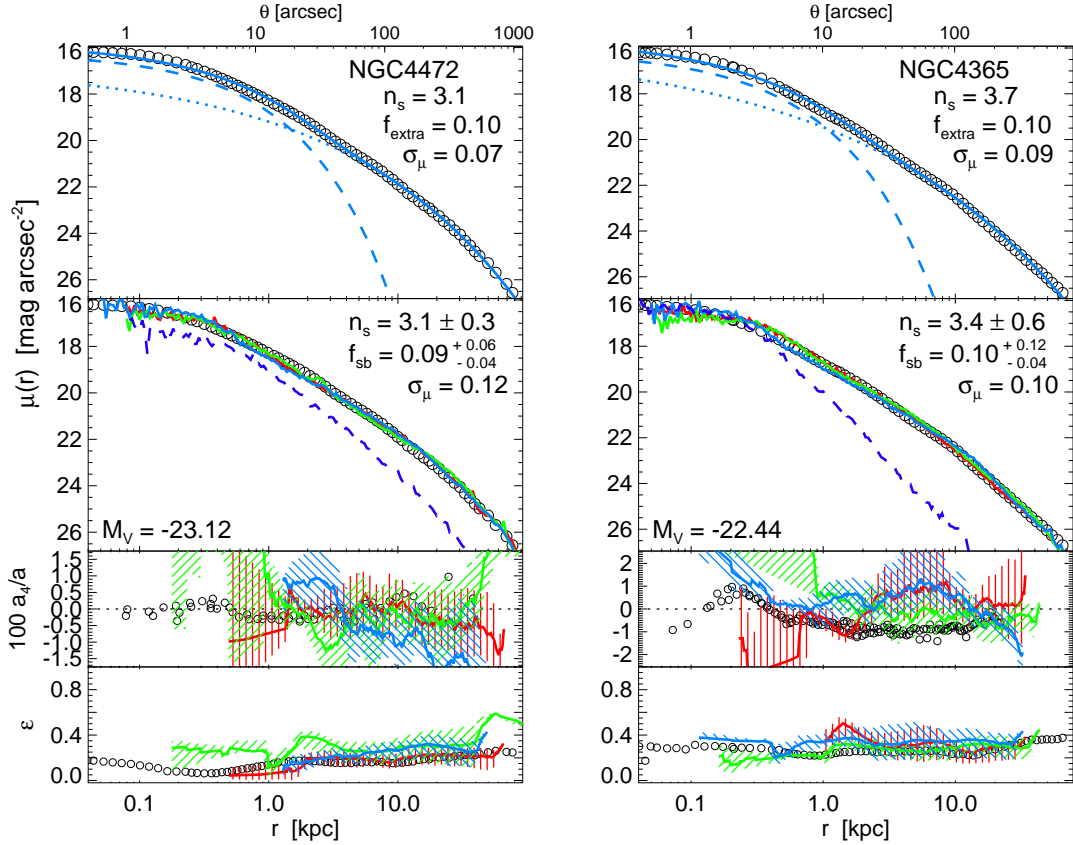


FIG. 33.— As Figure 10, but in log-log space. Surface brightness profiles – decomposed into dissipationless and dissipational/extra light components – are shown for core ellipticals in and around the Virgo cluster<sup>10</sup>. Open circles show the observations, from Kormendy et al. (2008). These are the highest-mass core ellipticals in Virgo ( $\sim 6-8M_*$ ). *Upper*: Observed V-band surface brightness profile with our two component best-fit model (solid, dashed, and dotted lines show the total, inner/extra light component, and outer/pre-starburst component). The best-fit outer Sersic index, extra light fraction, and rms residuals about the fit are shown. *Lower*: Colored lines show the corresponding surface brightness profiles from the three simulations in our library which correspond most closely to the observed system. Dashed line shows the profile of the starburst light in the best-matching simulation. The range of outer Sersic indices in the simulations (i.e. across sightlines for these objects) and range of starburst mass fractions which match the observed profile are shown, with the rms residuals of the observations about the best-fit simulation<sup>11</sup>. *Bottom*: Observed disk/boxy/ness ( $a_4$ ) and ellipticity profiles, with the median (solid) and 25–75% range (shaded) corresponding profile from the best-fitting simulations above. Note that these are not fitted for in any sense. Figures 34–37 show the other core ellipticals in the sample, ranked from most to least massive.

#### APPENDIX

##### FITS TO THE SAMPLE OF KORMENDY ET. AL. 2008

In Figures 33–37 we reproduce Figures 10–14, but with profiles shown in log-log projection as opposed to  $r^{1/4}$  projection.

FIG. 34.— The next most massive core ellipticals ( $\sim 5-6M_*$ ). (As Figure 11, but in log-log space.)FIG. 35.— Similar massive core ellipticals ( $\sim 4-5M_*$ ). (As Figure 12, but in log-log space.)



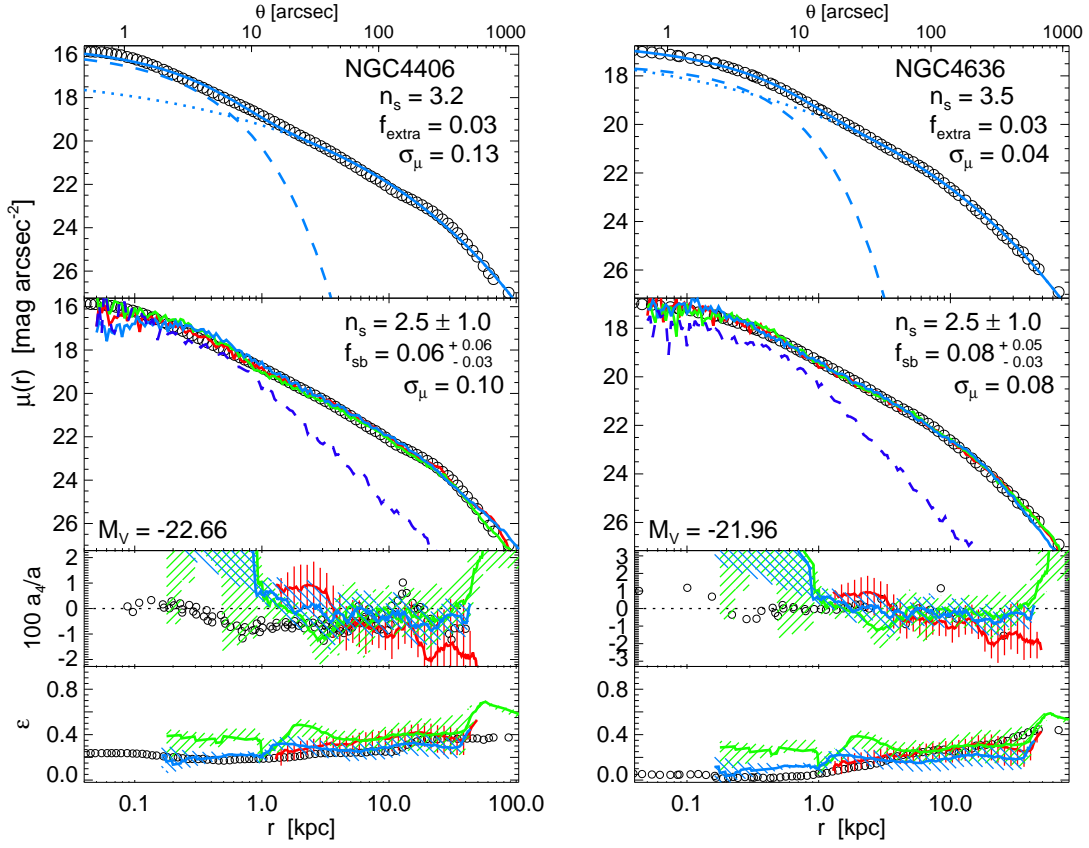


FIG. 36.— The next most massive core ellipticals ( $\sim 2-3M_*$ ). (As Figure 13, but in log-log space.)

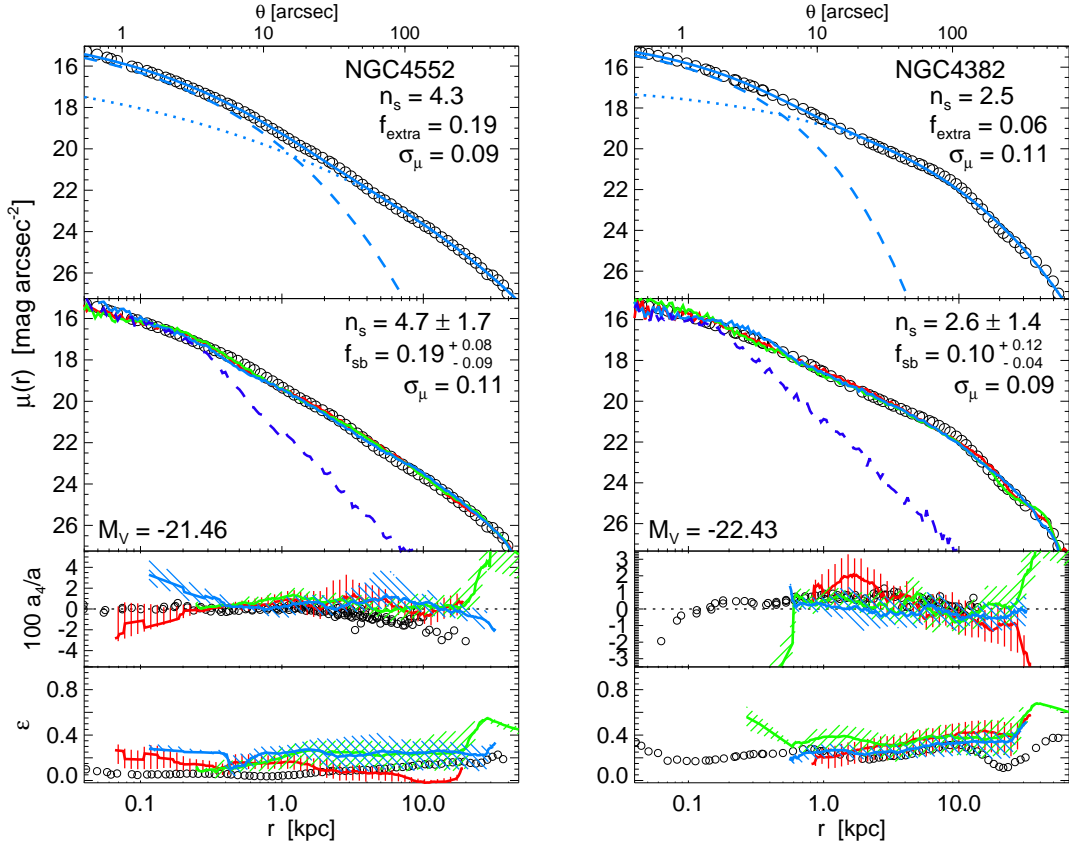


FIG. 37.— The least massive core ellipticals in the Kormendy et al. (2008) Virgo sample ( $\sim 1-2M_*$ ). (As Figure 14, but in log-log space.)